

การเตรียมฟิล์มผสมทั้งสแตนด์-ไทรออกไซด์-ไทเทเนียมไดออกไซด์
และการประยุกต์ใช้ในปฏิกิริยาโฟโตคะตะไลซิสแบบเฮเทอโรจีเนียส



นายอภิชน วัชรนทรวัรงค์

สถาบันวิทยบริการ

จุฬาลงกรณ์มหาวิทยาลัย

วิทยานิพนธ์นี้เป็นส่วนหนึ่งของการศึกษาตามหลักสูตรปริญญาวิทยาศาสตรดุษฎีบัณฑิต

สาขาวิชาการจัดการสิ่งแวดล้อม (สหสาขาวิชา)

บัณฑิตวิทยาลัย จุฬาลงกรณ์มหาวิทยาลัย

ปีการศึกษา 2550

ลิขสิทธิ์ของจุฬาลงกรณ์มหาวิทยาลัย

PREPARATION AND CHARACTERIZATION OF TUNGSTEN TRIOXIDE –
TITANIUM DIOXIDE COMPOSITE FILM AND ITS APPLICATIONS IN
HETEROGENEOUS PHOTOCATALYSIS



Mr. Apichon Watcharenwong

A Dissertation Submitted in Partial Fulfillment of the Requirements
for the Degree of Doctor of Philosophy Program in Environmental Management
(Interdisciplinary Program)

Graduate School

Chulalongkorn University

Academic Year 2007

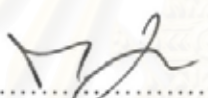
Copyright of Chulalongkorn University

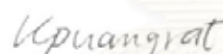
Thesis Title PREPARATION AND CHARACTERIZATION OF
TUNGSTEN TRIOXIDE – TITANIUM DIOXIDE
COMPOSITE FILM AND ITS APPLICATIONS IN
HETEROGENEOUS PHOTOCATALYSIS
By Mr. Apichon Watcharenwong
Field of Study Environmental Management
Thesis Advisor Associate Professor Puangrat Kajitvichyanukul, Ph.D.
Thesis Co-advisor Professor Krishnan Rajeshwar, Ph.D.

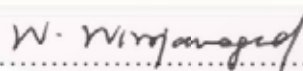
Accepted by the Graduate School, Chulalongkorn University in Partial
Fulfillment of the Requirements for the Doctoral Degree

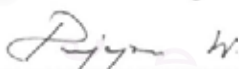

..... Dean of the Graduate School
(Assistant Professor M.R. Kalaya Tingsabadh, Ph.D.)

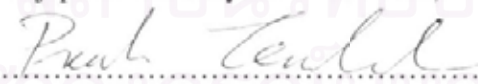
THESIS COMMITTEE



..... Chairman
(Manaskorn Rachakornkij, Ph.D.)


..... Thesis Advisor
(Associate Professor Puangrat Kajitvichyanukul, Ph.D.)


..... Member
(Associate Professor Wanpen Wirojanagud, Ph.D.)


..... Member
(Punjaporn Weschayanwiwat, Ph.D.)


..... Member
(Preecha Termsuksawad, Ph.D.)


..... External committee
(Associate Professor Duangrat Inthorn, Ph.D.)

อภิชน วิชาเรนทร์วงศ์ : การเตรียมฟิล์มผสมทั้งสเดนไดรออกไซด์-ไทเทเนียมไดออกไซด์ และการประยุกต์ใช้ในปฏิกิริยาโฟโตคะตะไลซิสแบบเฮเทอโรเจนีอัส (PREPARATION AND CHARACTERIZATION OF TUNGSTEN TRIOXIDE – TITANIUM DIOXIDE COMPOSITE FILM AND ITS APPLICATIONS IN HETEROGENEOUS PHOTOCATALYSIS) อ. ที่ปรึกษา : รศ. ดร. พวงรัตน์ ขจิตวิษยานุกูล, อ. ที่ปรึกษาร่วม: PROF. KRISHNAN RAJESHWAR, Ph.D. 161 หน้า.

งานวิจัยนี้มุ่งเน้นศึกษาการเตรียมและวิเคราะห์คุณลักษณะของไททาเนียมไดออกไซด์ ทั้งสเดนไดรออกไซด์ และฟิล์มผสมซึ่งได้จาก 2 วิธี คือ อิเล็กโตรเคมีโพสิชันและแอนโนไดเซชัน และสภาวะที่เหมาะสมในการเตรียมฟิล์มไททาเนียมไดออกไซด์ ทั้งสเดนไดรออกไซด์ และฟิล์มผสมโดยวิธีอิเล็กโตรเคมีโพสิชัน อีกทั้งยังศึกษาถึงความสัมพันธ์ระหว่างการเกิดรูปร่างลักษณะของชั้นไททาเนียมไดออกไซด์และชั้นทั้งสเดนไดรออกไซด์บนแผ่นตัวกลางของไททาเนียมและทั้งสเดนไดรออกไซด์ที่มีต่อการตอบสนองทางด้านปฏิกิริยาเคมีไฟฟ้าแสงในสารละลายโซเดียมซัลเฟตที่ความเข้มข้น 0.5 โมลาร์ ผลของการแปรเปลี่ยนค่าในการแอนโนไดเซชัน (ศักย์ไฟฟ้าและเวลา) และส่วนประกอบในสารละลาย (น้ำ กริเซอร์ออล โพลีเอทิลีนไกลคอล เอทิลีนไกลคอล) รวมทั้งความเข้มข้นของฟลูออไรด์ไอออนต่อการเกิดรูปร่างลักษณะของชั้นออกไซด์ และการตอบสนองต่อแสง พบว่าเมื่อใช้โลหะไทเทเนียมเป็นตัวกลางทำปฏิกิริยากับสารละลายที่มีฟลูออไรด์ไอออนผสมอยู่และถูกผสมด้วยโพลีเอทิลีนไกลคอล (น้ำหนักโมเลกุล 400) หรือเอทิลีนไกลคอลจะทำให้ได้ไทเทเนียมไดออกไซด์ที่มีลักษณะเป็นท่อขนาดเล็กในระดับนาโนเมตร ในขณะที่เมื่อใช้ทั้งสเดนเป็นตัวกลางจะไม่ให้ลักษณะเป็นท่อขนาดเล็ก ในการเตรียมฟิล์มผสมโดยวิธีโพสิชันแอนโนไดเซชัน ฟิล์มผสมสองแบบ (ทั้งสเดน/ทั้งสเดนไดรออกไซด์/ไททาเนียมไดออกไซด์ และไทเทเนียม/ไททาเนียมไดออกไซด์/ทั้งสเดนไดรออกไซด์) ให้ค่าการตอบสนองต่อปฏิกิริยาเคมีไฟฟ้าแสงดีกว่าฟิล์มเดี่ยวของทั้งสเดนไดรออกไซด์ และไทเทเนียมไดออกไซด์ ตามลำดับ นอกจากนี้ฟิล์มผสมไทเทเนียม/ไททาเนียมไดออกไซด์/ทั้งสเดนไดรออกไซด์ที่มีลักษณะเป็นท่อขนาดนาโนเมตรให้ค่าการตอบสนองต่อปฏิกิริยาเคมีไฟฟ้าแสงสูงถึง 7.7 มิลลิแอมแปร์ต่อตารางเซนติเมตร นอกจากนี้ยังมีการศึกษาปฏิกิริยาโฟโตคะตะไลติกรีดักชันของโครเมียมประจุบวก 6 และปฏิกิริยาโฟโตคะตะไลติกออกซิเดชันของเมทิลีนบลูภายใต้การฉายแสงอัลตราไวโอเล็ตโดยใช้ฟิล์มชนิดต่างๆ ที่เตรียมได้โดยวิธีแอนโนไดเซชัน และมีการศึกษาอัตราการสลายเมทิลีนบลูด้วยแสงขาวที่ความยาวคลื่นมากกว่า 400 นาโนเมตรและใช้แบบจำลองของ แลงเมียร์-ฮินเชลวูดศึกษาอัตรา การย่อยสลายพบว่า ได้ค่าคงของปฏิกิริยา (k) เท่ากับ 0.687 ไมโครโมลาร์ต่ออนาทีและค่าคงที่การดูดซับของแลงเมียร์ (K) เท่ากับ 0.021 ต่อไมโครโมลาร์

สาขาวิชาการจัดการสิ่งแวดล้อม
ปีการศึกษา 2550

ลายมือชื่อนิสิต
ลายมือชื่ออาจารย์ที่ปรึกษา.....
ลายมือชื่ออาจารย์ที่ปรึกษาร่วม.....

4789721320 : MAJOR ENVIRONMENTAL MANAGEMENT

KEY WORD: TiO_2 / WO_3 / COMPOSITE FILM / ELECTRODEPOSITION / ANODIZATION / TITANIUM NANOTUBE / CHROMIUM / METHYLENE BLUE / PHOTOCATALYSIS / VISIBLE LIGHT

APICHON WATCHARENWONG: PREPARATION AND CHARACTERIZATION OF TUNGSTEN TRIOXIDE – TITANIUM DIOXIDE COMPOSITE FILM AND ITS APPLICATIONS IN HETEROGENEOUS PHOTOCATALYSIS. THESIS ADVISOR: ASSOC. PROF. PUANGRAT KAJITVICHYANUKUL, Ph.D., THESIS CO-ADVISOR: PROF. KRISHNAN RAJESHWAR, Ph.D., 161 pp.

This research focuses on preparation and characterization of TiO_2 , WO_3 and composite films using two techniques: electrodeposition and anodization. Optimization of SS/ TiO_2 , SS/ WO_3 and composite films prepared by electrodeposition on the stainless steel (SS) type 304 was investigated. This study also probes the relationship between the morphology of anodic TiO_2 and WO_3 layers grown on Ti or W foil substrates and their subsequent photoelectrochemical response in 0.5 M Na_2SO_4 supporting electrolyte. The effects of anodization variables (voltage and time) and anodization medium composition [water, glycerol, poly(ethylene glycol) (PEG), ethylene glycol (EG)] along with fluoride ion concentration on the oxide layer morphology and photoresponse are described. Well define nanotube morphology of TiO_2 was observed when the fluoride ion containing electrolyte was modified by PEG400 or EG while the nanotube morphology could not be observed on W substrate. In fabrication of composite film by pulse anodization technique, two types of composite film ($\text{W}/\text{WO}_3/\text{TiO}_2$ and $\text{Ti}/\text{TiO}_2/\text{WO}_3$) were conducted. These composite films exhibit better photoelectrochemical response than the pure W/WO_3 and Ti/TiO_2 , respectively. In addition, the well organized composite $\text{Ti}/\text{TiO}_2/\text{WO}_3$ nanotube films were fabricated and gave the excellent photoelectrochemical performance reaching 7.7 mA cm^{-2} . Finally, photocatalytic reduction of hexavalent chromium and photocatalytic oxidation of methylene blue were studied under ultraviolet light using anodically growth Ti/TiO_2 , W/WO_3 and composite films. Furthermore, visible light ($\lambda > 400 \text{ nm}$) degradation of methylene blue using W/WO_3 films was studied. The photocatalytic degradation rate follow Langmuir–Hinshelwood model yields $k = 0.687 \mu\text{M min}^{-1}$ and $K = 0.021 \mu\text{M}^{-1}$.

Field of study Environmental Management
Academic year 2007

Student's signature

Advisor's signature

Co-advisor's signature.....

Abhis
Puangrat
Kajitvichyanukul

ACKNOWLEDGEMENTS

I would like to gratefully acknowledge my thesis advisor, Assoc. Prof. Dr. Puangrat Kajitvichyanukul and my thesis co-advisor, Prof. Dr. Krishnan Rajeshwar, for their encouragement, invaluable support, and guidance. Their comments and suggestions not merely provide valuable knowledge but broaden perspective in practical applications as well. Special gratitude goes to all committee members, Dr. Manaskorn Rachakornkij, Assoc. Prof. Dr. Wanpen Wirojanagud, Dr. Punjaporn Weschayanwiwat, Dr. Preecha Termsuksawad, and external committee, Assoc. Prof. Dr. Duangrat Inthorn for providing invaluable advices and their insightful suggestions.

I would like to extend my sincere appreciation to Dr. C. Ramannair Chenthamarakshan who has been abundantly helpful and to Prof. Dr. Norma R. de Tacconi for her explanations, supportive and fervent inspiration for being a good researcher. This work would not have been possible without their support and encouragement.

This work was supported in part by a grant from the U.S. Department of Energy (Office of Basic Energy Sciences) and partially granted by the National Center of Excellence for Environmental and Hazardous Waste Management (NCE-EHWM) Program, Thailand. Without these financial supports, my achievement should not become true.

Thanks to my colleagues from University of Texas at Arlington (Yogeeswaran Ganesan, Walter Alexander Morales, Hari Krishna Timmaji, Marly Eiko Osugi, Samantha de Zoysa and Sashikala Somasundaram) for their support, Jacob Alen Spharler for being good English teacher, Oliver's family for warmest welcome and thanks to all my colleagues from King Mongkut's University of Technology Thonburi (Jiraphat Ananpattarachai, Siriwan Pongpom, Suthatip Sinyoung, Janumas Boonsanit and Kiatsuda Somna) for their assistance and especially Wilaiwan Chanmanee for her plentifully help and suggestion.

Special thanks to my beloved family and Suporn Kiatmanaroj for supportiveness, understanding, encouragement, and patient support throughout my entire study and believed in me even from the distance away.

CONTENTS

	Page
ABSTRACT IN THAI.....	iv
ABSTRACT IN ENGLISH.....	v
ACKNOWLEDGEMENTS.....	vi
CONTENTS.....	vii
LIST OF TABLES.....	xiii
LIST OF FIGURES	xv
NOMENCLATURES.....	xxii
CHAPTER I INTRODUCTION.....	1
1.1 Research rationale.....	1
1.2 Objectives.....	3
1.3 Hypotheses.....	4
1.4 Scopes of work.....	4
CHAPTER II BACKGROUNDS AND LITERATURE REVIEWS.....	5
2.1 Electrodeposition	5
2.1.1 Electrodeposition of semiconductors	7
2.1.2 Electrodeposition of TiO ₂	9
2.1.3 Electrodeposition of WO ₃	10
2.2 Anodization	11
2.3 Review of WO ₃ /TiO ₂	14
2.4 Photocatalytic process	16
2.4.1 Photocatalysis using WO ₃ /TiO ₂	17
2.4.2 Review of photocatalysis of chromium	18
2.4.3 Review of photocatalysis of methylene blue	20
CHAPTER III METHODOLOGY.....	22
3.1 Cathodic electrodeposition	22

3.1.1 Chemicals and Materials	22
3.1.2 Thin films preparation	22
3.2 Anodization	24
3.2.1 Ti/TiO ₂ films prepared by anodization	24
3.2.1.1 Chemicals and Materials	24
3.2.1.2 Electrosynthesis	24
3.2.2 W/WO ₃ films prepared by anodization	25
3.2.2.1 Chemicals and Materials	25
3.2.2.2 Electrosynthesis	25
3.2.3 Composite films prepared by anodization	27
3.2.3.1 Electrosynthesis	27
- Part I W/WO ₃ /TiO ₂ nanoporous	27
- Part II Ti/TiO ₂ /WO ₃ nanoporous	28
- Part III Effect of electrolyte composition on the resulting W/WO ₃ /TiO ₂ and Ti/TiO ₂ /WO ₃ nanoporous films.....	29
- Part IV Ti/TiO ₂ /WO ₃ nanotubes	30
3.3 Photoelectrochemistry	32
3.3.1 Photocurrent measurement	32
3.3.2 Photon flux measurement	32
3.4 Photocatalysis	33
3.4.1 Ultraviolet (UV) light photocatalysis	33
3.4.2 Visible light photocatalysis	34
3.5 Other Instrumentation	34
CHAPTER IV RESULTS AND DISCUSSION.....	36
4.1 WO ₃ , TiO ₂ , and composite film preparation by cathodic electrodeposition on stainless steel (SS) type 304	36
4.1.1 Effect of electrodeposition time on film preparation	36
4.1.2 Effect of electrodeposition potential on film preparation ...	37
4.1.3 Effect of multilayer films of electrodeposition on photocurrent performance	40
4.1.3.1 Multilayer WO ₃ thin film electrodeposition	40

4.1.3.2 Multilayer TiO ₂ thin film electrodeposition	40
4.1.4 Effect of composite films of electrodeposition on photocurrent performance	41
4.1.4.1 Composite film SS/WO ₃ /TiO ₂ obtained by different electrodeposition steps	41
4.1.4.2 Composite SS/WO ₃ /TiO ₂ films prepared in different number of films layer	43
4.1.4.3 Composite film SS/TiO ₂ /WO ₃ obtained by different electrodeposition steps	44
4.1.4.4 Composite SS/TiO ₂ /WO ₃ films prepared in different number of films layer	45
4.1.5 Evaluation of the capability of electrodeposition technique in fabrication of TiO ₂ , WO ₃ and composite films on stainless steel AISI 304	46
4.2 TiO ₂ , WO ₃ , and composite film preparation by anodization	47
4.2.1 Ti/TiO ₂ prepared by anodization	47
4.2.1.1 Anodic growth of TiO ₂ films: variables	47
4.2.1.2 Effect of anodization time	51
4.2.1.3 Effect of poly(ethylene glycol) of different molecular weights	54
4.2.1.4 Effect of anodization voltage	56
4.2.1.5 Effect of fluoride ion concentration	58
4.2.2 W/WO ₃ prepared by anodization	60
4.2.2.1 Anodic growth of WO ₃ films: variables	60
4.2.2.2 Effect of anodization voltage	62
4.2.2.3 Effect of anodization time	65
4.2.2.4 Effect of poly(ethylene glycol) of different molecular weights	67
4.2.3 W/WO ₃ /TiO ₂ nanoporous film prepared by pulse anodization	68
4.2.3.1 Effect of pulsing voltage on morphology of composite W/WO ₃ /TiO ₂ films	68

4.2.3.2 Effect of pulsing voltage on photoelectrochemical performance of composite W/WO ₃ /TiO ₂ films	70
4.2.4 Ti/TiO ₂ /WO ₃ nanoporous film prepared by pulse anodization	74
4.2.4.1 Effect of pulsing voltage on morphology of composite Ti/TiO ₂ /WO ₃ films	74
4.2.4.2 Effect of pulsing voltage on photoelectrochemical performance of composite Ti/TiO ₂ /WO ₃ films	76
4.2.5 Effect of electrolyte composition on the resulting W/WO ₃ /TiO ₂ and Ti/TiO ₂ /WO ₃ composites prepared by pulse anodization..	80
4.2.5.1 Effect of electrolyte composition on morphology of W/WO ₃ /TiO ₂ and Ti/TiO ₂ /WO ₃ composites	80
4.2.5.2 Effect of electrolyte composition on photocurrent performance of W/WO ₃ /TiO ₂ and Ti/TiO ₂ /WO ₃ composites	86
4.2.6 Ti/TiO ₂ /WO ₃ nanotubes prepared by pulse anodization	87
4.2.6.1 Effect of constant polarization time and pulsing time on morphology and photoelectrochemical performance of nanotubes Ti/TiO ₂ /WO ₃ films	87
4.3 Photocatalysis application for TiO ₂ , WO ₃ , and composite film preparation by anodization	95
4.3.1 Ultraviolet (UV) light photocatalysis of Hexavalent Chromium, Cr(VI) by TiO ₂ , WO ₃ , and composite films prepared by anodization	95
- Effect of modifier in Ti/TiO ₂ film fabrication on photocatalytic reduction of Cr(VI)	97
- Comparison of composite W/WO ₃ /TiO ₂ films on photocatalytic reduction of Cr(VI)	99
- Comparison of composite Ti/TiO ₂ /WO ₃ films on photocatalytic reduction of Cr(VI)	101
- Comparison of Ti/TiO ₂ nanotube film and Ti/TiO ₂ /WO ₃ nanotube film on photocatalytic reduction of Cr(VI)	104

- Quantum efficiencies on photocatalytic reduction of hexavalent chromium, Cr(VI)	106
4.3.2 Ultraviolet (UV) light photocatalysis of Methylene blue, MB by TiO ₂ , WO ₃ , and composite films prepared by anodization	107
- Effect of modifier in Ti/TiO ₂ film fabrication on photocatalytic oxidation of MB	110
- Comparison of composite W/WO ₃ /TiO ₂ films on photocatalytic oxidation of MB	112
- Comparison of composite Ti/TiO ₂ /WO ₃ films on photocatalytic oxidation of MB	114
- Comparison of Ti/TiO ₂ nanotube film and Ti/TiO ₂ /WO ₃ nanotube film on photocatalytic oxidation of MB	116
- Quantum efficiencies on photocatalytic oxidation of methylene blue, MB	119
4.3.3 Visible light photocatalysis oxidation of Methylene blue, MB By W/WO ₃ film preparation by anodization	120
CHAPTER V CONCLUSIONS AND SUGGESTIONS FOR FUTURE WORKS	124
5.1 Conclusions.....	124
5.1.1 WO ₃ , TiO ₂ , and composite film preparation by cathodic electrodeposition on stainless steel (SS) AISI 304	124
5.1.2 TiO ₂ , WO ₃ , and composite film preparation by anodization...	125
5.1.3 Photocatalysis application for TiO ₂ , WO ₃ , and composite film preparation by anodization.....	126
5.2 Suggestions for future works.....	126
REFERENCES.....	128
APPENDICES.....	136
APPENDIX A Photocurrent and photocatalytic performances of films prepared by electrodeposition and anodization techniques..	137

APPENDIX B Photon flux and quantum yield calculations	157
APPENDIX C Journal publication list	159
BIOGRAPHY.....	161



สถาบันวิทยบริการ
จุฬาลงกรณ์มหาวิทยาลัย

LIST OF TABLES

Table	Page
3.1 Effect of parameters on film growth	23
3.2 Anodization conditions on Ti substrates.....	25
3.3 Anodization conditions on W substrates.....	26
3.4 Anodization conditions for W/WO ₃ /TiO ₂ nanocomposite film preparation.....	28
3.5 Anodization conditions for Ti/TiO ₂ /WO ₃ nanocomposite film preparation.....	29
3.6 Anodization conditions for the study of effect of electrolyte composition on the resulting W/WO ₃ /TiO ₂ and Ti/TiO ₂ /WO ₃ nanoporous films.....	30
3.7 Anodization conditions for Ti/TiO ₂ /WO ₃ nanotubes film preparation.....	31
4.1 Photocurrent density of SS/WO ₃ electrodeposition films with varying electrodeposition time.....	36
4.2 Photocurrent density of SS/TiO ₂ electrodeposition films with varying electrodeposition time.....	37
4.3 Photocurrent density of SS/WO ₃ electrodeposition films with varying electrodeposition potential.....	38
4.4 Photocurrent density of SS/TiO ₂ electrodeposition films with varying electrodeposition potential.....	38
4.5 Photocurrent density of SS/WO ₃ /WO ₃ /... multilayer films.....	40
4.6 Photocurrent density of SS/TiO ₂ /TiO ₂ /... multilayer films.....	40
4.7 Photocurrent density of SS/WO ₃ /TiO ₂ films obtained by different electrodeposition steps.....	41
4.8 Photocurrent density of SS/WO ₃ /TiO ₂ films prepared in different number of films layer.....	43
4.9 Photocurrent density of SS/TiO ₂ /WO ₃ films obtained by different electrodeposition steps.....	44
4.10 Photocurrent density of SS/TiO ₂ /WO ₃ films prepared in different number of films layer.....	45
4.11 Anodization conditions, photoelectrochemical performance and morphology of TiO ₂ nanotubes in this study.....	48

4.12 Anodization conditions, photoelectrochemical performance and morphology of nanoporous WO_3 in this study.....	60
4.13 Ti:W composition for composite $\text{W}/\text{WO}_3/\text{TiO}_2$ and $\text{Ti}/\text{TiO}_2/\text{WO}_3$ films analyzed by XPS analysis.....	81
4.14 Ti:W composition for composite nanotubes $\text{Ti}/\text{TiO}_2/\text{WO}_3$ films analyzed by XPS analysis.....	87
4.15 Photoelectrochemical performance and kinetic parameters on photocatalytic reduction of Cr(VI) for Ti/TiO_2 films prepared by anodization technique.....	98
4.16 Photoelectrochemical performance and kinetic parameters on photocatalytic reduction of Cr(VI) for composite $\text{W}/\text{WO}_3/\text{TiO}_2$ films prepared by anodization technique.....	100
4.17 Photoelectrochemical performance and kinetic parameters on photocatalytic reduction of Cr(VI) for composite $\text{Ti}/\text{TiO}_2/\text{WO}_3$ films prepared by anodization technique.....	103
4.18 Photoelectrochemical performance and kinetic parameters on photocatalytic reduction of Cr(VI) for Ti/TiO_2 nanotube film and $\text{Ti}/\text{TiO}_2/\text{WO}_3$ nanotube film prepared by anodization technique.....	105
4.19 Photoelectrochemical performance and kinetic parameters on photocatalytic reduction of MB for Ti/TiO_2 films prepared by anodization technique.....	111
4.20 Photoelectrochemical performance and kinetic parameters on photocatalytic oxidation of MB for composite $\text{W}/\text{WO}_3/\text{TiO}_2$ films prepared by anodization technique.....	113
4.21 Photoelectrochemical performance and kinetic parameters on photocatalytic oxidation of MB for composite $\text{Ti}/\text{TiO}_2/\text{WO}_3$ films prepared by anodization technique.....	115
4.22 Photoelectrochemical performance and kinetic parameters on photocatalytic oxidation of MB for Ti/TiO_2 nanotube film and $\text{Ti}/\text{TiO}_2/\text{WO}_3$ nanotube film prepared by anodization technique.....	118
4.23 Effect of initial methylene blue (MB) concentration on the kinetics parameters.....	122

LIST OF FIGURES

Figure	Page
2.1 Schematic of electrodeposition process	6
2.2 Road map of electrodeposition of main inorganic semiconductors established from the analysis of many References and Current Contents data base (2000–April 2002).....	8
2.3 Number of published papers from Current Contents data base (2000–April 2002) as a function of the nature of the semiconductor. Other: MoS ₂ , In ₂ Se ₃ , SnSe, Sb ₂ Se ₃ , In ₂ S ₃ , PbTe, FeS ₂ , CuSnSb, Ag ₂ S, Cu ₂ S, InSb, InAsSb, CoS, Bi ₂ Se ₃ , WS ₂ , SnSb, CuZnTe, Ge NiS, CuI, CuSCN, InFe(CN) ₆ , SnO ₂	9
2.4 Hexagonal cell structure of aluminum oxide layer	12
2.5 Schematic diagram of the evolution of a nanotube array at constant anodization voltage	13
2.6 Schematic of photocatalytic process	17
2.7 Energy diagram for the WO ₃ -TiO ₂ composite system.....	18
3.1 Total potential waveform for W/WO ₃ /TiO ₂ nanocomposite film preparation.....	27
3.2 Total potential waveform for Ti/TiO ₂ /WO ₃ nanocomposite film preparation.....	29
3.3 Total potential waveform for Ti/TiO ₂ /WO ₃ nanotubes film preparation	31
4.1 SEM images of after annealed (a) WO ₃ (-400 mV, 10 min) and (b) TiO ₂ (-950 mV, 30 min) films on stainless steel type 304 prepared by optimum electrodeposition potential and time.....	39
4.2 SEM images of composite SS/WO ₃ /TiO ₂ film (SS/5/15 min, 2 layers) which gave highest photocurrent reach to 230 μA/cm ²	42

- 4.3 (A) Photovoltammograms of nanoporous TiO₂ films grown in poly(ethylene glycol) (PEG) of different molecular weights (as shown) containing 0.15 M NH₄F electrolyte. (B) Bar diagram comprising of photocurrent density at 1.5 V for nanoporous TiO₂ films grown under various conditions..... 50
- 4.4 Effect of anodization time on the morphology of nanoporous TiO₂ films as probed by SEM. The films were grown in 0.15 M NH₄F electrolyte at 20 V for (a) 1, (b) 3, and (c) 10 h.51
- 4.5 Comparison of SEM images of TiO₂ nanotubes obtained by anodization of Ti foil in 0.15 M NH₄F + glycerol (~2-3% water) at 20 V for (a) 5 and (b) 10 h. 52
- 4.6 Effect of anodization time on the morphology of nanoporous TiO₂ films as probed by SEM. The films were grown in 0.15 M NH₄F + glycerol (1% water) at 20 V for (a) 3, (b) 5, and (c) 10 h. 53
- 4.7 Comparison of SEM data for TiO₂ nanotubes obtained by anodization of Ti foil at 20 V for 5 h in 0.15 M NH₄F with poly(ethylene glycol) (PEG) of different molecular weights, (a) PEG 200, (b) PEG 400, (c) PEG 600, and (d) PEG 1000 with a ratio of PEG:H₂O of 90:10 in each case.55
- 4.8 Effect of anodization voltage on the morphology of TiO₂ nanotubes as probed by SEM (cross-sectional views). The films were grown in 0.36 M NH₄F + ethylene glycol:H₂O (90:10) for 5 h at (a) 20, (b) 40, and (d) 60 V, respectively..... 57
- 4.9 Effect of fluoride ion concentration on the morphology of TiO₂ nanotubes as probed by SEM. The films were grown at 20 V for 5 h in (a) 0.15 M NH₄F + glycerol (~2-3% water) and (b) 0.36 M NH₄F + glycerol (~2-3% water).....58
- 4.10 Comparison of the lengths of TiO₂ nanotubes as probed by cross-sectional SEM. The nanotube arrays were prepared by anodization of Ti foil at 20 V for 5 h in (a) 0.15 M NH₄F + ethylene glycol:H₂O (90:10) and (b) 0.36 M NH₄F + ethylene glycol:H₂O (90:10).....59
- 4.11 (A) Photovoltammograms of nanoporous WO₃ films grown in 0.15 NaF electrolyte at 60 V for (a) 2, (b) 3, and (c) 6 h, respectively. (B) Bar diagram comprising of photocurrent density at 2 V for nanoporous WO₃ films grown under various conditions..... 61

- 4.12 Effect of anodization voltage on the morphology of WO_3 nanoporous films as probed by SEM. The films were grown in 0.15 M NaF for 3 h at (a) 20, (b) 40, and (c) 60 V, respectively.....63
- 4.13 Effect of anodization voltage on the morphology of WO_3 nanoporous films as probed by SEM. The films were grown in 0.3 M oxalic acid for 2 h at (a) 20, (b) 40, and (c) 60 V, respectively..... 64
- 4.14 Comparison of SEM images of WO_3 nanoporous films obtained by anodization of tungsten foil in 0.15 M NaF at 60 V for (a) 2, (b) 4, and (c) 6 h, respectively.....66
- 4.15 Comparison of SEM data for WO_3 nanoporous films obtained by anodization of tungsten foil at 20 V for 3 h in 0.15 M NaF with PEG of different molecular weights: (a) PEG 200, (b) PEG 400, (c) PEG 600, and (d) PEG 1000 with a ratio of PEG:H₂O of 40:60 in each case.....67
- 4.16 SEM images of composite W/ WO_3 /TiO₂ nanoporous film prepared with initial stage of constant anodization 60 V, 1 h and second stage of pulse waveform (60/-4 V) with different pulsing anodization time (A1) 20 min, (A2) 40 min, (A3) 1 h, (A4) 2 h and (A5) 3 h.....68
- 4.17 SEM images of composite W/ WO_3 /TiO₂ nanoporous film prepared with initial stage of constant anodization 60 V, 1 h and second stage of pulse waveform (60/0 V) with different pulsing anodization time (B1) 20 min, (B2) 40 min, (B3) 1 h, (B4) 2 h and (B5) 3 h.....69
- 4.18 Bar diagram comprising of photocurrent density at 2 V for composite W/ WO_3 /TiO₂ films grown under various conditions.....70
- 4.19 Photovoltammograms for selected W/ WO_3 /TiO₂ grown under the two pulsing waveforms (60/-4 V and 60/0 V) compare with neat WO_372
- 4.20 SEM images of composite Ti/TiO₂/ WO_3 nanoporous film prepared with initial stage of constant anodization 20 V, 30 min and second stage of pulse waveform (20/-4 V) with different pulsing anodization time (C1) 30 min, (C2) 1 h, (C3) 2 h and (C4) 3 h.....74

4.21 SEM images of composite Ti/TiO ₂ /WO ₃ nanoporous film prepared with initial stage of constant anodization 20 V, 30 min and second stage of pulse waveform (20/0 V) with different pulsing anodization time (D1) 30 min, (D2) 1 h, (D3) 2 h and (D4) 3 h.....	75
4.22 Bar diagram comprising of photocurrent density at 2 V for composite Ti/TiO ₂ /WO ₃ films grown under various conditions.....	77
4.23 Photovoltammograms for selected Ti/TiO ₂ /WO ₃ grown under the two pulsing waveforms (20/-4 V and 20/0 V) compare with neat TiO ₂	79
4.24 Band positions of TiO ₂ and WO ₃ in solution pH 7.....	80
4.25 Comparison of SEM images of W/WO ₃ /TiO ₂ films grown with initial stage of constant anodization 60 V, 1 h and second stage of pulse waveform 60/-4 V 20 min with different volume ratios of 0.15 M NaF and TiO ₂ precursor solution, (a) 100:0, (b) 90:10, (c) 70:30 and (d) 50:50.....	82
4.26 Comparison of SEM images of W/WO ₃ /TiO ₂ films grown with initial stage of constant anodization 60 V, 1 h and second stage of pulse waveform 60/0 V 40 min with different volume ratios of 0.15 M NaF and TiO ₂ precursor solution, (a) 100:0, (b) 90:10, (c) 70:30 and (d) 50:50.....	83
4.27 Comparison of SEM images of Ti/TiO ₂ /WO ₃ films grown with initial stage of constant anodization 20 V, 30 min and second stage of pulse waveform 20/-4 V 30 min with different volume ratios of 0.15 M NH ₄ F and WO ₃ precursor solution, (a) 100:0, (b) 90:10, (c) 70:30 and (d) 50:50....	84
4.28 Comparison of SEM images of Ti/TiO ₂ /WO ₃ films grown with initial stage of constant anodization 20 V, 30 min and second stage of pulse waveform 20/0 V 30 min with different volume ratios of 0.15 M NH ₄ F and WO ₃ precursor solution, (a) 100:0, (b) 90:10, (c) 70:30 and (d) 50:50....	85
4.29 Comparison of the effect of electrolyte ratio on the photocurrent performance for W/WO ₃ /TiO ₂ and Ti/TiO ₂ /WO ₃ at the two pulsing waveform.....	86
4.30 Comparison of SEM images of Ti/TiO ₂ /WO ₃ films grown with initial stage of constant anodization 20 V, 10 min (CA 10 min) and second stage of pulse waveform (20/0V) with different pulsing anodization time (CT1) 10 min, (CT2) 30 min, and (CT3) 1 h.....	88

4.31	Comparison of SEM images of Ti/TiO ₂ /WO ₃ films grown with initial stage of constant anodization 20 V, 30 min (CA 30 min) and second stage of pulse waveform 20/0 V with different pulsing anodization time (CT4) 10 min, (CT5) 30 min, and (CT6) 1 h.....	89
4.32	Comparison of SEM images of Ti/TiO ₂ /WO ₃ films grown with initial stage of constant anodization 20 V, 1 h and second stage of pulse waveform 20/0 V with different pulsing anodization time (CT7) 10 min, (CT8) 30 min, and (CT9) 1 h.....	90
4.33	Compares photocurrent performance for the films shown in Figures 4.30, 4.31 and 4.32.....	91
4.34	Comparison of SEM images of Ti/TiO ₂ /WO ₃ films grown with initial stage of constant anodization 20 V, 2 h and second stage of pulse waveform 20/0 V with different pulsing anodization time (CT10) 30 min, (CT11) 1 h, (CT12) 2 h and (CT13) 3 h.....	92
4.35	Comparison of SEM images of Ti/TiO ₂ /WO ₃ films grown with initial stage of constant anodization 20 V, 3 h and second stage of pulse waveform 20/0 V with different pulsing anodization time (CT14) 30 min, (CT15) 1 h, (CT16) 2 h and (CT17) 3 h.....	93
4.36	Comparison of photocurrent performance for the films shown in Figures 4.34 and 4.35.....	94
4.37	Effect of modifier in Ti/TiO ₂ film fabrication on photocatalytic reduction of Cr(VI).....	97
4.38	Zero order plot of photocatalytic reduction of Cr(VI) by Ti/TiO ₂ films	97
4.39	Comparison of composite W/WO ₃ /TiO ₂ films on photocatalytic reduction of Cr(VI).....	99
4.40	Zero order plot of photocatalytic reduction of Cr(VI) by composite W/WO ₃ /TiO ₂ films.....	100
4.41	Comparison of composite Ti/TiO ₂ /WO ₃ films on photocatalytic reduction of Cr(VI).....	102
4.42	Zero order plot of photocatalytic reduction of Cr(VI) by composite Ti/TiO ₂ /WO ₃ films.....	102

4.43	Comparison of Ti/TiO ₂ nanotube film and Ti/TiO ₂ /WO ₃ nanotube film on photocatalytic reduction of Cr(VI).....	104
4.44	Zero order plot of photocatalytic reduction of Cr(VI) by Ti/TiO ₂ nanotube film and composite Ti/TiO ₂ /WO ₃ nanotube film.....	105
4.45	Photogenerated electrons (e ⁻) at the surface of oxide layer reacted with chromium species.....	107
4.46	Photocatalytic degradation pathway of methylene blue.....	109
4.47	Effect of modifier in Ti/TiO ₂ film fabrication on photocatalytic oxidation of MB.....	110
4.48	Pseudo first-order plot of photocatalytic oxidation of MB by Ti/TiO ₂ films...	111
4.49	Comparison of composite W/WO ₃ /TiO ₂ films on photocatalytic oxidation of MB.....	112
4.50	Pseudo first-order plot of photocatalytic oxidation of MB by composite W/WO ₃ /TiO ₂ films.....	113
4.51	Comparison of composite Ti/TiO ₂ /WO ₃ films on photocatalytic oxidation of MB.....	114
4.52	Pseudo first-order plot of photocatalytic oxidation of MB by composite Ti/TiO ₂ /WO ₃ films.....	115
4.53	Comparison of Ti/TiO ₂ nanotube film and Ti/TiO ₂ /WO ₃ nanotube film on photocatalytic oxidation of MB.....	117
4.54	Pseudo first-order plot of photocatalytic oxidation of MB by Ti/TiO ₂ nanotube film and composite Ti/TiO ₂ /WO ₃ film.....	117
4.55	Hydroxyl radical (OH [•]) at the surface of oxide layer reacted with methylene blue, MB.....	119
4.56	(a) Langmuir adsorption plot of methylene blue with different initial solution concentrations on nanoporous WO ₃ film obtained by anodization of W foil at 60 V for 2 h in 0.15M NaF electrolyte. The line was simply drawn through the data points. (b) Variation of initial rate (R _{initial}) with initial methylene blue (MB) concentration. The line is a least-squares fit.....	120

- 4.57 (a) Visible light ($k > 400$ nm) decomposition of methylene blue at different initial concentrations by nanoporous WO_3 films obtained by anodization of tungsten foil at 60 V for 2 h in 0.15M NaF electrolyte. The lines are simply drawn through the data points. (b) Corresponding pseudo first-order plot of these data. The line is a least-squares fit..... 121
- 4.58 Plots of $t_{1/2}$ and $t^*_{1/2}$ values versus initial methylene blue concentration for the nanoporous WO_3 films in this study. The lines are least-squares fits.....123



สถาบันวิทยบริการ
จุฬาลงกรณ์มหาวิทยาลัย

NOMENCLATURES

AISI	=	American Iron and Steel Institute
SS	=	stainless steel
Ti	=	titanium
W	=	tungsten
TiO ₂	=	titanium dioxide
WO ₃	=	tungsten trioxide
NH ₄ F	=	ammonium fluoride
NaF	=	sodium fluoride
N ₂	=	nitrogen gas
O ₂	=	oxygen gas
PEG	=	polyethylene glycol
EG	=	ethylene glycol
H ₂ O ₂	=	hydrogen peroxide
CO ₂	=	carbon dioxide gas
H ⁺	=	hydrogen ions
OH ⁻	=	hydroxide ion
h	=	hour
min	=	minute
M	=	molar
k _{app}	=	apparent rate constant
r _{initial}	=	initial reaction rate
t _{1/2}	=	half life
Φ _{app}	=	apparent quantum yield
j _{ph}	=	photocurrent density

CHAPTER I

INTRODUCTION

1.1 Research rationale

Advance oxidation processes (AOPs) have demonstrated their usefulness in the purification of the air, drinking water and cleaning of industrial wastewater (Schrank *et al.*, 2002). The industrial wastewater consists of organic and inorganic species. The presence of heavy metals in aquatic bodies has been known to cause pollution problems. Heavy metal is an important inorganic pollutant and some species are toxic and carcinogenic. The major source of heavy metals is the improper discharge of various industrial wastewater. Precipitation, activated carbon adsorption, ion exchange, and membrane separation are common methods for the disposal or recovery of metal ions in wastewater. However, these methods have their own advantages and disadvantages. Drawbacks of precipitation are the high cost of chemical used; the disposal of metal sludge and it cannot complete heavy metal removal. For adsorption, ion exchange and membrane separation only transfer the heavy metal from one source to another source, for example, moving from wastewater to solid media. These methods could not reduce the toxicity or degrade the pollutant.

Photocatalysis is one branch of AOPs. For treatment of wastewater, heterogeneous photocatalysis has special advantages in decontamination in wastewater system as shown below (Herrmann, 1999):

- cheap chemicals in use,
- low cost of photocatalyst (Titania~10 FF/kg or 1.54 EURO/kg),
- low inhibition by ions generally present in water,
- completeness for the metal ions reduction,
- great deposition capacity for noble metal recovery,
- total mineralization achieved for many organic species,
- possible combination with other decontamination method (in particular biological).

Photocatalytic technique is suitable for heavy metal wastewater which requires high removal efficiency or wastewater containing precious metal such as silver and gold. Moreover, this technique can be used with organic wastewater which containing high toxic pollutants such as pesticides which is hard to remove by biological treatment.

In the field of heterogeneous photocatalysis, many studies have been done on the photocatalytic removal of environmental pollutants using semiconductors like TiO_2 , ZnO , WO_3 , and CdS (Rajeshwar *et al.*, 2001). Among these semiconductors, TiO_2 is the most popular semiconductor used in this field because of its many advantages such as high surface activity, corrosion stability and environmental friendly nature (Oppenlander, 2003). When a semiconductor such as TiO_2 absorbs a photon of energy greater than its bandgap, an electron is transferred from the valence band to the conduction band where it can generate reduction reaction, leaving a hole in the valence band that is a strong oxidizing entity. Pure TiO_2 has the energy bandgap between the valence and conduction bands around 3.2 eV and thus UV-light is necessary to excite electrons on the TiO_2 surface.

Powder form of TiO_2 was generally used as the photocatalyst. However, it contains several problems (Lee *et al.*, 2003): (1) Separation of the catalyst from suspension after the reaction is difficult. (2) The suspended particles tend to aggregate at high concentrations. (3) The efficiency was limited by turbidity effect. TiO_2 thin films have recently been prepared by many methods to avoid these problems such as sol-gel (Bockmeyer and Löbmann, 2007; Kajitvichyanukul and Amornchat, 2005; Sonawane *et al.*, 2003), electrodeposition (Somasundaram *et al.*, 2006; Lincot, 2005; de Tacconi *et al.*, 2003 and 2004) and anodization (Mor *et al.*, 2006; Liu *et al.*, 2006; Tsuchiya *et al.*, 2005). Among these techniques, both electrodeposition and anodization methods apply electrochemical process to fabricate TiO_2 thin films. These two techniques gave a thin film with high quality, high uniformity and could directly control the film thickness by controlling processing parameters. These processes occur at low temperature and at atmospheric pressure.

Increasing of the photocatalytic and photoelectrochemical efficiency of these films can be done by increasing the wavelength response range (i.e., excitation of wide bandgap semiconductors by visible light) and by reducing recombination of

electron-hole pairs by increasing the charge separation. Composite semiconductors provide an interesting way to increase the efficiency of a photocatalytic process by increasing the charge separation and extending the energy range of photoexcitation to the visible range of solar spectrum. This then constitutes the focus of this research. This research work focuses on increasing the photocatalytic and photoelectrochemical efficiency of TiO_2 thin films prepared by electrodeposition and anodization techniques. Preparation and characterization of WO_3/TiO_2 composite films were conducted. After the preparation of the composite films, its application on hazardous waste removal was carried out. Hexavalent chromium, Cr(VI) and methylene blue, MB were used as probe reactions.

1.2 Objectives

This research consists of 3 main objectives:

1. Preparation of semiconductor WO_3 , TiO_2 , WO_3/TiO_2 composite film, using electrodeposition and anodization techniques.
 - 1.1 To evaluate the properties of the semiconductors prepared by both techniques.
 - 1.2 To select the better technique for semiconductors preparation (Anodization technique was selected that will be explained in this document).
2. Modification of the anodization
 - 2.1 To evaluate the effect of anodization parameters such as electrolyte/medium modifier, anodization voltage and time, on oxide film growth and morphology using W and Ti metal substrates.
 - 2.2 To evaluate the effect of anodization parameters such as pulsing voltage and time, electrolyte composition on morphology and photoelectrochemical response of the composite nanoporous $\text{W}/\text{WO}_3/\text{TiO}_2$, $\text{Ti}/\text{TiO}_2/\text{WO}_3$ and nanotube $\text{Ti}/\text{TiO}_2/\text{WO}_3$ films.
3. Investigation of hazardous waste removal
 - 3.1 To investigate the efficiency of hazardous waste removal using the composite films prepared by anodization process.

- 3.2 To compare the efficiency of hazardous waste removal with pure TiO₂ and pure WO₃ films.

1.3 Hypotheses

1. Nanotube morphology of self organized TiO₂ and WO₃ film has better photoelectrochemical response than that of nanoporous morphology.
2. Composite WO₃/TiO₂ material film has higher efficiency on hazardous waste removal than pure WO₃ or TiO₂ film.

1.4 Scopes of work

1. Electrodeposition and anodization techniques were used to make TiO₂, WO₃ and composite WO₃/TiO₂ films.
2. Hexavalent chromium (Cr(VI)) was used as pollutant model for photoreduction and methylene blue (MB) was used as pollutant model for photooxidation in photocatalytic study.
3. All photocatalytic processes were done with only synthetic wastewater using methylene blue oxidation and Cr(VI) reduction as probe reactions.

สถาบันวิทยบริการ
จุฬาลงกรณ์มหาวิทยาลัย

CHAPTER II

BACKGROUNDS AND LITERATURE REVIEWS

2.1 Electrodeposition

An electrodeposition applies cathodic reaction of electrolytic process which is useful for many industrial applications. The electrodeposition of metal or electroplating is mainly used for decorative and protective purposes. In this process metal is recovered from natural ores by deposition in massive form from aqueous solution. To achieve a metal deposit of the highest quality the following factors should be consider; *adherent*, *coherent*, *continuous*, and *uniform* (Potter, 1956).

Adherent coating to be formed the basis metal must be free from grease and corrosion products (e.g. rust oxides, sulphides, and other tarnishing films). The basis metal should also have a grain or crystal structure and a ductility which are compatible with that of the deposited metal, so that the most efficient factor of the deposit to its substrate may take place. The cleaning of surfaces to be plated is often done by electrolytic process or by acid etching. Roughening of the basis metal surface by etching improve adhesive property of the surface, an electropolished surface (with its regular and undistorted grain structure) also provides a good key for electroplated metal.

Coherent coatings the electrodeposited metal should be fine-grained and relatively pure. The grain of the deposit is controlled by attention to such variables as electrolyte composition, current density, and temperature. High current density and elevated temperature usually give the production of coarse-grained, loose deposits. As a general rule, finer-grained and more compact deposits are obtained from electrolytes in which the plated ion is present at very low concentration.

Continuity in a coating of electroplated metal may lack in two main ways. Either the coating may be punctured with pores so that many small areas of basis metal are exposed, or, the coating may be so uneven that comparatively large areas of basis metal remain visibly uncovered. The porosity of an electrodeposit can decreases

with increasing thickness and with more thorough surface cleaning of the basis metal. Greater attention to the purity and the clarity of the plating solution is also conducive to less porosity in an electrodeposit.

The overall *uniformity* of an electrodeposit is essential for protection of the basis metal from corrosion. Not only the surface must be covered adequately and uniformly, but also crevices and recessed areas must be coated. The shapes of the electrodes and the distances between them are factors which may yield a uniformity electrodeposit.

Electrodeposition offers rigid control of film thickness, uniformity, and deposition rate and is especially attractive owing to its low equipment cost and starting materials. Due to the use of an electric field, electrodeposition is particularly suited for the formation of uniform films on substrates of complicated shape, impregnation of porous substrates, and deposition on selected areas of the substrates (Zhitomirsky, 2000). This technique consists of an electrochemical cell and accessories for applying controlled current at a certain voltage. The cell usually contains a reference electrode, a designed cathode, and an anode or counter electrode. Schematic of electrodeposition device was shown in figure 2.1.

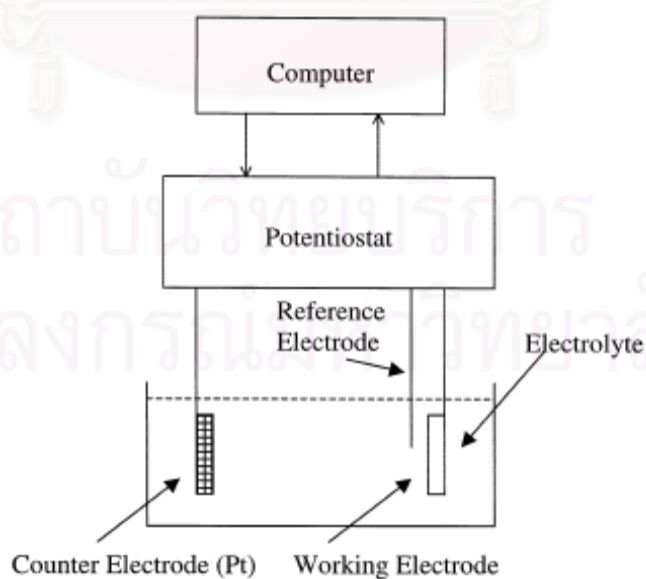


Figure 2.1 Schematic of electrodeposition process (Attenborough *et al.*, 2000)

2.1.1 Electrodeposition of semiconductors

Recently, Electrodeposition is well known for depositing metals and metallic alloys at the industrial level, with a wide range of applications from large area surface treatments (i.e. zinc electroplating) to most advanced electronic industries (copper deposition on chips, magnetic heads, etc.). Electrodeposition of semiconducting materials thus represents a new challenge, not only from the academic point of view, but also from the economic point of view, since this method presents interesting characteristics for large area, low cost and generally low temperature and soft processing of materials.

Lincot, 2005 tried to represent a road map of the electrodeposition of main inorganic semiconductors based on a personal analysis as shown in Figure 2.2. Important information is indicated (dates, solvents, tendencies).

Several points deserve the attention. Firstly, Si was the first semiconducting material prepared by electrodeposition, well before the electronic age, in 1865. At this stage, electrodeposition was considered for raw materials preparation like metals. High temperature molten salt routes were operating mostly at early periods of preparation of Si, Ge, GaAs, InP. Then it appears that electrodeposition tends to decline for these materials from mid-1980s, probably due to the lack of sufficient electronic quality for applications. On the contrary, the semiconductors based on column VI elements, mainly II–VI chalcogenides, started more later, in the 1980s and experienced a continuous development (CdTe, CdSe, and CuInSe₂ (CIS)). This can be related to the fact that thin films (in the micrometer thickness range) can be easily prepared by simple low temperature deposition processes, using water or non-aqueous solvents. Moreover the films present sufficient quality for being used in real application.

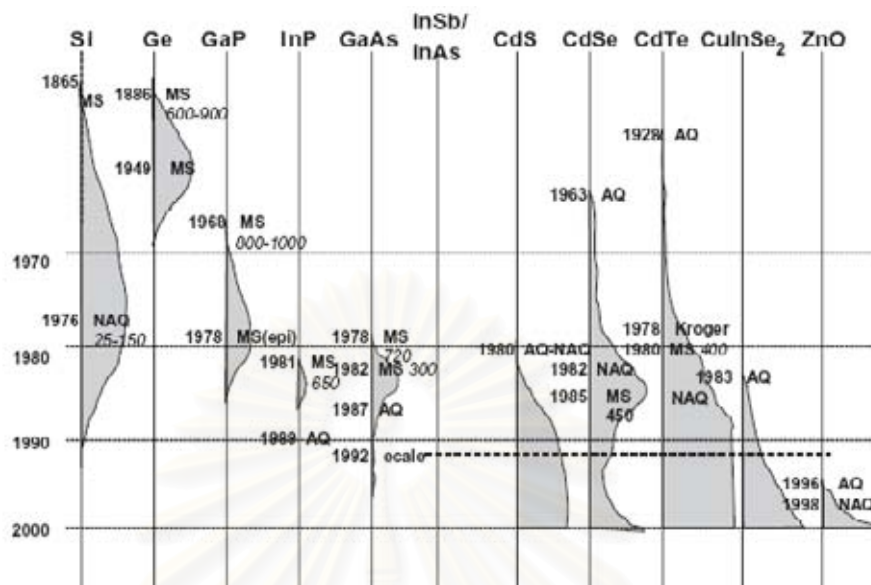


Figure 2.2 Road map of electrodeposition of main inorganic semiconductors established from the analysis of many References and Current Contents data base (2000–April 2002). Grey areas correspond to research intensity. MS: molten salts; AQ: aqueous solvent; NAQ: non-aqueous solvent; ECALE: Electrochemical Atomic Layer Electrodeposition. Numbers in bold letters are years, numbers in italic letters are temperatures in °C (Lincot, 2005).

In 1996, development of the electrodeposition of oxides, led by ZnO, was introduced. Electrodeposition appears very well suited for oxides (Therese and Kamath, 2000); most of them are semiconducting materials. These compounds are also highly ionic which is expected to be a favorable criterion. He reviewed papers which appeared in the period January 2000 – April 2002, on the basis of Current Contents data base and sorted the results by the number of papers for specific compounds (shown in Figure 2.3).

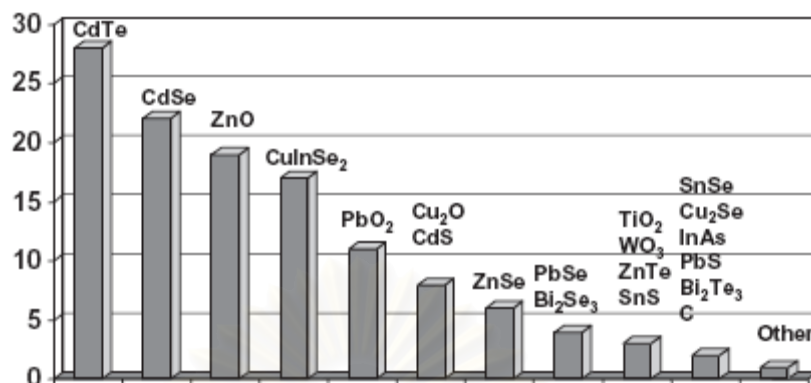


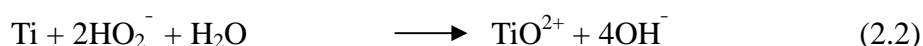
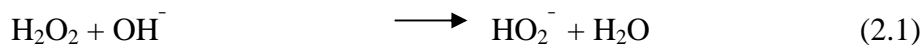
Figure 2.3 Number of published papers from Current Contents data base (2000–April 2002) as a function of the nature of the semiconductor. Other: MoS₂, In₂Se₃, SnSe, Sb₂Se₃, In₂S₃, PbTe, FeS₂, CuSnSb, Ag₂S, Cu₂S, InSb, InAsSb, CoS, Bi₂Se₃, WS₂, SnSb, CuZnTe, Ge NiS, CuI, CuSCN, InFe(CN)₆, SnO₂.

The results indicated that published papers on CdTe and CdSe are still at the top, but ZnO is now just behind and then CuInSe₂. Interestingly, Oxides are also appearing markedly (Cu₂O, PbO₂, TiO₂ and WO₃).

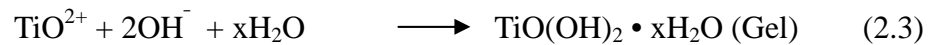
2.1.2 Electrodeposition of TiO₂

Firstly, the Ti-precursor solution was prepared based on the following steps, using a reported procedure (Natarajan and Nogami, 1996) and the possible reactions at the respective steps are given.

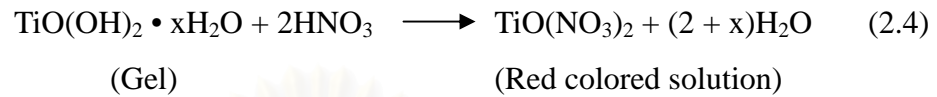
1. The Ti powder was dissolved in H₂O₂ and ammonia solution



2. After all the Ti powder is dissolved; the solution is stirred for 2 days. The excess H₂O₂ and ammonia was decomposed and consequently, a yellow colored gel was obtained.



3. By dissolving the yellow gel in 2 M HNO₃, a red colored solution was obtained.



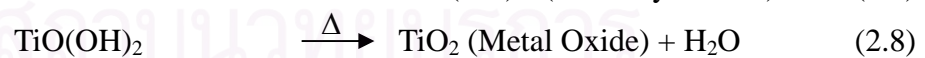
The red solution was used as the stock solution for preparation of TiO₂ films by electrodeposition. Thus, the electrolyte for electrodeposition consists of a mixture this red colored solution, ethanol and distilled water. Possible reaction that can occur when cathodic potential was applied at the working electrode immersed in the electrodeposition solution bath;



At the cathode the NO₃⁻ ion is reduced according to reaction (6) (Natarajan and Nogami, 1996)



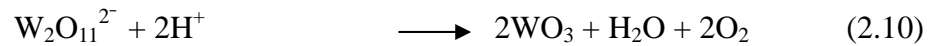
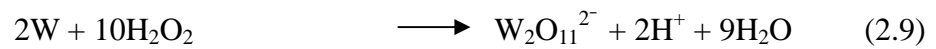
The production of OH⁻ increases the local pH, resulting in the precipitation of titanyl hydroxide and a subsequent heat treatment leads to the formation of an oxide, reactions (2.7) and (2.8)



2.1.3 Electrodeposition of WO₃

The cathodic electrodeposition of WO₃ from a peroxy tungstate precursor starts with preparation of the solution by mixing Na₂WO₄• 2H₂O, 3% hydrogen peroxide and water. The pH of the resulting solution ranged between 10.5 and 10.8. To this solution, 6 M HNO₃ was added subsequently in order to adjust the pH down to 1.4. The precursor species is assumed to involve in reactions leading to formation of a dimeric peroxy-tungstate species which undergoes reduction to the oxide as shown by

the following reactions (Chenthamarakshan *et al.*, 2004):



2.2 Anodization

Anodization process or anodizing is one of anodic technique of electrolytic process in which the overall effect is a thickening of the natural oxide film on the metal (Potter, 1956). The anodizing process firstly introduced by the Bengough - Stuart process developed in 1923 (Wernick *et al.*, 1987). The anodic layer formed by this process consists of an oxide layer with pores having a very small diameter and therefore looking almost as a barrier oxide layer. It has been known since 1932 that the aluminum oxide layer consists of a thin compact oxide layer, called the barrier layer, and a porous oxide layer, as shown in figure 4 (Wernick *et al.*, 1987). This barrier layer has a thickness of around 0.1 - 2.0% of the total film thickness and is mostly affected by the concentration of the electrolyte and by the forming voltage. As the formation of oxide continues in sulfuric acid, an arrangement of cells will be produced until finally a well-defined hexagonal cell pattern is apparent (Wernick *et al.*, 1987 and Diggle *et al.*, 1969). The pore and cell wall form the unit-cell as seen in Figure 2.4a). Figure 2.4b) shows a plane view of the porous oxide layer. The growth of the oxide layer is continuing from the bottom of the pores, more precisely in the barrier layer. This means that all the oxide has been a part of the barrier layer before becoming a porous oxide layer.

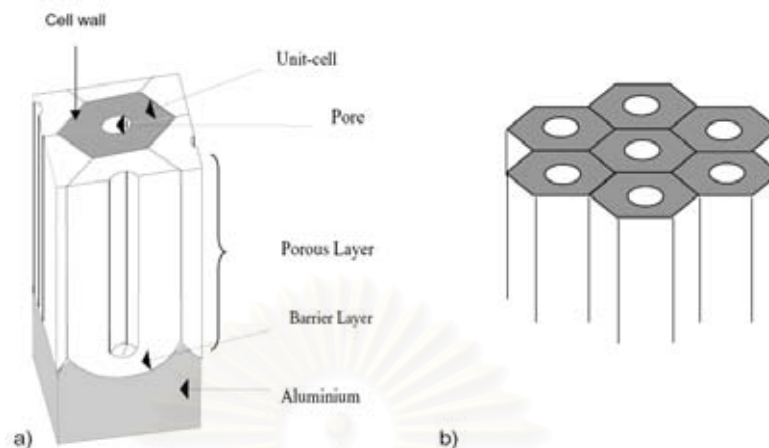


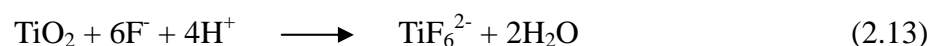
Figure 2.4 Hexagonal cell structure of aluminum oxide layer

(Wernick *et al.*, 1987)

Mor *et al.*, 2006, suggest that anodic formation of nanoporous alumina and titania appear to be the same and are fundamental to the formation of straight titania nanotubes. As the anodization process begins the initial oxide layer (Thompson, 1997), formed due to interaction of the surface Ti^{4+} ions with oxygen ion (O^{2-}) in the electrolyte. The overall reaction of anodic oxidation of titanium can be represented as



In the initial state of the anodization process, field-assisted dissolution dominates chemical dissolution due to the relatively large electric field across the thin oxide layer. Small pits formed due to the localized dissolution of the oxide (in a F^- containing electrolyte), represented by following reaction, act as pore forming centers:



Then, these pits convert into bigger pores and the pore density increases. After that, the pores spread uniformly over the surface. The pore growth occurs due to the inward movement of the oxide layer at the pore bottom (barrier layer) due to processes (2.11)-(2.13).

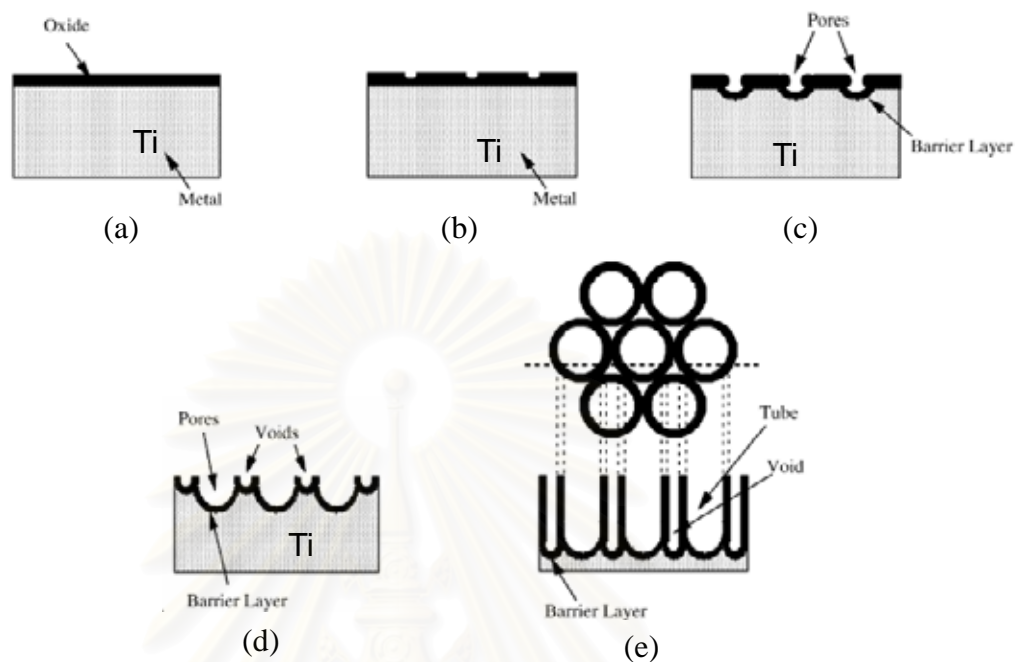


Figure 2.5 Schematic diagram of the evolution of a nanotube array at constant anodization voltage: (a) oxide layer formation, (b) pit formation on the oxide layer, (c) growth of the pit into scallop shaped pores, (d) metallic part between the pores undergoes oxidation and field assisted dissolution, and (e) fully developed nanotube array with a corresponding top view. (Mor *et al.*, 2006)

Figure 2.5 shows the evolution of a nanotube array at constant anodization voltage. A thin layer of oxide forms on the titanium surface (Fig. 5a). Small pits originate in this oxide layer due to the localized dissolution of the oxide (Fig. 5b) making the barrier layer at the bottom of the pits relatively thin which, in turn, increases the electric field intensity across the remaining barrier layer resulting in further pore growth (Fig. 5c). The pore entrance is not affected by electric field-assisted dissolution and hence remains relatively narrow, while the electric field distribution in the curved bottom surface of the pore causes pore widening, as well as deepening of the pore. As the Ti-O bond energy is high (323 kJ/mol), in the case of titania it is reasonable to assume that only pores having thin walls can be formed due to the relatively low ion mobility and relatively high chemical solubility of the oxide

in the electrolyte, hence un-anodized metallic portions can initially exist between the pores. As the pores become deeper the electric field in these protruded metallic regions increases enhancing the field-assisted oxide growth and oxide dissolution, hence simultaneously with the pores well-defined inter-pore voids start forming (Fig. 5d). Thereafter, both voids and tubes grow in equilibrium. The nanotube length increases until the electrochemical etch rate equals the chemical dissolution rate of the top surface of the nanotubes. After this point is reached the nanotube length will be independent of the anodization duration, as determined for a given electrolyte concentration and anodization potential.

2.3 Review of WO_3/TiO_2

TiO_2 is the excellent photocatalyst for degradation of several environmental contaminants both in polluted air and waste water. In heterogeneous photocatalysis system, the degradation reactions take place at the surface of TiO_2 when it was irradiate with UV light. It has been shown that the photocatalytic activity of TiO_2 is influenced by the crystal structure, surface area, size distribution, porosity, Band gap, and surface hydroxyl group (Damme, 1989; Harada and Ueda, 1984; Bickly *et al.*, 1991) so many techniques have been studied in order to improve the photocatalytic activity of TiO_2 . Three benefits of modifications to photocatalytic semiconductor systems have been studied: (1) inhibiting recombination by increasing the charge separation and therefore the efficiency of the photocatalytic process; (2) increasing the wavelength response range; and (3) changing the selective or yield of a particular product (Linsebigler *et al.*, 1995).

Composite semiconductor is one technique to increase the efficiency of TiO_2 by increasing the charge separation and extending the energy range of photoexcitation for the photocatalytic process. Many studies have been done on WO_3/TiO_2 composite semiconductor as following.

Do *et al.*, 1994 studied effect of WO_3 on the photocatalytic activity of TiO_2 . The composite WO_3/TiO_2 powder was made and used for degradation of 1-4 dichlorobenzene (DCB). They found that the addition of WO_3 to TiO_2 greatly increased its photocatalytic behavior.

Shiyanovskaya and Hepel, 1999 studied the morphology, structure, fundamental absorption edge, flatband potential, vibration spectra, and photocurrent response of the amorphous WO_3 films and nanocrystalline TiO_2 films and compared with bicomponent WO_3/TiO_2 films. Thin films of WO_3 were deposited by thermal vacuum evaporation of WO_3 polycrystalline powder and thin TiO_2 films were deposited onto the conductive glass substrates with and without the WO_3 layer from the colloidal dispersion of TiO_2 particles by dropping of the colloidal dispersion and spread onto the substrate. They found that in bicomponent WO_3/TiO_2 films, the porous films of the tungsten trioxide with a high open surface area can serve as substrates for nanocrystalline TiO_2 films to increase the efficiency of photocurrent generation at band gap excitation.

Kwon *et al.*, 2000 studied the photocatalytic behavior of WO_3/TiO_2 in film form (by dropping the suspension of WO_3/TiO_2 powder on substrate and dried at 50 °C) using methylene blue as probe. The photocatalytic activity of WO_3/TiO_2 is only 1.4-1.5 times of pure TiO_2 in decomposing the coated methylene blue.

Song *et al.*, 2001 prepared transparent photocatalytic films WO_3/TiO_2 by incipient wetness method. It has also been found that the photocatalytic activity of WO_3/TiO_2 film is 2.8-3 times that of pure TiO_2 film in decomposing gas-phase 2-propanol.

de Tacconi *et al.*, 2004 used a new pulsed deposition technique to prepared WO_3/TiO_2 composite films over a wide compositional range in precursor bath mix for each component and their electrochromic behavior was studied. It is shown that the progressive coloration of an initially transparent conducting oxide glass substrate, as a result of oxide film growth, offers a versatile spectroelectrochemical probe of the film electrosynthesis process itself. Both the blue shift undergone by the absorption threshold of the oxide film (as a result of electron accumulation during the electrochromic process), and the coloration dynamics are favorably influenced by the presence of small amounts of TiO_2 in the WO_3 film.

Georgieva *et al.*, 2005 synthesized bilayer WO_3/TiO_2 films from acidic aqueous solutions of peroxytungstate and titanium oxosulfate, by cathodic electrodeposition/electrosynthesis steps using stainless steel 304 (SS 304) substrates. The resulting deposits were annealed at 350 or 400 °C to obtain crystalline WO_3

(monoclinic) and TiO₂ (anatase) coatings respectively. The deposits had a particulate, “cracked mud” structure, characterized by 5–20 μm large patches. SEM/EDS analysis of the bilayer samples indicated and Auger Electron Spectroscopy confirmed that TiO₂ grows preferentially in the center of the WO₃ islands of the deposit underlayer. Photoelectrochemical characterization of the TiO₂/SS 304, WO₃/SS 304 and TiO₂/WO₃/SS 304 photoelectrodes was carried out by photovoltammetry and photoamperometry under UV or visible light illumination, in sulfate and oxalate solutions. It was found that bilayer TiO₂/WO₃-coated electrodes were more active not only than TiO₂-coated electrodes upon UV illumination but also, than WO₃-coated electrodes under visible light excitation.

Somasundaram *et al.*, 2006 made composite WO₃/TiO₂ semiconductor films by cathodic electrodeposition using sequential deposition of WO₃ and TiO₂ from aqueous baths containing peroxytungstate and titanyl precursor species, respectively. The composite films were prepared by switching the baths for five cycles of deposition at -0.45 V (for WO₃) and -0.95 V (for TiO₂). These new films were compared and contrasted with composite WO₃/TiO₂ films prepared by pulsed electrodeposition from a mixed bath. Neat WO₃ films were also included for this comparison; the best photoelectrochemical response was shown by the composite films obtained from the new procedure.

2.4 Photocatalytic process

Photocatalytic process is an advance oxidation technology for water and air purification. Photocatalytic process occurs when a suitable photocatalyst is irradiated by photons. The first step in photocatalysis is the absorption of photons of appropriate energy to excite an electron from the valence band (VB) to the conduction band (CB) of the semiconductor, thus creating an electron-hole pair. Each species must then migrate to the surface before recombination occurs. If this happens the electron can be transferred to a surface adsorbed molecule, eventually reducing it. In the same manner the photogenerated hole is capable of catalyzing an oxidation reaction at the surface. The positions of the band edges are critical for each step of this process. First of all, only light with energy greater than the bandgap (E_g) will be absorbed. Secondly, the

potential of the electron acceptor (A/A^-) should be more positive than the conduction band (CB) in order to allow the transfer electrons, while the potential of the electron donor (D/D^+) should be more negative than the valence band (VB) of the semiconductor.

The overall process is illustrated in the figure 2.6 below.

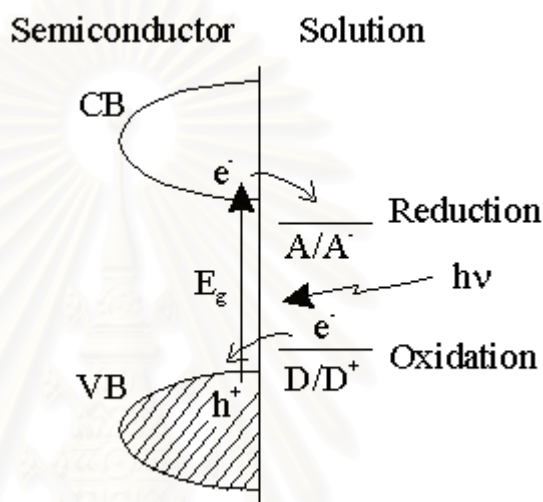


Figure 2.6 Schematic of photocatalytic process (Woodward)

2.4.1 Photocatalysis using WO_3/TiO_2

TiO_2 has been proven to be an excellent photocatalyst. A lot of investigations have focused on the improvement of TiO_2 photocatalysis. The efficiency of a photocatalytic reaction is improved in a heterogeneous semiconductor system because fast transfer of the photogenerated charges between different types of semiconductor particles suppresses the direct recombination of the photogenerated carriers. One of the heterogeneous semiconductor systems, WO_3/TiO_2 , has been investigated for its photocatalytic reactions (Keller *et al.*, 2003; Song *et al.*, 2001; Kwon *et al.*, 2000; Do *et al.*, 1994). Song *et al.*, 2001 reported the photocatalytic activity of WO_3/TiO_2 films is around 3 times of pure TiO_2 films for the gas-phase oxidation of 2-propanol and Kwon *et al.*, 2000 indicated the photocatalytic activity of WO_3/TiO_2 is around 1.4-1.5 times of pure TiO_2 in decomposing the coated methylene blue.

The bandgap of TiO_2 and WO_3 nanoclusters are all in the ultraviolet, these oxides are both semiconductors with optical bandgap in the 2.8-3.3 eV range and TiO_2 has slightly larger band gap than WO_3 . Both the top of the valence band and the bottom of the conduction band of WO_3 are lower than those of TiO_2 (as shown in Figure 2.7). WO_3 and TiO_2 can both be excited by UV-light but only WO_3 can be excited by visible light. The photogenerated holes can transfer from the WO_3 valence band to the TiO_2 valence band and the photogenerated electrons can transfer from the TiO_2 conduction band to the WO_3 conduction band. As a result, the photogenerated carriers can be effectively separated. A higher photoresponse was observed for bilayered WO_3/TiO_2 films relative to single component films (Shiyanovskaya and Hapel, 1998).

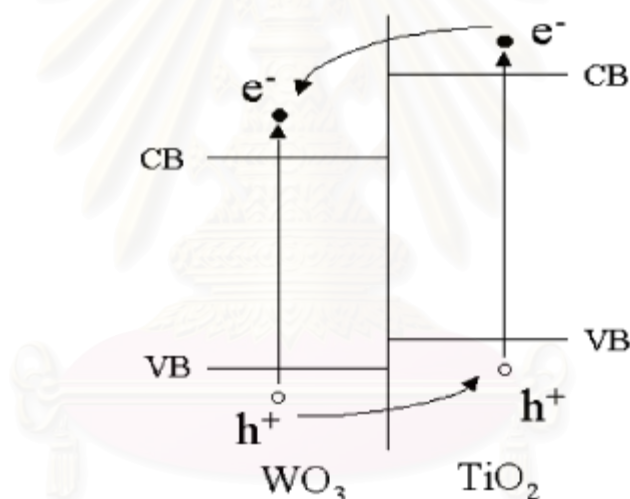


Figure 2.7 Energy diagram for the $\text{WO}_3\text{-TiO}_2$ composite system (He *et al.*, 2003)

2.4.2 Review of photocatalysis of chromium

Chromium is a naturally-occurring element in rocks, animals, plants, soil, and volcanic dust and gases. In form of a metal, it is a steel-gray solid with a high melting point and an atomic weight of 51.996 g/mol (ATSDR, 1998). The oxidation states of chromium are ranging from chromium (-II) to chromium (+VI). The trivalent chromium (Cr III) and hexavalent chromium (Cr VI) are the predominant species of chromium in the environment. The trivalent chromium (Cr III) occurs naturally and is an essential nutrient. The trivalent chromium salts such as chromium polynicotinate,

chromium chloride and chromium picolinate (CrP) are used as micronutrients and nutritional supplements and have been demonstrated to exhibit a significant number of health benefits in animals and humans (Anderson, 2000).

The hexavalent chromium, which, along with the less common metallic chromium (III) is most commonly produced by industrial processes. The most important industrial sources of chromium in the atmosphere are those related to ferrochrome production. Ore refining, chemical and refractory processing, cement-producing plants, automobile brake lining and catalytic converters for automobiles, leather tanneries, and chrome pigments also contribute to the atmospheric contribution of chromium. (USEPA, 1998). The metal chromium is mainly used for making steel and other alloys (ATSDR, 1998). Chromium compounds, in either the chromium (III) or chromium (VI) forms, are used for chrome plating, the manufacture of dyes and pigments, leather and wood preservation, and treatment of cooling tower water. Smaller amounts are used in drilling muds, textiles, and toner for copying machines (ATSDR, 1998)

Chromium forms a large number of compounds, in both the chromium (III) and the chromium (VI) forms. Chromium compounds are stable in the trivalent state, with the hexavalent form being the second most stable state (ATSDR, 1998). The chromium (III) compounds are sparingly soluble in water and may be found in water bodies as soluble chromium (III) complexes, while the chromium (VI) compounds are readily soluble in water.

The photocatalytic reduction of Cr (VI) in aqueous suspensions of semiconductors such as TiO_2 , ZnO , CdS , ZnS , and WO_3 under UV illumination has been widely studied (Domenech, J., and Munoz, 1987; Prairie, *et al.*, 1993; Navo, *et al.*, 1998) and constitutes the basis of promising new decontamination technologies. It has also been shown that the photocatalytical reduction of Cr (VI) in aqueous suspensions of ZnO can take place under sunlight (3). The optimum conditions to treat chromium using TiO_2 was well established from the previous works (Kajitvichyanukul and Vatcharenwong, 2005; Ku and Jung, 2001). It was found that Cr (VI) was well removed from wastewater at the reaction pH of 3. The efficiency in Cr (VI) removal can be enhanced with the addition of hole scavenger (for example; formate ions) which eliminate the recombination effect. The photocatalytic reduction

rate of Cr (VI) was found to be linearly increased with light intensity until a certain optimum light intensity was reached (Ku and Jung, 2001).

2.4.3 Review of photocatalysis of methylene blue

Methylene blue (phenothiazin-5-ium, 3,7-bis(dimethylamino)-, chloride) is a heterocyclic aromatic chemical compound with molecular formula: $C_{16}H_{18}ClN_3S$ and an atomic weight of 139.86 g/mol (U.S. EPA). At room temperature it appears as a solid, odorless, dark green crystals or crystalline powder, having a bronze-like luster. Solutions in water or alcohol have a deep blue color. It has been used in a range of different fields, such as biology or chemistry. Methylene blue is widely used a redox indicator in analytical chemistry. Solutions of this substance are blue when in an oxidizing environment, but will turn colorless if exposed to a reducing agent. Also it is used as a bacteriologic stain and as an indicator. It inhibits guanylate cyclase, and has been used to treat cyanide poisoning and to lower levels of methemoglobin.

Methylene blue is a common dye in the textile industry. Textile dyes and other industrial dyestuffs constituted one of the largest groups of organic compounds representing an increasing environmental danger (Zollinger, 1991). Dyes were widely used and therefore wastewater was discharged into natural and domestic water systems including rivers, lakes and public sewage. As a result, they were highly contaminated (Houas, *et al.*, 2001 and Bianco-Prevot, *et al.*, 2001). Colored water was no longer attractive and caused more and more complaints. Moreover, concerns were expressed about the potential toxicity of dyes and of their precursors. Environmental pollution caused by organic dyes also set a severe ecological problem, which increased because most of them were difficult to degrade using standard methods (Galindo, *et al.*, 2001). Generally, traditional physical techniques could be efficiently employed to remove such recalcitrant pollutants. However, they were non-destructive, because they just transferred organic matter from water to sludge. This led to the requirement of regeneration of the adsorbent materials and post-treatment of solid wastes.

Alternatives to conventional treatment methods are advanced oxidation processes (AOPs), which are based on the generation of very reactive species such as

hydroxyl radicals that oxidize a broad range of organic pollutants quickly and nonselectively (Park, *et al.*, 2003). This photocatalytic method was based on the reactive properties of photogenerated electron–hole pairs. They were generated in the semiconductor (TiO₂) particles under irradiation at suitable wavelengths ($\lambda \leq 400$ nm). These electrons and holes could also recombine. Since the hole was a powerful oxidizing agent, it could decompose water and/or contaminants adsorbed on the TiO₂ surface. TiO₂ photocatalysis is an effective method for decoloring and oxidizing methylene blue in wastewater (Zhang, *et al.*, 2001). Hasnat *et al.*, 2005 investigated the photocatalytic degradation of methylene blue and procion red in TiO₂ dispersion under visible light. The rate of degradation followed first-order kinetics based on the Langmuir–Hinshelwood model.



สถาบันวิทยบริการ
จุฬาลงกรณ์มหาวิทยาลัย

CHAPTER III

METHODOLOGY

3.1 Cathodic electrodeposition

3.1.1 Chemicals and Materials

All chemicals used in this work were analytical reagent grade and were used without further purification. Ti powder 99.9 % metal basis (Alfa Aesar) and $\text{Na}_2\text{WO}_4 \cdot 2\text{H}_2\text{O}$ 99.0-101.0 % (Alfa Aesar) were used to prepare titanyl ion precursor bath and peroxytungstate precursor solution for electrodeposition, respectively. Stainless steel foil AISI 304 (0.2 mm thick, and 0.5 cm \times 2.5 cm from Alfa Aesar) which has a deposited area 0.75 cm² was used as substrate. Before using, stainless steel was degreased with acetone and etched in 1:1 HCl/H₂O mixture for 60 s, washed with distilled water and dried at room temperature.

3.1.2 Thin films preparation

A Bioanalytical Systems (BAS) Model 100A Electrochemical Analyzer was used for the electrodeposition experiments. A standard single compartment, three-electrode electrochemical cell was used for film preparation. Pt wire was used as counter electrode and an Ag|AgCl|satd. KCl as reference electrode. Stainless steel foil was used as working electrode.

Tungsten trioxide films were cathodically electrosynthesized from a peroxytungstate deposition bath that has been described in previous chapter. Briefly, the bath consists of 25 mM Na_2WO_4 and 3% H_2O_2 with the pH adjusted to 1.4 with HNO_3 . The precursor bath was used immediately after preparation. Films were grown with applied potential in the range of -250 to -550 mV (vs. Ag|AgCl|satd. KCl reference; all potentials are quoted with respect to this reference) for a various time as shown in Table 3.1. They were then subjected to a post-deposition thermal anneal at

450 °C for 30 min.

Titanium dioxide films were cathodically electrosynthesized from a titanyl ion precursor bath also containing nitrate ion. The bath preparation has been described in previous chapter but briefly consists of dissolving Ti powder in a solution containing H_2O_2 and NH_3 . The gel initially formed is redissolved in HNO_3 . The pH of the solution is then adjusted to 1.7 with dilute NH_3 . Film formation occurs in this process by the initial electrogeneration of base and an increase in the local pH at the substrate/solution interface. The precursor bath was used immediately after preparation. Films were grown with applied potential in the range of -850 to -1050 mV for a various time as shown in Table 3.1. The deposited titanium oxy-hydroxide films were subjected to a post-deposition thermal anneal at 450 °C for 30 min.

Composite films were prepared by sequential deposition from two separate baths using electrodeposition time and voltage as shown in Table 3.1 and multilayer films of WO_3 or TiO_2 were also studied.

Table 3.1 Effect of parameters on film growth

No.	Parameters	Conditions
1.	Time of electrodeposition	SS/ WO_3 ; 5, 10, 15, 20, 25 and 30 min SS/ TiO_2 ; 15, 30, 45, 60 and 90 min
2.	Applied potential during electrodeposition process	SS/ WO_3 ; -250, -300, -350, -400, -450 and -550 mV SS/ TiO_2 ; -850, -950 and -1050 mV
3.	Multilayer films	SS/ WO_3 ; 1 layer of SS/10 min 2 layers of SS/10 min 3 layers of SS/10 min SS/ TiO_2 ; 1 layer of SS/15 min 2 layers of SS/15 min 3 layers of SS/15 min 4 layers of SS/15 min
4.	Composite films	SS/ WO_3 / TiO_2 ; 1 layer of SS/10/30 min 2 layers of SS/5/15 min 5 layers of SS/2/6 min SS/ TiO_2 / WO_3 ; 1 layer of SS/30/10 min 2 layers of SS/15/5 min 5 layers of SS/6/2 min

3.2 Anodization

3.2.1 Ti/TiO₂ films prepared by anodization

3.2.1.1 Chemicals and Materials

All chemicals were from commercial sources and were of the highest purity available. Deionized water (18 MΩ cm) was used in all cases for making solutions. Ammonium fluoride (Alfa Aesar, 98.0%), glycerol (Mallinckrodt Chemicals), poly(ethylene glycol) (M_n ca. 200, 400, 600, and 1000, Aldrich), and ethylene glycol (Spectrum Chemical) were used as received. Titanium foil (Alfa Aesar, 0.25 mm thick, 99.95%) was used as the substrate for oxide film growth. Before using, the foil was cut (1.4 cm × 1.4 cm), mechanically polished to mirror finish using silicon carbide sandpaper of successively finer roughness (220, 240, 400, 800, 1000 and 1500 grit), and cleaned for three 5 min steps in ultrasonicated acetone, 2-propanol, and finally ultrapure water. Subsequently, the substrate was dried in ultrapure N₂ stream and used immediately.

3.2.1.2 Electrosynthesis

Nanoporous films of TiO₂ were grown in a two-electrode electrochemical cell using a large Pt coil as counter electrode and Ti foil as working electrode. In all the cases, NH₄F was used as the major electrolyte and a selected medium modifier such as glycerol, poly(ethylene glycol) (PEG) and ethylene glycol (EG) was used to form the nanoporous oxide layer. Anodization employed a multioutput power supply (Switching System International, CA). The electrochemical cell was connected in series to a variable resistor (100 kΩ) that was decreased to zero to simulate a voltage ramp of ~0.2 V/s, and then the voltage was held at the preselected level for anodization times varying from 1 to 10 h. The Ti foil was pressed between a set of O rings in the electrochemical cell, leaving 0.63 cm² exposed to the electrolyte, and the electric contact was located on the backside of the sample. After the oxide films were grown, the anodized Ti foils were removed from the O-ring assembly and carefully washed by immersion in deionized water and then dried in a N₂ stream. A summary of anodization conditions for TiO₂ films are shown in Tables 3.2.

Table 3.2 Anodization conditions on Ti substrates

No.	Metal substrate	Electrolyte, medium modifier	Anodization voltage	Anodization Time
1	Ti	0.15 M NH ₄ F	20 V	1 h
2		0.15 M NH ₄ F	20 V	3 h
3		0.15 M NH ₄ F	20 V	5 h
4		0.15 M NH ₄ F	20 V	10 h
5	Ti	0.15 M NH ₄ F/glycerol	20 V	3 h
6		0.15 M NH ₄ F/glycerol	20 V	5 h
7		0.15 M NH ₄ F/glycerol	20 V	10 h
8		0.36 M NH ₄ F/ glycerol	20 V	5 h
9	Ti	0.15 M NH ₄ F/ PEG 200:H ₂ O (90:10)	20 V	5 h
10		0.15 M NH ₄ F/ PEG 400:H ₂ O (90:10)	20 V	5 h
11		0.15 M NH ₄ F/ PEG 600:H ₂ O (90:10)	20 V	5 h
12		0.15 M NH ₄ F/ PEG 1000:H ₂ O (90:10)	20 V	5 h
13	Ti	0.15 M NH ₄ F/EG:H ₂ O (90:10)	20 V	5 h
14		0.36 M NH ₄ F/EG:H ₂ O (90:10)	20 V	5 h
15		0.36 M NH ₄ F/EG:H ₂ O (90:10)	40 V	5 h
16		0.36 M NH ₄ F/EG:H ₂ O (90:10)	60 V	5 h

3.2.2 W/WO₃ films prepared by anodization

3.2.2.1 Chemicals and Materials

All chemicals were from commercial sources and were of the highest purity available. Deionized water (18 MΩ cm) was used in all cases for making solutions. Sodium fluoride (Alfa Aesar, 98.0%), oxalic acid (Sigma, 98.5%), poly(ethylene glycol) (M_n ca. 200, 400, 600, and 1000, Aldrich), and ethylene glycol (Spectrum Chemical) were used as received. Tungsten foil (Alfa Aesar, 0.25 mm thick, 99.95%) was used as the substrate for oxide film growth. Before use, the foil was cut (1.4 cm × 1.4 cm), mechanically polished to mirror finish using silicon carbide sandpaper of successively finer roughness (220, 240, 400, 800, 1000 and 1500 grit), and cleaned in three 5 min steps in ultrasonicated acetone, 2-propanol, and finally ultrapure water. Subsequently, the substrate was dried in ultrapure N₂ stream and used immediately.

3.2.2.2. Electrosynthesis

Nanoporous films of WO₃ were grown in a two-electrode electrochemical cell using a large Pt coil as counter electrode and tungsten foil as the working electrode. NaF was used as the major electrolyte and selected medium modifiers [e.g.,

poly(ethylene glycol) and ethylene glycol] were used to form the nanoporous oxide layer. In addition, oxalic acid was also used as an electrolyte for film growth. Anodization employed a multi-output power supply (Switching System International, CA). The electrochemical cell was connected in series to a variable resistor (100 k Ω) that was decreased to zero to simulate a voltage ramp of ~ 0.2 V/s, and then the voltage was held at the preselected level for anodization times varying from 1 to 6 h. The W foil was pressed between a set of O rings in the electrochemical cell, leaving 0.63 cm² exposed to the electrolyte, and the electric contact was located on the backside of the sample. After the oxide films were grown, the anodized W foils were removed from the O-ring assembly and carefully washed by immersion in deionized water and then dried in a N₂ stream. A summary of anodization conditions for WO₃ films are shown in Tables 3.3.

Table 3.3 Anodization conditions on W substrates

No.	Metal substrate	Electrolyte, medium modifier	Anodization voltage	Anodization Time
1	W	0.15 M NaF	20 V	3 h
2		0.15 M NaF	40 V	3 h
3		0.15 M NaF	60 V	3 h
4		0.15 M NaF	80 V	3 h
5	W	0.15 M NaF	60 V	1 h
6		0.15 M NaF	60 V	2 h
7		0.15 M NaF	60 V	3 h
8		0.15 M NaF	60 V	4 h
9		0.15 M NaF	60 V	6 h
10	W	0.30 M Oxalic acid	20 V	2 h
11		0.30 M Oxalic acid	40 V	2 h
12		0.30 M Oxalic acid	60 V	2 h
13		0.30 M Oxalic acid	80 V	2 h
14	W	0.30 M Oxalic acid	60 V	1 h
15		0.30 M Oxalic acid	60 V	2 h
16		0.30 M Oxalic acid	60 V	3 h
17		0.30 M Oxalic acid	60 V	4 h
18		0.30 M Oxalic acid	60 V	6 h
19		0.30 M Oxalic acid	60 V	10 h
20	W	0.15 M NaF / PEG 200:H ₂ O (40:60)	20 V	3 h
21		0.15 M NaF / PEG 400:H ₂ O (40:60)	20 V	3 h
22		0.15 M NaF / PEG 600:H ₂ O (40:60)	20 V	3 h
23		0.15 M NaF / PEG 1000:H ₂ O (40:60)	20 V	3 h
24	W	0.15 M NaF / EG:H ₂ O (40:60)	20 V	3 h

3.2.3 Composite films prepared by anodization

3.2.3.1 Electrosynthesis

In this experiment composite films were grown in a two-electrode electrochemical cell using a large Pt coil as counter electrode and tungsten or titanium foil as the working electrode. The experiments were separated into 4 parts as following, (1) W/WO₃/TiO₂ nanoporous, (2) Ti/TiO₂/WO₃ nanoporous, (3) effect of electrolyte composition on the resulting W/WO₃/TiO₂ and Ti/TiO₂/WO₃ nanoporous, and (4) Ti/TiO₂/WO₃ nanotubes.

Part I W/WO₃/TiO₂ nanoporous

W/WO₃/TiO₂ nanocomposite films were prepared with a two-step procedure: a) nanoporous WO₃ films were grown in 0.15 M NaF at 60 V for 1 h using W foil as the working electrode; b) under constant potential, the electrolyte solution was modified with titanyl ion electrodeposition solution in a 90:10 ratio (volume of electrolyte (NaF) to volume of electrodeposition solution added during pulse anodization) and pulse anodization waveform was applied. Two different limits were used; 60/-4 V and 60/0 V during pre-selected time (20 min, 40 min, 1 h, 2 h, 3 h). The waveform was adjusted to 3 min at the higher voltage and 15 s at the lower one. The total potential perturbation is shown in Figure 3.1. A summary of anodization conditions for W/WO₃/TiO₂ nanocomposite films are shown in Tables 3.4.

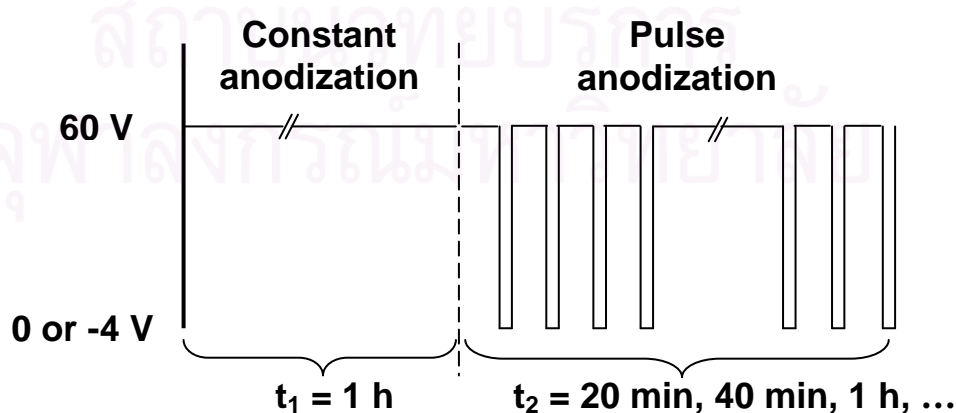


Figure 3.1 Total potential waveform for W/WO₃/TiO₂ nanocomposite film preparation.

Table 3.4 Anodization conditions for W/WO₃/TiO₂ nanocomposite film preparation.

No.	Metal substrate	Constant Anodization	Pulse Anodization	Ratio
A1	W	0.15 M NaF, 60 V, 1 h	Add TiO(NO ₃) ₂ , 60 V/ -4 V, 20 min	90:10
A2		0.15 M NaF, 60 V, 1 h	Add TiO(NO ₃) ₂ , 60 V/ -4 V, 40 min	90:10
A3		0.15 M NaF, 60 V, 1 h	Add TiO(NO ₃) ₂ , 60 V/ -4 V, 1 h	90:10
A4		0.15 M NaF, 60 V, 1 h	Add TiO(NO ₃) ₂ , 60 V/ -4 V, 2 h	90:10
A5		0.15 M NaF, 60 V, 1 h	Add TiO(NO ₃) ₂ , 60 V/ -4 V, 3 h	90:10
B1	W	0.15 M NaF, 60 V, 1 h	Add TiO(NO ₃) ₂ , 60 V/ 0 V, 20 min	90:10
B2		0.15 M NaF, 60 V, 1 h	Add TiO(NO ₃) ₂ , 60 V/ 0 V, 40 min	90:10
B3		0.15 M NaF, 60 V, 1 h	Add TiO(NO ₃) ₂ , 60 V/ 0 V, 1 h	90:10
B4		0.15 M NaF, 60 V, 1 h	Add TiO(NO ₃) ₂ , 60 V/ 0 V, 2 h	90:10
B5		0.15 M NaF, 60 V, 1 h	Add TiO(NO ₃) ₂ , 60 V/ 0 V, 3 h	90:10

Part II Ti/TiO₂/WO₃ nanoporous

Ti/TiO₂/WO₃ nanocomposite films were prepared with a two- step procedure: a) nanoporous TiO₂ films were grown in 0.15 M NH₄F at 20 V for 30 min using Ti foil as the working electrode; b) under constant potential the electrolyte solution was modified with peroxytungstate electrodeposition solution in a 90:10 ratio (volume of electrolyte (NH₄F) to volume of electrodeposition solution added during pulse anodization) and pulse anodization waveform was applied. Two different limits were used; 20/-4 V and 20/0 V during pre-selected time (20 min, 40 min, 1 h, 2 h, 3 h). The waveform was adjusted to 3 min at the higher voltage and 15 s at the lower one. The total potential perturbation is shown in Figure 3.2. A summary of anodization conditions for Ti/TiO₂/WO₃ nanocomposite films are shown in Tables 3.5.

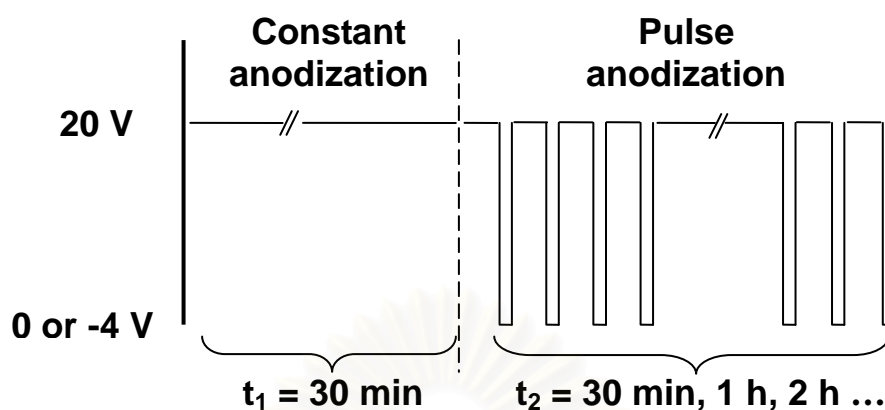


Figure 3.2 Total potential waveform for Ti/TiO₂/WO₃ nanocomposite film preparation

Table 3.5 Anodization conditions for Ti/TiO₂/WO₃ nanocomposite film preparation.

No.	Metal substrate	Constant Anodization	Pulse Anodization	Ratio
C1	Ti	0.15 M NH ₄ F, 20 V, 30 min	Add W ₂ O ₁₁ ²⁻ , 20 V/-4 V, 30 min	90:10
C2		0.15 M NH ₄ F, 20 V, 30 min	Add W ₂ O ₁₁ ²⁻ , 20 V/-4 V, 1 h	90:10
C3		0.15 M NH ₄ F, 20 V, 30 min	Add W ₂ O ₁₁ ²⁻ , 20 V/-4 V, 2 h	90:10
C4		0.15 M NH ₄ F, 20 V, 30 min	Add W ₂ O ₁₁ ²⁻ , 20 V/-4 V, 3 h	90:10
D1	Ti	0.15 M NH ₄ F, 20 V, 30 min	Add W ₂ O ₁₁ ²⁻ , 20 V/0 V, 30 min	90:10
D2		0.15 M NH ₄ F, 20 V, 30 min	Add W ₂ O ₁₁ ²⁻ , 20 V/0 V, 1 h	90:10
D3		0.15 M NH ₄ F, 20 V, 30 min	Add W ₂ O ₁₁ ²⁻ , 20 V/0 V, 2 h	90:10
D4		0.15 M NH ₄ F, 20 V, 30 min	Add W ₂ O ₁₁ ²⁻ , 20 V/0 V, 3 h	90:10

Part III Effect of electrolyte composition on the resulting W/WO₃/TiO₂ and Ti/TiO₂/WO₃ nanoporous films

In this experiment, all films were prepared in the same procedure as in part I and II. However, different volume ratios of added semiconductor precursors for cathodic electrodeposition of one of them on the other which is simultaneously grown by anodic polarization was studied. The total potential waveforms for W/WO₃/TiO₂ and Ti/TiO₂/WO₃ films were the same as in Figure 3.1 and Figure 3.2, respectively. A summary of anodization conditions for W/WO₃/TiO₂ and Ti/TiO₂/WO₃

nanocomposite films are shown in Table 3.6.

Table 3.6 Anodization conditions for the study of effect of electrolyte composition on the resulting W/WO₃/TiO₂ and Ti/TiO₂/WO₃ nanoporous films

No.	Metal substrate	Constant Anodization	Pulse Anodization	Ratio
1	W	0.15 M NaF, 60 V, 1 h	Add TiO(NO ₃) ₂ , 60 V/ -4 V, 20 min	100:0
2		0.15 M NaF, 60 V, 1 h	Add TiO(NO ₃) ₂ , 60 V/ -4 V, 20 min	90:10
3		0.15 M NaF, 60 V, 1 h	Add TiO(NO ₃) ₂ , 60 V/ -4 V, 20 min	70:30
4		0.15 M NaF, 60 V, 1 h	Add TiO(NO ₃) ₂ , 60 V/ -4 V, 20 min	50:50
5	W	0.15 M NaF, 60 V, 1 h	Add TiO(NO ₃) ₂ , 60 V/ 0 V, 40 min	100:0
6		0.15 M NaF, 60 V, 1 h	Add TiO(NO ₃) ₂ , 60 V/ 0 V, 40 min	90:10
7		0.15 M NaF, 60 V, 1 h	Add TiO(NO ₃) ₂ , 60 V/ 0 V, 40 min	70:30
8		0.15 M NaF, 60 V, 1 h	Add TiO(NO ₃) ₂ , 60 V/ 0 V, 40 min	50:50
9	Ti	0.15 M NH ₄ F, 20 V, 30 min	Add W ₂ O ₁₁ ²⁻ , 20 V/-4 V, 30 min	100:0
10		0.15 M NH ₄ F, 20 V, 30 min	Add W ₂ O ₁₁ ²⁻ , 20 V/-4 V, 30 min	90:10
11		0.15 M NH ₄ F, 20 V, 30 min	Add W ₂ O ₁₁ ²⁻ , 20 V/-4 V, 30 min	70:30
12		0.15 M NH ₄ F, 20 V, 30 min	Add W ₂ O ₁₁ ²⁻ , 20 V/-4 V, 30 min	50:50
13	Ti	0.15 M NH ₄ F, 20 V, 30 min	Add W ₂ O ₁₁ ²⁻ , 20 V/0 V, 30 min	100:0
14		0.15 M NH ₄ F, 20 V, 30 min	Add W ₂ O ₁₁ ²⁻ , 20 V/0 V, 30 min	90:10
15		0.15 M NH ₄ F, 20 V, 30 min	Add W ₂ O ₁₁ ²⁻ , 20 V/0 V, 30 min	70:30
16		0.15 M NH ₄ F, 20 V, 30 min	Add W ₂ O ₁₁ ²⁻ , 20 V/0 V, 30 min	50:50

Part IV Ti/TiO₂/WO₃ nanotubes

Ti/TiO₂/WO₃ nanotubes were prepared by a 2 step method. The initial growth of TiO₂ nanotubes is performed at constant anodization at 20 V in a PEG400:water mixture (90:10) containing 0.15 M NH₄F. This growth stage was performed for different times from 10 min to 3 h. After this stage was completed, a 10 % v/v of WO₃ precursor was added to the electrolytic bath and a pulse waveform of 20/0V was applied for different time form 10 min to 3 h. The total potential perturbation is shown in Figure 3.3. A summary of anodization conditions for Ti/TiO₂/WO₃ nanotubes films are shown in Tables 3.7.

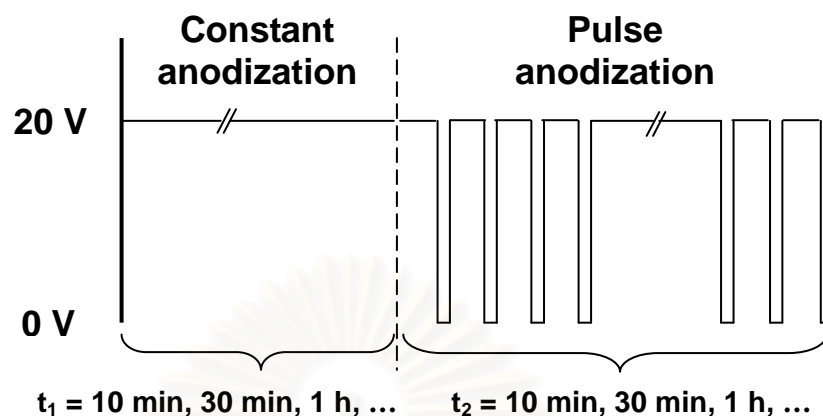


Figure 3.3 Total potential waveform for Ti/TiO₂/WO₃ nanotubes film preparation.

Table 3.7 Anodization conditions for Ti/TiO₂/WO₃ nanotubes film preparation

No.	Metal substrate	Constant Anodization	Pulse Anodization	Ratio
CT1	Ti	0.15 M NH ₄ F/PEG400:H ₂ O (90:10), 20 V, 10 min	Add W ₂ O ₁₁ ²⁻ , 20 V/0 V, 10 min	90:10
CT 2		0.15 M NH ₄ F/PEG400:H ₂ O (90:10), 20 V, 10 min	Add W ₂ O ₁₁ ²⁻ , 20 V/0 V, 30 min	90:10
CT 3		0.15 M NH ₄ F/PEG400:H ₂ O (90:10), 20 V, 10 min	Add W ₂ O ₁₁ ²⁻ , 20 V/0 V, 1 h	90:10
CT 4	Ti	0.15 M NH ₄ F/PEG400:H ₂ O (90:10), 20 V, 30 min	Add W ₂ O ₁₁ ²⁻ , 20 V/0 V, 10 min	90:10
CT 5		0.15 M NH ₄ F/PEG400:H ₂ O (90:10), 20 V, 30 min	Add W ₂ O ₁₁ ²⁻ , 20 V/0 V, 30 min	90:10
CT 6		0.15 M NH ₄ F/PEG400:H ₂ O (90:10), 20 V, 30 min	Add W ₂ O ₁₁ ²⁻ , 20 V/0 V, 1 h	90:10
CT 7	Ti	0.15 M NH ₄ F/PEG400:H ₂ O (90:10), 20 V, 1 h	Add W ₂ O ₁₁ ²⁻ , 20 V/0 V, 10 min	90:10
CT 8		0.15 M NH ₄ F/PEG400:H ₂ O (90:10), 20 V, 1 h	Add W ₂ O ₁₁ ²⁻ , 20 V/0 V, 30 min	90:10
CT 9		0.15 M NH ₄ F/PEG400:H ₂ O (90:10), 20 V, 1 h	Add W ₂ O ₁₁ ²⁻ , 20 V/0 V, 1 h	90:10
CT 10	Ti	0.15 M NH ₄ F/PEG400:H ₂ O (90:10), 20 V, 2 h	Add W ₂ O ₁₁ ²⁻ , 20 V/0 V, 30 min	90:10
CT 11		0.15 M NH ₄ F/PEG400:H ₂ O (90:10), 20 V, 2 h	Add W ₂ O ₁₁ ²⁻ , 20 V/0 V, 1 h	90:10
CT 12		0.15 M NH ₄ F/PEG400:H ₂ O (90:10), 20 V, 2 h	Add W ₂ O ₁₁ ²⁻ , 20 V/0 V, 2 h	90:10
CT 13		0.15 M NH ₄ F/PEG400:H ₂ O (90:10), 20 V, 2 h	Add W ₂ O ₁₁ ²⁻ , 20 V/0 V, 3 h	90:10
CT 14	Ti	0.15 M NH ₄ F/PEG400:H ₂ O (90:10), 20 V, 3 h	Add W ₂ O ₁₁ ²⁻ , 20 V/0 V, 30 min	90:10
CT 15		0.15 M NH ₄ F/PEG400:H ₂ O (90:10), 20 V, 3 h	Add W ₂ O ₁₁ ²⁻ , 20 V/0 V, 1 h	90:10
CT 16		0.15 M NH ₄ F/PEG400:H ₂ O (90:10), 20 V, 3 h	Add W ₂ O ₁₁ ²⁻ , 20 V/0 V, 2 h	90:10
CT 17		0.15 M NH ₄ F/PEG400:H ₂ O (90:10), 20 V, 3 h	Add W ₂ O ₁₁ ²⁻ , 20 V/0 V, 3 h	90:10

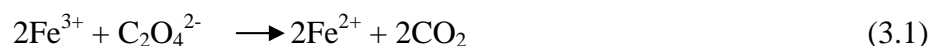
3.3 Photoelectrochemistry

3.3.1 Photocurrent measurement

A standard single-compartment, three-electrode electrochemical cell was used for the photoelectrochemical measurements. A large Pt coil and an Ag|AgCl|satd. KCl reference electrode (Microelectrode Inc., NH), along with the working electrode, completed the cell setup. All potentials in the photoelectrochemical data below are quoted with respect to this reference electrode. The UV light source was a 150 W xenon arc lamp (Oriel, Stratford, CT). The radiation source was placed 8 cm away from the working electrode surface. The incident power on the electrode surface was 11 mW/cm^2 for the UV wavelength region between 270- 400 nm. Photovoltammetry profiles were recorded on a Model CV-27 Voltammograph (Bioanalytical Systems, West Lafayette, IN) equipped with a Model VP-6414S Soltec X-Y recorder in 0.5 M Na_2SO_4 electrolyte. The photovoltammograms were obtained using a slow potential sweep (2 mV/s) in conjunction with interrupted irradiation of the semiconductor film. All electrolyte solutions were sparged with ultrapure N_2 for at least 20 min prior to use. All measurements described below were performed at the laboratory ambient temperature ($25 \pm 2 \text{ }^\circ\text{C}$) unless otherwise noted.

3.3.2 Photon flux and quantum yield measurement

The method of photon flux measurement is potassium ferrioxalate actinometry (Braun *et al.*, 1991). The overall photochemical reaction of a ferrioxalate solution consists of the reduction of ferric ions to ferrous ions:



Normally, the moles of Fe^{2+} formed are determined spectrophotometrically by development with 1,10-phenanthroline (phen) to form the red $[\text{Fe}(\text{phen})_3]^{2+}$ moiety ($\lambda_{\text{max}} = 510.0 \text{ nm}$) (Demas *et al.*, 1981).

In the calibration of a photon source, it is assumed that quantum yield ($\Phi_{\text{Fe}^{2+}}$) of this reaction is accurately known. For the ferrioxalate actinometer, the generally accepted quantum yields have been obtained in the classic work of Hatchard and Parker, 1956. The photon flux (P) was calculated by (Braun *et al.*, 1991):

$$P = \left[\frac{(A_s - A_b) \times V_d \times V_p \times N_A}{\epsilon_{\text{Fe}^{2+}} \times l \times \Phi_{\text{Fe}^{2+} \text{ at } 0.006M} \times V_a \times t} \right] \quad (3.2)$$

where P is the photon flux in photon s^{-1} ; A_s and A_b are the developed absorbance of sample and blank, respectively, at 510.0 nm; V_d , V_p and V_a are the final developed, photolyzed, and aliquot volumes, respectively (all in liters); N_A is Avogadro number (6.023×10^{23}); $\epsilon_{\text{Fe}^{2+}}$ is the specific molar absorbance for $[\text{Fe}(\text{phen})_3]^{2+}$ at 510.0 nm ($11,110 \text{ L cm}^{-1} \text{ mol}^{-1}$); l is the spectrophotometer cell path length (cm); $\Phi_{\text{Fe}^{2+}}$ is quantum yield for the photoreduction of the ferrioxalate ions ($\Phi_{\text{Fe}^{2+}} = 0.9\text{-}1.25$, Kuhn *et al.*, 2004); and t is the irradiation time in seconds.

The apparent quantum yield (Φ_{app}) of the reaction can be defined as the initial degradation rate of pollutant (r_{initial}) (photon/s) divided by the photon flux (P) (photon/s).

$$\Phi_{\text{app}} = \frac{r_{\text{initial}}}{P} \quad (3.3)$$

3.4 Photocatalysis

3.4.1 Ultraviolet (UV) light photocatalysis

The selected oxide films prepared from anodization technique (adsorption area around 0.63 cm^2) were used in the photocatalysis experiments. The 150 W xenon arc lamp (Oriel, Stratford, CT) was used as the light source for ultraviolet (UV) light photocatalysis. For photoreduction study, hexavalent chromium solutions ($100 \mu\text{M}$, 10 ml), containing 0.01 M formate species as sacrificial electron donor and adjusted

to pH 3 was used and Cr(VI) solutions were sparged with ultrapure N₂ for 30 min prior and throughout the photocatalysis reaction. For photooxidation study, methylene blue solution (30 μM, 10 ml) at pH 9 was used and pre-purified O₂ gas was sparged through the solution during the 30 min dark adsorption (equilibration) period and throughout the photocatalysis experiments. The concentrations of the Cr(VI) and methylene blue were spectrophotometrically monitored at analytical wavelengths of 660 nm and 350 nm respectively on an Agilent Model 8453 instrument.

3.4.2 Visible light photocatalysis

Nanoporous WO₃ films prepared from 0.15 M NaF electrolyte at 60 V for 2 h (adsorption area around 0.63 cm²) were used in the photocatalysis experiments. For visible light photocatalysis, the 150 W xenon arc lamp (Oriel, Stratford, CT) was used as the light source combined with a 400 nm cutoff filter. Ten milliliter of methylene blue solution at pH 9 was prepared in different initial concentrations and pre-purified O₂ gas was sparged through the solution during the 30 min dark adsorption (equilibration) period and throughout the photocatalysis experiments. The concentrations of the methylene blue were spectrophotometrically monitored at analytical wavelengths of 660 nm on an Agilent Model 8453 instrument.

3.5 Other Instrumentation

For scanning electron microscopy (SEM), a Zeiss Supra 55 instrument with a nominal electron beam voltage of 5 kV was used. Most of the films in this study were subjected to a thermal anneal in a model 650-14 Isotemp Programmable Muffle Furnace (Fisher Scientific) in air before characterization and photoelectrochemical measurements. A linear heat ramp (at 25 °C/min) from room temperature to a preselected final temperature of 450 °C was followed by 30 min equilibration at the final temperature. The samples were then allowed to cool via natural convection in the furnace back to the ambient condition. The oxide films as prepared were amorphous and become crystalline only after the thermal anneal step noted above.

For X-ray photoelectron spectroscopy (XPS), a Perkin Elmer/Physical Electronics Model 5000C was used to analyze the Ti and W composition in composite film.



สถาบันวิทยบริการ
จุฬาลงกรณ์มหาวิทยาลัย

CHAPTER IV

RESULTS AND DISCUSSION

4.1 WO₃, TiO₂, and composite film preparation by cathodic electrodeposition on stainless steel (SS) AISI 304

Photocurrent density was measured after deposited film was annealed at 450 °C for 30 min. The photocurrent density of all electrodeposited films was measured at 1.0 V for WO₃ and 0.8 V for TiO₂.

4.1.1 Effect of electrodeposition time on film preparation

Table 4.1 and 4.2 show the photocurrent density of WO₃ and TiO₂ electrodeposition films on stainless steel AISI 304 prepared by varying electrodeposition time.

Table 4.1 Photocurrent density of SS/WO₃ electrodeposition films with varying electrodeposition time

Film	Electrodeposition Potential (mV)	Electrodeposition Time (min)	Photocurrent density ($\mu\text{A}/\text{cm}^2$)	
			1 st series	2 nd series
WO ₃	-450	5	253.3	186.7
		10	746.7	440.0
		15	53.3	26.7
		20	40.0	13.3
		25	26.7	13.3
		30	13.3	13.3

Table 4.2 Photocurrent density of SS/TiO₂ electrodeposition films with varying electrodeposition time

Film	Electrodeposition Potential (mV)	Electrodeposition Time (min)	Photocurrent density ($\mu\text{A}/\text{cm}^2$)	
			1 st series	2 nd series
TiO ₂	-950	15	21.3	9.3
		30	28.0	13.3
		45	16.0	8.0
		60	18.7	5.3
		90	14.7	5.3

From the photocurrent measurements, it was found that optimum electrodeposition time for the WO₃ film on stainless steel AISI 304 at the potential of -450 mV is 10 min and for the TiO₂ film on stainless steel AISI 304 at the potential of -950 mV is 30 min. Also, the photocurrent density decreases with increase in the electrodeposition time with values higher at 10 min for WO₃ (30 min in the case of TiO₂). This could be explained that the increase in thickness of electrodeposited films by increasing the time of deposition which resulted in cracking on film after annealing at 450 °C. When working electrode was immersed into electrolyte, films peeled off and fell down into the solution. As the films are not physically stable, their photocurrent densities decrease.

4.1.2 Effect of electrodeposition potential on film preparation

Table 4.3 and 4.4 show the photocurrent density of WO₃ and TiO₂ electrodeposited films on stainless steel AISI 304 prepared by varying electrodeposition potential.

Table 4.3 Photocurrent density of SS/WO₃ electrodeposition films with varying electrodeposition potential

Film	Electrodeposition Potential (mV)	Electrodeposition Time (min)	Photocurrent density ($\mu\text{A}/\text{cm}^2$)	
			1 st series	2 nd series
WO ₃	-250	10	200.0	160.0
	-300	10	213.3	360.0
	-350	10	426.7	653.3
	-400	10	480.0	453.3
	-450	10	386.7	186.7
	-550	10	133.3	40.0
			3 rd series	
WO ₃	-350	10	426.7	
	-350	10	480.0	
	-400	10	546.7	
	-400	10	493.3	

Table 4.4 Photocurrent density of SS/TiO₂ electrodeposition films with varying electrodeposition potential

Film	Electrodeposition Potential (mV)	Electrodeposition Time (min)	Photocurrent density ($\mu\text{A}/\text{cm}^2$)	
			1 st series	2 nd series
TiO ₂	-850	30	8.0	6.7
	-950	30	12.0	9.3
	-1050	30	6.7	6.7

From the results of photocurrent measurement it was found that -400 mV is the optimum potential for WO₃ electrodeposition on SS 304 and -950 mV is the optimum potential for TiO₂ electrodeposition on SS 304. By increasing the potential, it resulted in faster deposition of the ions in the precursor solution and increase in the thickness of the film. The SEM images of WO₃ and TiO₂ prepared by optimum

electrodeposition potential and time after annealed at 450 °C for 30 min were shown in Figure 4.1.

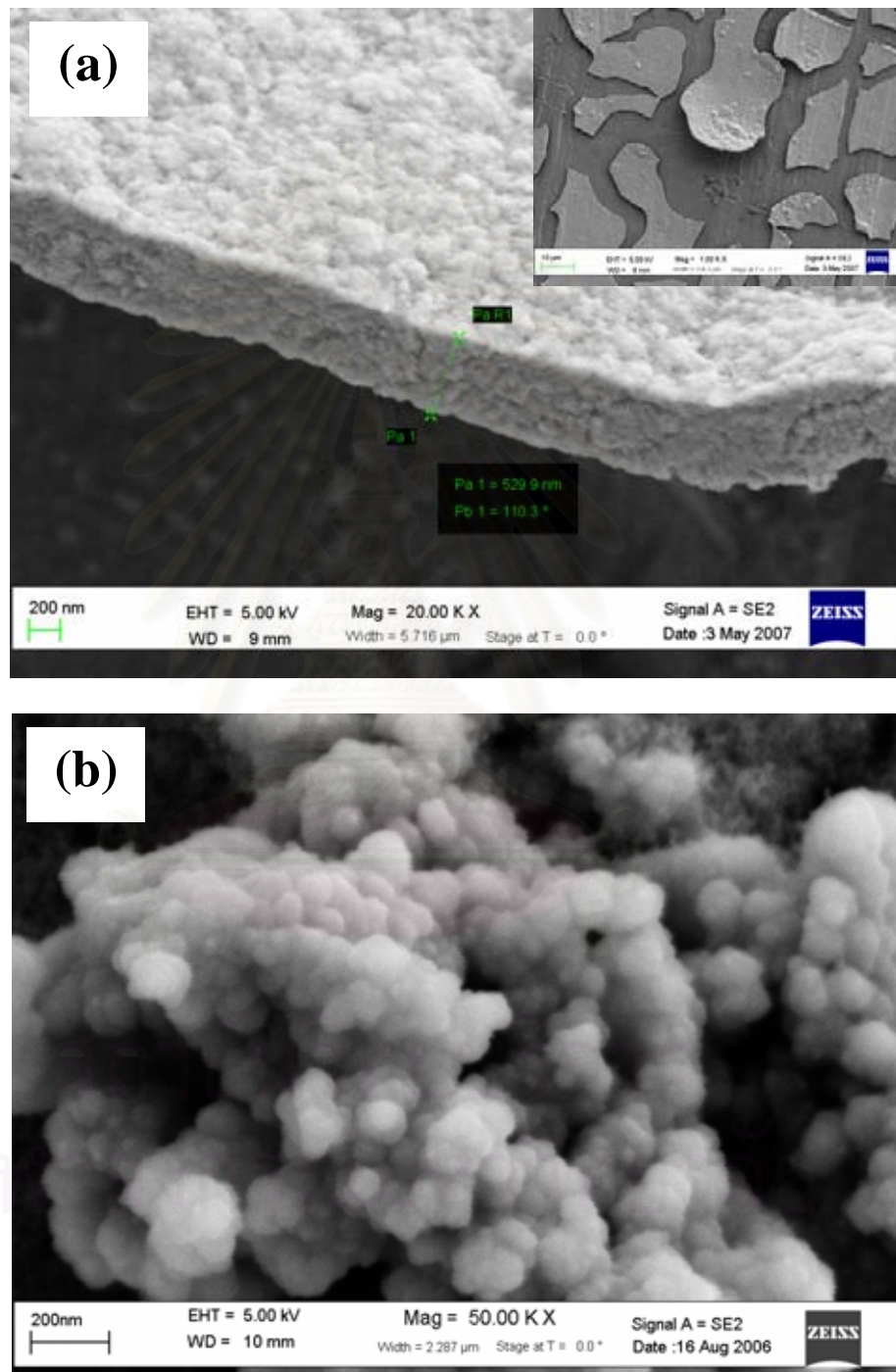


Figure 4.1 SEM images of after annealed (a) WO₃ (-400 mV, 10 min) and (b) TiO₂ (-950 mV, 30 min) films on stainless steel AISI 304 prepared by optimum electrodeposition potential and time.

4.1.3 Effect of multilayer films of electrodeposition on photocurrent performance

4.1.3.1 Multilayer WO_3 thin film electrodeposition.

Multilayer WO_3 film obtained by deposited first layer film at -450 mV for 10 min and annealed at 450 °C for 30 min and then second layer film was deposited for 10 min and annealed for 30 min as before. The designated code for this condition is “10 + 10” as shown in Table 4.5. The electrodeposition and annealing steps were repeated for selected time as shown in the same table.

Table 4.5 Photocurrent density of SS/ WO_3 / WO_3 /... multilayer films

Film	Electrodeposition Potential (mV)	Electrodeposition Time (min)	Photocurrent density ($\mu A/cm^2$)	
			1 st series	2 nd series
WO_3	-450	10	533.3	546.7
		10 + 10	280.0	386.7
		10 + 10 + 10	333.3	160.0

4.1.3.2 Multilayer TiO_2 thin film electrodeposition.

Multilayer TiO_2 film obtained by depositing first layer film at -950 mV for 15 min and annealing at 450 °C for 30 min. The second layer film was deposited for 15 min and annealed for 30 min as before. The designated code for this condition is “15 + 15” as shown in Table 4.6. The electrodeposition and annealing steps were repeated for selected time as shown in the same table.

Table 4.6 Photocurrent density of SS/ TiO_2 / TiO_2 /... multilayer films

Film	Electrodeposition Potential (mV)	Electrodeposition Time (min)	Photocurrent density ($\mu A/cm^2$)	
			1 st series	2 nd series
TiO_2	-950	15	15.4	10.0
		15 + 15	7.7	3.3
		15 + 15 + 15	7.7	6.7
		15 + 15 + 15 + 15	7.7	6.7

From the photocurrent results of this experiment it was found that only one layer of the electrodeposited films gave the highest photocurrent compared with multilayer films. This trend occurred with both WO_3 and TiO_2 films. It could be explained that in multilayer films, cracking occurred after annealing at $450\text{ }^\circ\text{C}$ for 30 min. Due to this explanation, when the next layer film was deposited and annealed, the film became non-continuous and non-uniform and gave less current as shown.

4.1.4 Effect of composite films of electrodeposition on photocurrent performance

4.1.4.1 Composite film $\text{SS}/\text{WO}_3/\text{TiO}_2$ obtained by different electrodeposition steps

WO_3 and TiO_2 films were deposited at -400 and -950 mV for 10 min and 30 min, respectively. All films were grown for same total electrodeposition time but were applied in different sequence as shown in Table 4.7. For example, film 2 layers of $\text{SS}/5/15$ min, stainless steel was immersed in WO_3 electrodeposition bath and then WO_3 film was deposited at -400 mV for 5 min. Next bath solution was changed to TiO_2 precursor solution and then TiO_2 film was deposited at -950 mV for 15 min. As-deposited film was annealed at $450\text{ }^\circ\text{C}$ for 30 min. After that second layer of WO_3/TiO_2 film was deposited at the same voltage and time and was annealed at same condition.

Table 4.7 Photocurrent density of $\text{SS}/\text{WO}_3/\text{TiO}_2$ films obtained by different electrodeposition steps

Film	Electrodeposition	Electrodeposition	Photocurrent density	
	Potential (mV)	Time (min)	($\mu\text{A}/\text{cm}^2$)	
$\text{SS}/\text{WO}_3/\text{TiO}_2$	$\text{SS}/\text{WO}_3/\text{TiO}_2$	$\text{SS}/\text{WO}_3/\text{TiO}_2$	1 st series	2 nd series
	$\text{SS}/-400/-950$	$\text{SS}/10/30$ min (1 layer)	44.0	177.3
		$\text{SS}/5/15$ min (2 layers)	229.3	201.3
		$\text{SS}/2/6$ min (5 layers)	44.0	104.0

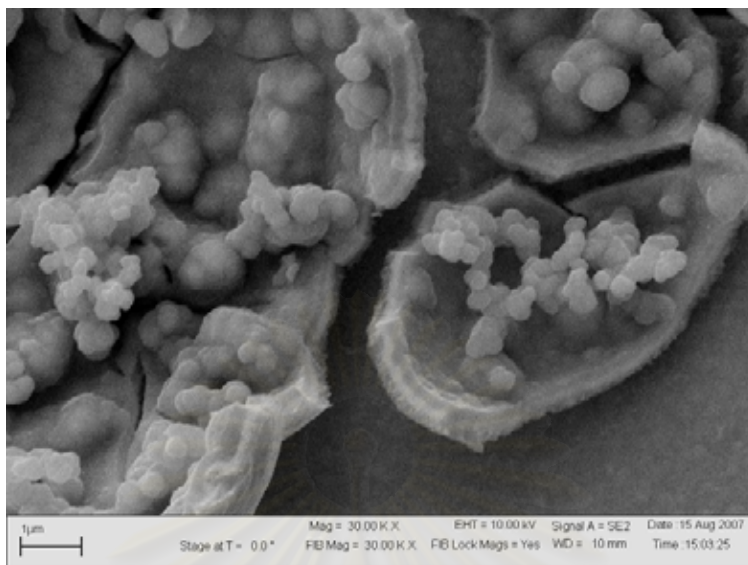


Figure 4.2 SEM images of composite SS/WO₃/TiO₂ film (SS/5/15 min, 2 layers) which gave the highest photocurrent reach to 230 $\mu\text{A}/\text{cm}^2$.

When composite SS/WO₃/TiO₂ film was irradiated, electron in conduction band of TiO₂ can move to conduction band of WO₃ due to conduction band of TiO₂ has more negative reduction potential than conduction band of WO₃. The hole in valence band of WO₃ has more positive reduction potential than valence band of TiO₂ therefore, it can move to valence band of TiO₂. When hole was trapped in TiO₂ film and electron was trapped in WO₃ film, electron-hole paired separation occurred and electrons moved to back contact and gave highest photocurrent.

From results of photocurrent, composite SS/WO₃/TiO₂ film (SS/5/15 min, 2 layers) gave highest photocurrent density (230 $\mu\text{A}/\text{cm}^2$). Figure 4.2 shows SEM images of composite SS/WO₃/TiO₂ film (SS/5/15 min, 2 layers). Obviously, the multilayer of crystalline WO₃ and TiO₂ film was seen after annealed at 450 °C for 30 min. This SS/5/15 min, 2 layers film gave photocurrent density higher than other types of deposited films (SS/10/30 min and SS/2/6 min, 5 layers). This could be explained by light penetration that SS/10/30 min film has thicker layer of outer TiO₂ film than SS/5/15 min, 2 layers film. When the former film was irradiated electron was generated less than the latter film where light may reach inner WO₃ layer and electron can be generated as well. Consequently the latter film gave higher current

density. While SS/2/6, 5 layers film was deposited and annealed for 5 times causing part of film to peel off, thus giving less current density. In addition, the composite SS/WO₃/TiO₂ film (SS/5/15 min, 2 layers) gave higher photocurrent density than those of other synthesized SS/TiO₂ films.

4.1.4.2 Composite SS/WO₃/TiO₂ films prepared in different number of films layer

WO₃ and TiO₂ films were deposited at -400 and -950 mV for 2 min and 6 min, respectively. Then a composite film was annealed at 450 °C for 30 min and measured for photocurrent density. Again, the second layer was deposited on the same films, annealed, and measured for the photocurrent density. Next layer films also followed the same steps. The photocurrent density was measured after each successive layer of WO₃/TiO₂ deposition and annealing as shown in Table 4.8.

Table 4.8 Photocurrent density of SS/WO₃/TiO₂ films prepared in different number of films layer

Film	Electrodeposition Potential (mV)	Electrodeposition Time (min)	Photocurrent density (μA/cm ²)
SS/WO ₃ /TiO ₂	SS/WO ₃ /TiO ₂	SS/WO ₃ /TiO ₂	1 st series
	SS/-400/-950	SS/2/6 min, 1 layer	176.0
		SS/2/6 min, 2 layers	56.0
		SS/2/6 min, 3 layers	52.0
		SS/2/6 min, 4 layers	77.3
		SS/2/6 min, 5 layers	44.0

From this experiment it was found that only one layer composite SS/WO₃/TiO₂ film gave the highest photocurrent density when compared with multilayer composite film. In composite film, after finishing each step of WO₃/TiO₂, deposition film increased in thickness and after annealing and emerging into the electrolyte for measured photocurrent, film was peeled off and gave less current.

4.1.4.3 Composite film SS/TiO₂/WO₃ obtained by different electrodeposition steps

TiO₂ and WO₃ films were deposited at -950 and -400 mV for 30 min and 10 min, respectively. All films were grown for same total electrodeposition time but were applied in different sequence as shown in Table 4.9. For example, film SS/15/5min, 2 layers, stainless steel was immersed in TiO₂ electrodeposition bath and then TiO₂ film was deposited at -950 mV for 15 min. Next bath solution was changed to WO₃ precursor solution and then WO₃ film was deposited at -400 mV for 5 min and then the deposited film was annealed at 450 °C for 30 min. After that second layer of TiO₂/WO₃ film was deposited at the same voltage and time and was annealed at the same condition.

Table 4.9 Photocurrent density of SS/TiO₂/WO₃ films obtained by different electrodeposition steps

Film	Electrodeposition	Electrodeposition	Photocurrent density	
	Potential (mV)	Time (min)	(μA/cm ²)	
SS/TiO ₂ /WO ₃	SS/TiO ₂ /WO ₃	SS/TiO ₂ /WO ₃	1 st series	2 nd series
	SS/-950/-400	SS/30/10 min (1 layer)	40.0	66.7
		SS/15/5 min (2 layers)	40.0	53.3
		SS/6/2 min (5 layers)	26.7	40.0

Result from this experiment shows that composite film SS/TiO₂/WO₃ gave smaller photocurrent density than composite SS/WO₃/TiO₂ films. This can be explained that when composite SS/TiO₂/WO₃ film was irradiated, the electron in conduction band of WO₃ which has more positive reduction potential than conduction band of TiO₂, could not move to conduction band of TiO₂ and hole in valence band of TiO₂ which has more negative reduction potential than valence band of WO₃, could not move to valence band of WO₃. In addition, electron from conduction band of WO₃ can move to hole in valence band of TiO₂ faster than move to conduction band of TiO₂. Thus electron hole recombination occurred. Electron was removed by

recombination process thus this composite SS/TiO₂/WO₃ film gave less photocurrent density.

4.1.4.4 Composite SS/TiO₂/WO₃ films prepared in different number of films layer

TiO₂ and WO₃ films were deposited at -950 and -400 mV for 6 min and 2 min, respectively. Then a composite film was annealed at 450 °C for 30 min and measured for photocurrent density. Then the second layer was deposited on the same films, annealed, and measured for the photocurrent density again. Next layer films followed the same steps. The photocurrent density was measured after each successive layer of TiO₂/WO₃ deposition and annealing as shown in Table 4.10.

Table 4.10 Photocurrent density of SS/TiO₂/WO₃ films prepared in different number of films layer

Film	Electrodeposition Potential (mV)	Electrodeposition Time (min)	Photocurrent density (μA/cm ²)
SS/TiO ₂ /WO ₃	SS /TiO ₂ /WO ₃	SS/TiO ₂ /WO ₃	1 st series
	SS/-950/-400	SS/6/2 min, 1 layer	66.7
		SS/6/2 min, 2 layers	53.3
		SS/6/2 min, 3 layers	40.0
		SS/6/2 min, 4 layers	26.7
		SS/6/2 min, 5 layers	26.7

From the photocurrent results of this experiment it was found that only one layer composite SS/TiO₂/WO₃ film gave the highest photocurrent density than those of other multilayer composite films. This shows that it resulted and can be explained in the same way as done on experiment 4.1.2.

In photocurrent comparison between this film (SS/TiO₂/WO₃) and SS/WO₃ film we found that the latter film gives much higher photocurrent than former film. This maybe due to the time when the composite SS/TiO₂/WO₃ film was irradiated

with UV light so the electron-hole recombination occurred as described before, therefore, giving less photocurrent than SS/WO₃ film.

4.1.5 Evaluation of the capability of electrodeposition technique in fabrication of TiO₂, WO₃ and composite films on stainless steel AISI 304

In summary, the appropriate electrodeposition time and electrodeposition potential for WO₃, TiO₂ and composite films are shown below.

- For WO₃ cathodic electrodeposition on stainless steel (SS) AISI 304, the best electrodeposition time and electrodeposition potential studied in this work are 10 min and -400 mV, respectively which gave photocurrent density up to 546.7 $\mu\text{A}/\text{cm}^2$.

- For TiO₂ cathodic electrodeposition on stainless steel (SS) AISI 304, the best electrodeposition time and electrodeposition potential studied in this work are 30 min and -950 mV, respectively which gave photocurrent density up to 28.0 $\mu\text{A}/\text{cm}^2$.

The effect of multilayer films of electrodeposition on photocurrent performance was also studied. Interestingly, both types of semiconductors show the same result that only one layer of film on stainless steel (SS) AISI 304 show better photocurrent performances than multilayer film.

For composite film preparations, SS/WO₃/TiO₂ films were prepared in different electrodeposition steps. The result shows that film SS/WO₃/TiO₂ in the type of SS/5/15min (2 layers) gave the highest photocurrent density up to 229.3 $\mu\text{A}/\text{cm}^2$. For SS/TiO₂/WO₃ films, the SS/30/10 min (1 layer) gave the highest photocurrent density up to 66.7 $\mu\text{A}/\text{cm}^2$. In comparison, film SS/WO₃/TiO₂ show better photocurrent performance than film SS/TiO₂/WO₃. The composite film SS/WO₃/TiO₂ is relevant to the theory of composite film WO₃/TiO₂ which TiO₂ should be the outer part and WO₃ should be the inner part. Conduction band of TiO₂ has more negative reduction potential than that of WO₃, so photogenerated electron in conduction band of TiO₂ can move down to conduction band of WO₃. This reduces recombination of e⁻ - h⁺ pair in the composite semiconductor, thus film SS/WO₃/TiO₂ show better performance.

In evaluation of the practicability of electrodeposition technique in fabrication of TiO₂, WO₃ and composite films, it is found that all synthesized films are not physically stable. These cathodic electrodeposition films were easily peeled off from substrate after prepared and annealing steps. These films demonstrated low adhesion, discontinuity, and non-uniformity properties. The multilayer film fabrication does not improve the film quality. Consequently, the photocurrent densities obtaining from these films are in variation according to the film quality. Even though, the best electrodeposition time and electrodeposition potential in this study could be identified, the obtaining photocurrent densities from duplicate experiment are very different as shown in Table 4.2-4.7. From the results shown in this section, it can be concluded that the electrodeposition technique can not provide the high quality film to be used for photocatalysis application. Thus, the further film preparation conditions were focused only on anodization technique.

4.2 TiO₂, WO₃, and composite film preparation by anodization

4.2.1 Ti/TiO₂ prepared by anodization

4.2.1.1 Anodic growth of TiO₂ films: variables

Anodic growth of oxide layers on Ti substrates relies on the controlled balance between oxide formation and chemical/electrochemical dissolution phenomena (Mor *et al.*, 2003 and Grimes 2007). Thus a wide range of fluoride-based electrolytes have been deployed in previous studies, including HF (Gong *et al.*, 2001), KF or NaF (Cai *et al.*, 2005), and HNO₃-HF (Ruan *et al.*, 2006) or H₂SO₄-HF (Beranek *et al.*, 2003) mixtures. Other electrolyte compositions include NH₄F/(NH₄)₂SO₄ or NaF/Na₂SO₄ mixtures (Beranek *et al.*, 2005, Tsuchiya *et al.*, 2005, Macak *et al.*, 2005) and various acids such as boric acid, citric acid (Cai *et al.*, 2005), or acetic acid (Tsuchiya *et al.*, 2005). In this study, NH₄F containing electrolytes without (entries 1-4, Table 4.11) or with a medium modifier, glycerol (entries 5-8, Table 4.11) were used. Two different NH₄F concentrations (0.15 M and 0.36 M) were used (entries 6 and 8, Table 4.11). The influence of another bath additive, poly(ethylene glycol) or PEG, was also

examined using PEG of varying molecular weights (entries 9-12, Table 4.11). Entries 14-16 in Table 4.11 pertain to the effect of anodization voltage using ethylene glycol as the predominant electrolyte supporting medium. It must be noted that the water content of the anodization medium runs the gamut from completely aqueous (entries 1-4, Table 4.11) to a relatively small fraction by mass (entries 5-8, Table 4.11) with the other experiments (entries 9-16) featuring an intermediate water content. The effect of anodization time is probed for two sets of experiments with (entries 5-7, Table 4.11) or without “wet” glycerol (entries 1-4, Table 4.11) to support the NH_4F electrolyte.

Table 4.11 Anodization conditions, photoelectrochemical performance and morphology of TiO_2 nanotubes in this study

entry no.	electrolyte, medium modifier	voltage, time	$j_{\text{ph}}/$ $\text{mA cm}^{-2 \text{ a)}$	morphology
1	0.15 M NH_4F	20 V, 1 h	2.10	disordered NT ^{b)}
2	”	20 V, 3 h	1.83	disordered NT
3	”	20 V, 5 h	1.47	disordered NT
4	”	20 V, 10 h	1.43	disordered NT
5	0.15 M $\text{NH}_4\text{F}/$ glycerol (~ 2-3% H_2O)	20 V, 3 h	2.38	S-O ^{c)} NT, ~21 nm ^{d)}
6	”	20 V, 5 h	2.58	S-O NT, ~20 nm
7	”	20 V, 10 h	2.82	S-O NT, ~20 nm
8	0.36 M $\text{NH}_4\text{F}/$ glycerol (~ 2-3% H_2O)	20 V, 5 h	n.d. ^{e)}	L-S-O ^{f)} NT, ~62 nm
9	0.15 M $\text{NH}_4\text{F}/$ PEG 200: H_2O (90:10)	20 V, 5 h	1.13 ^{g)}	S-O NT, ~77 nm
10	PEG 400: H_2O (90:10)	20 V, 5 h	2.65 ^{g)}	S-O NT, ~80 nm
11	PEG 600: H_2O (90:10)	20 V, 5 h	1.55 ^{g)}	S-O NT, ~47 nm
12	PEG 1000: H_2O (90:10)	20 V, 5 h	1.39 ^{g)}	S-O NT, ~56 nm
13	0.15 M $\text{NH}_4\text{F}/$ ethylene glycol: H_2O (90:10)	20 V, 5 h	1.31	S-O NT, ~67 nm
14	0.36 M $\text{NH}_4\text{F}/$ ethylene glycol: H_2O (90:10)	20 V, 5 h	n.d.	L-S-O NT, ~63 nm
15	”	40 V, 5 h	n.d.	L-S-O NT, ~65 nm
16	”	60 V, 5 h	n.d.	L-S-O NT, ~100 nm

^{a)} j_{ph} = stationary photocurrent density in 0.5 M Na_2SO_4

^{b)} NT = nanotubes

^{c)} S-O = self-organized

^{d)} nanopore inner diameter

^{e)} n.d. = can not be determined

^{f)} L-S-O = lift-off self-organized

^{g)} average value (see appendix A)

Figure 4.3 contains representative assessment of the quality of the anodic oxide layers using linear sweep photovoltammetry (Mishra and Rajeshwar, 1989, Zhou *et al.*, 1996). This technique is described elsewhere (Rajeshwar, 2001) but briefly consists of a slow scan of the potential while the film irradiation is periodically interrupted. In this manner, both the “dark” and the light-induced photoresponse of the oxide layers can be assessed in a single experiment.

Note the excellent rectification quality of the anodic TiO₂ layers in this study as diagnosed by the flat baseline response in the “dark” (Fig. 4.3(A)) over a potential range spanning ~ 4.0 V. The anodic photocurrents arise from the photooxidation of adsorbed hydroxyl groups or water molecules in the 0.5 M Na₂SO₄ electrolyte.

For a “snapshot” assessment of the photoresponse quality as a function of a given anodization parameter, the photocurrent *density* (photocurrent/surface area of the film) at a fixed potential (1.5 V vs. Ag|AgCl) may be utilized as shown in Fig. 4.3(B). Thus, samples grown in 0.15 M NH₄F/glycerol for 10 h at 20 V or in 0.15 M NH₄F/PEG 400 for 5 h at 20 V gave excellent photoresponses (approaching 2.74 mA cm⁻²) (Fig. 4.3(B)).

A clear picture about the effect of light absorption length on the photoelectrochemical behavior of the nanotube arrays can be obtained under monochromatic light irradiation. Incident photon to electron conversion efficiencies (IPCE) of up to 90% at 330 nm (i.e., at the maximum of the photoaction spectrum) for water photooxidation were obtained with films prepared by 10 h anodization at 20 V in 0.15 M NH₄F/glycerol (see Figs. 5 and 15 from de Tacconi *et al.*, 2006). Since the IPCE is defined as the ratio of the number of electrons in the external circuit produced by an incident photon at a given wavelength, the IPCE values of these nanotube arrays translate to a high light harvesting efficiency when the light absorption length ($1/\alpha$, where α is the absorption coefficient of TiO₂) of the monochromatic light is in the 100-200 nm range. For example, at 300 nm, the reported values of light absorption length ($1/\alpha$) is 30 nm, and at 340 nm it is 200 nm (Wahl and Augustynski, 1998, Somasundaram *et al.*, 2005) while our films are in the 1-3 μ m range depending on the anodization time and electrolyte composition. Efficient collection of the photogenerated electrons with very low charge recombination and high electron mobility through the nanotube walls must be occurring in to sustain such IPCE

values. The latter are significantly better than reported values of $\sim 40\%$ at 340 nm for films formed with TiO_2 gels of nanotubes and nanowires synthesized by molecular assemblies composed of surfactant molecules and titanium alkoxide modified with acetylacetone (Shen *et al.*, 2006).

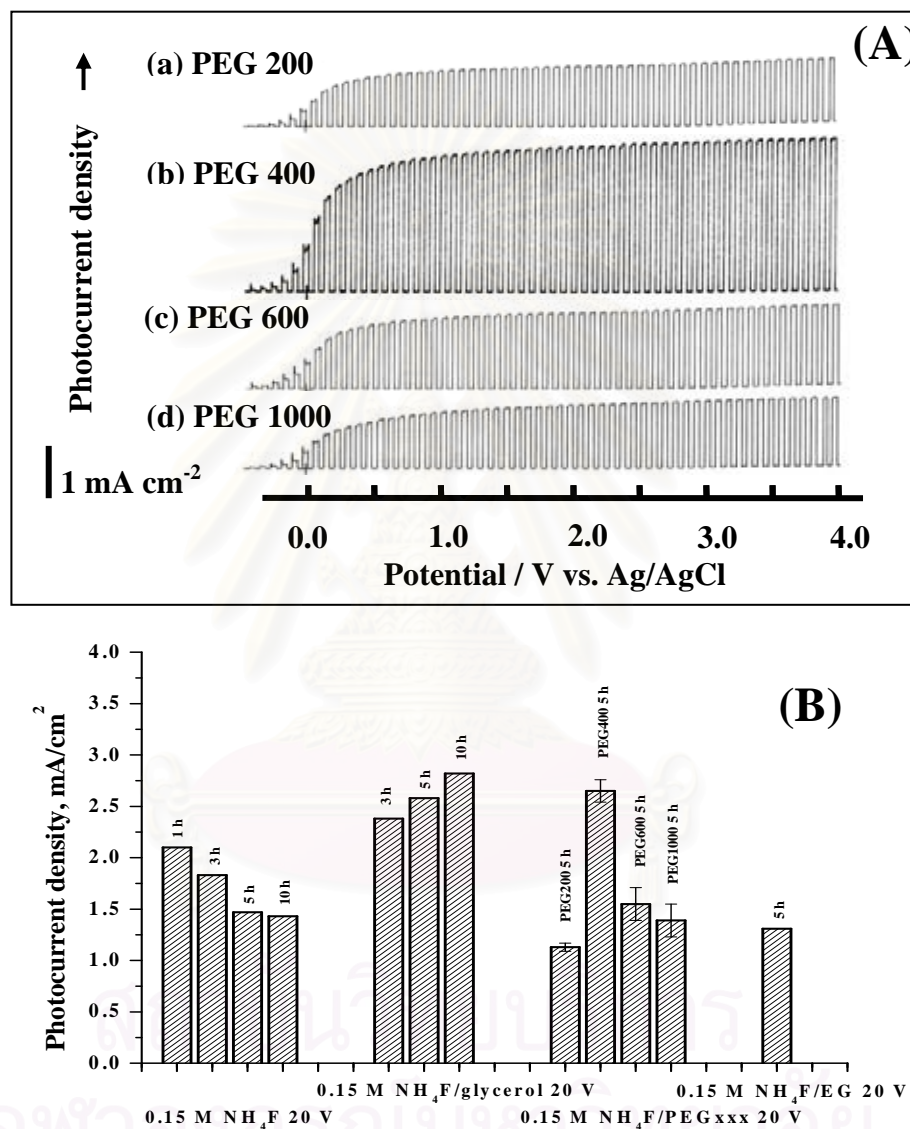


Figure 4.3 (A) Photovoltammograms of nanoporous TiO_2 films grown in poly(ethylene glycol) (PEG) of different molecular weights (as shown) containing 0.15 M NH_4F electrolyte. (B) Bar diagram comprising of photocurrent density at 1.5 V for nanoporous TiO_2 films grown under various conditions. All the photovoltammograms were obtained at 0.05 Hz chopped irradiation in 0.5 M Na_2SO_4 with a scan rate of 2 mV/s using the full output of a 150 W Xe lamp.

4.2.1.2. Effect of anodization time

Figure 4.4 contains representative SEM data showing the influence of anodization time on the growth of TiO₂ nanoporous structure in 0.15 M NH₄F as electrolyte at 20 V. When the anodization time was short, e.g., 1 h (Fig. 4.4a), the resultant TiO₂ nanostructure was more organized than the use of a longer time, e.g., 3 h or 10 h (Figs. 4.4b and 4.4c) where a rough and cross-linked structure was obtained. Accordingly, the photocurrent decreases when the anodization time increases as seen in Fig. 4.3b.

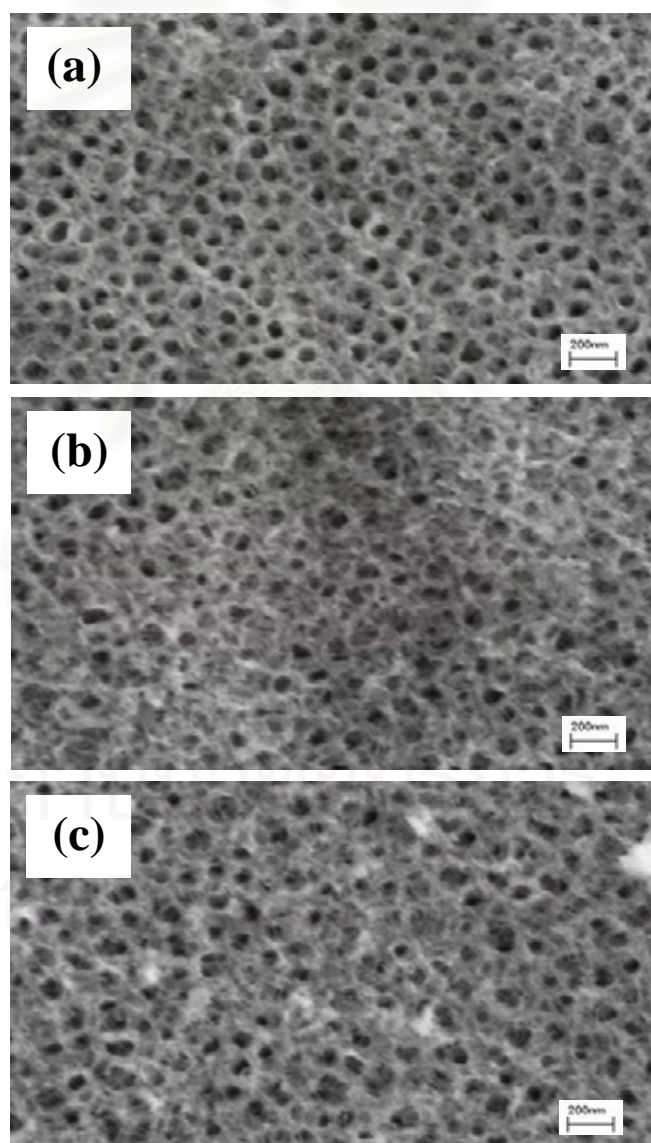


Figure 4.4 Effect of anodization time on the morphology of nanoporous TiO₂ films as probed by SEM. The films were grown in 0.15 M NH₄F electrolyte at 20 V for (a) 1, (b) 3, and (c) 10 h.

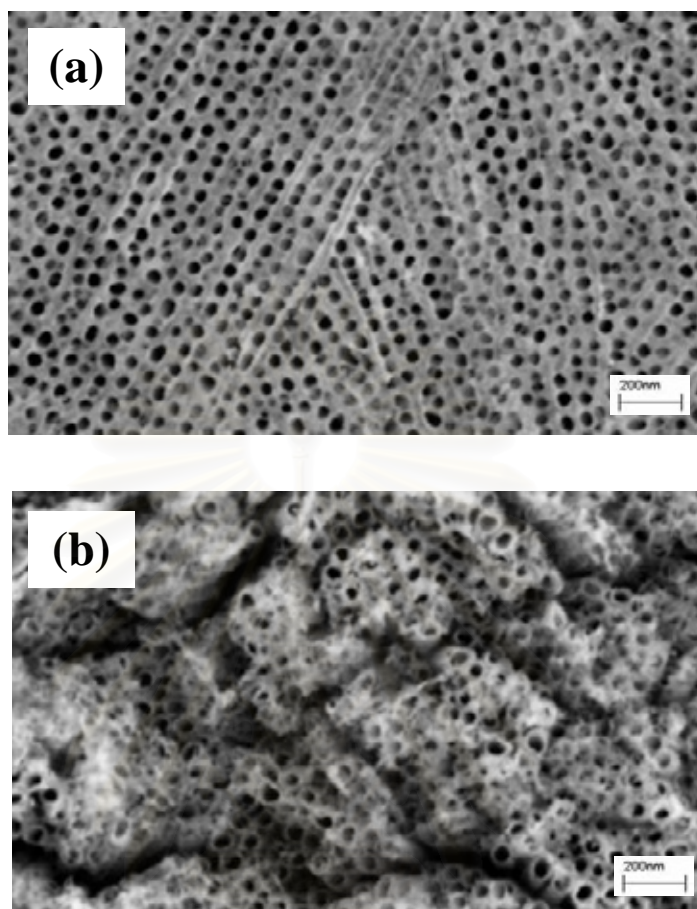


Figure 4.5 Comparison of SEM images of TiO₂ nanotubes obtained by anodization of Ti foil in 0.15 M NH₄F + glycerol (~2-3% water) at 20 V for (a) 5 and (b) 10 h.

Clearly, electron transport in well organized nanotubes is faster than in a less organized nanostructure. In the presence of glycerol as a medium modifier in NH₄F electrolyte with a small amount of water (~2-3%), for shorter periods of anodization (5 h), the nanotube openings appear aligned along the grooves (Fig. 4.5a) while for longer periods of anodization time (10 h), the TiO₂ nanotubes can be seen more clustered as in groups or bundles with a higher exposure of the more deeper areas of the film (Fig. 4.5b). Correspondingly, the photocurrent increases with anodization time because of the higher surface area. Thus TiO₂ nanotubes obtained from anodization at 20 V for 10 h in 0.15 M NH₄F gave the highest photocurrent density reaching 2.82 mA cm⁻².

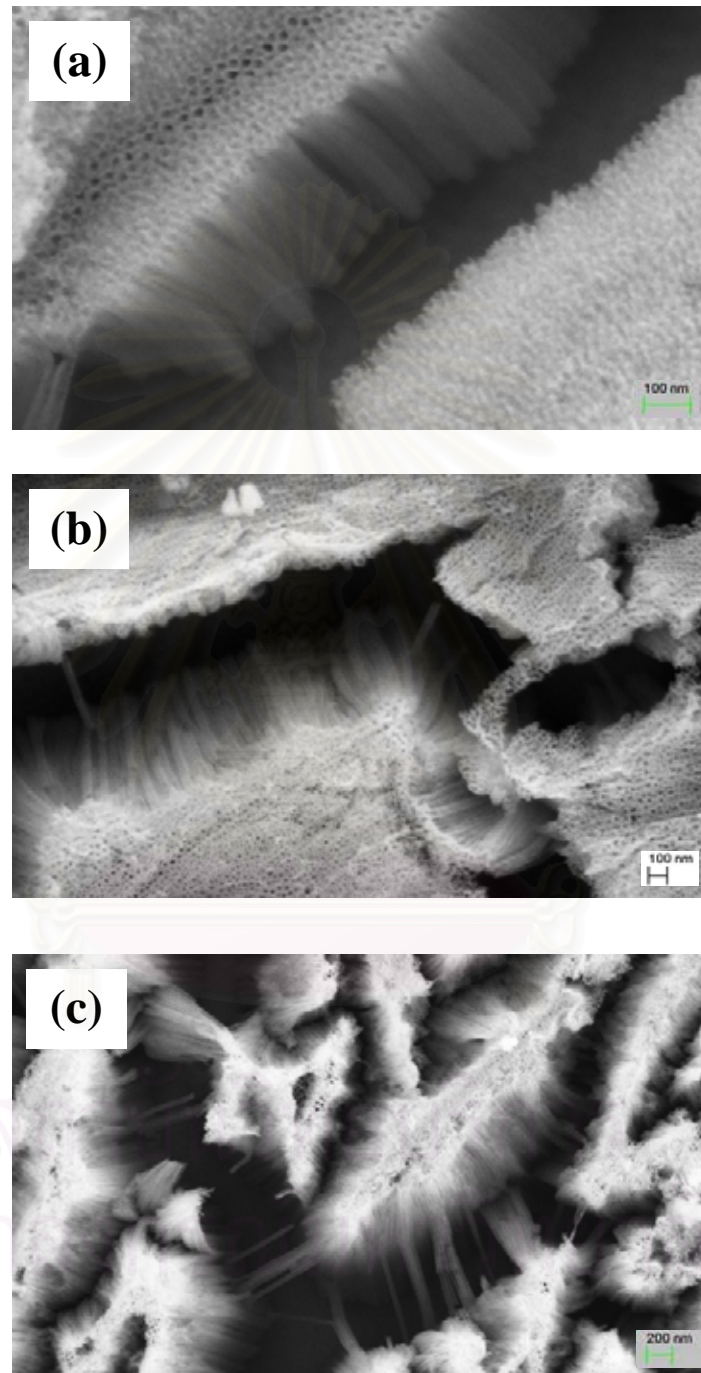


Figure 4.6 Effect of anodization time on the morphology of nanoporous TiO₂ films as probed by SEM. The films were grown in 0.15 M NH₄F + glycerol (1% water) at 20 V for (a) 3, (b) 5, and (c) 10 h.

Interestingly, when the glycerol medium contains only 1% water, the morphology of the resulting films contrasts with that shown in Fig. 4.5. In fact, data on the effect of polarization time for 1% water (Fig. 4.6) clearly show that although the nanotubes grow longer with time, cracking of the films also grows significantly. Collapse of the nanotubes is also seen at long term polarization. Specifically, nanotubes grown for 3 h reach a length of 320 nm (Fig. 4.6a) and kept growing to 660 nm at 5 h (Fig. 4.6b) and to 720 nm at 10 h (Fig. 4.6c). For good photoelectrochemical performance, it is necessary to have long nanotubes with a continuous, extended morphology. The structure in Fig. 4.5b is clearly more extended and continuous than that in Fig. 4.6c and the magnitude of the photoresponse is correspondingly better (2.82 mA cm^{-2} vs. 1.63 mA cm^{-2}).

4.2.1.3 Effect of poly(ethylene glycol) of different molecular weights

Preliminary data on the effects of these additives were reported by de Tacconi *et al.* in 2006. There is also precedence in the literature on the effect of PEG on the morphologies of *nanoporous* oxide semiconductor materials. For example, in the case of WO_3 film growth, PEG was used as a surface modulator (Wolcott *et al.*, 2006) and preferential orientation of crystals were reported. Moreover, in the case of colloidal growth of Fe_3O_4 , PEG was used as a surfactant to attain preferential crystal orientation and better morphology (Zou *et al.*, 2005). In addition, film thickness and smoothness of dip-coated TiO_2 can be controlled by the highly viscous PEG (Miki *et al.*, 2004). For WO_3 , PEG 300 was found to be the most efficient organic additive influencing significantly the film porosity (Santato *et al.*, 2001). For the specific case of oxide nanotubes, additives such as PEG, glycerol, mannitol, and ethylene glycol can be used to control the morphology and growth mechanism. Preferential adsorption and the high viscosity of these additives improve the quality of the resulting film by affecting the degree of oxide dissolution at high positive potentials.

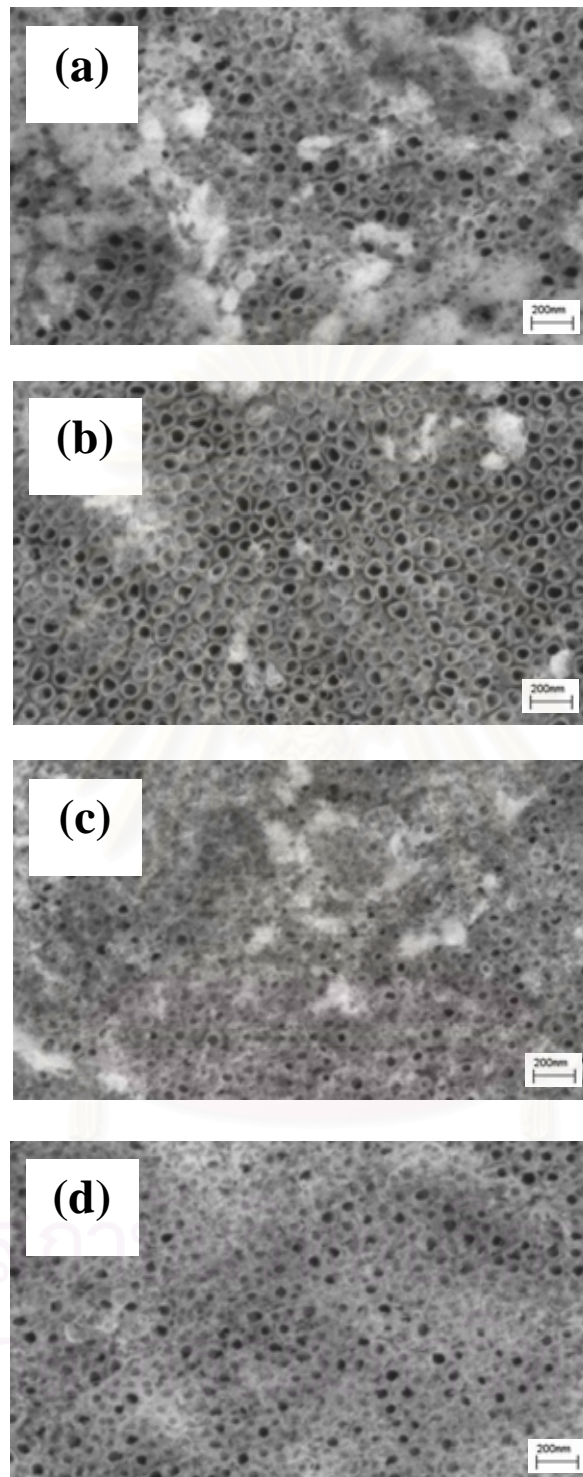


Figure 4.7 Comparison of SEM data for TiO₂ nanotubes obtained by anodization of Ti foil at 20 V for 5 h in 0.15 M NH₄F with poly(ethylene glycol) (PEG) of different molecular weights, (a) PEG 200, (b) PEG 400, (c) PEG 600, and (d) PEG 1000 with a ratio of PEG:H₂O of 90:10 in each case.

Figure 4.7 shows SEM images of self-organized TiO₂ nanotubes which were prepared in PEG of different molecular weights. PEG 200, 400, 600, or 1000 were used as the medium modifier in 0.15 M NH₄F electrolyte (10% water was added to dissolve NH₄F before adding PEG). In all the cases, the TiO₂ nanotubes were grown for 5 h at 20 V. Clearly, TiO₂ nanotubes obtained from PEG 400 as medium modifier, which has nanotube inner diameter around 80 nm, were well organized compared to the other cases (Fig. 4.7). TiO₂ nanotubes obtained from PEG 200 as medium modifier has a less homogenous pore structure and pore formation in this case did not extend over the entire surface. Additionally, there were cloudy precipitates on approximately half the area of the surface. TiO₂ nanotubes obtained from PEG 600 and PEG 1000 as medium modifiers have inner tube diameters around 47 nm and 56 nm, respectively, smaller than the nanotubes obtained in PEG 400. In comparison, PEG 1000 as medium modifier affords a slightly larger tube diameter- perhaps a consequence of the slightly higher temperature that was employed for the anodization in this case. (This is because PEG 1000 is a solid at room temperature.) A similar trend was reported for glycerol, namely the higher the temperature, the larger the diameter of the nanotubes (Macak and Schmuki, 2006). Thus pore diameters do not scale with the molecular weight of poly(ethylene glycol) from PEG 400, 600, to 1000 where an expected decrease in pore diameter with an increase in viscosity should have occurred. TiO₂ nanotubes obtained from PEG 400 gave the highest photocurrent density up to 2.74 mA cm⁻² in the PEG series of experiments (entries 9-12, Table 1).

4.2.1.4 Effect of anodization voltage

Figure 4.8 shows cross-section SEM images of TiO₂ nanotubes prepared in 0.36 M NH₄F with ethylene glycol as medium modifier (10% water was added to dissolve NH₄F before mixing with ethylene glycol) for 5 h with different anodization voltages 20 V, 40 V, and 60 V, respectively. After anodization, in all the cases (20 V, 40 V, and 60 V), the oxide layer appeared to lift-off from the substrate; hence, photocurrent measurements on these films could not be performed. In Fig. 4.8a, at 20 V, 5 h gives a nanotube length around 1.5 μm while at 40 V and 5 h (Fig. 4.8b), a nanotube length up to 2.8 μm is obtained with the nanotube tips tending to coalesce.

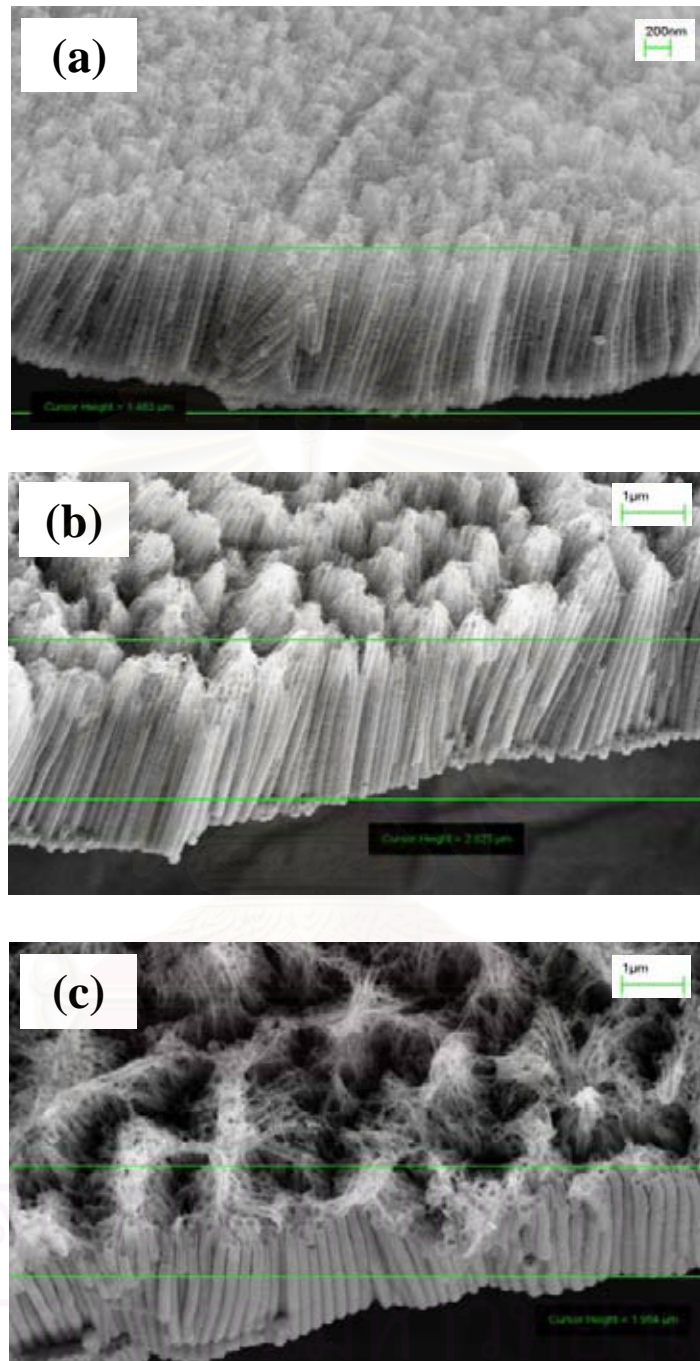


Figure 4.8 Effect of anodization voltage on the morphology of TiO₂ nanotubes as probed by SEM (cross-sectional views). The films were grown in 0.36 M NH₄F + ethylene glycol:H₂O (90:10) for 5 h at (a) 20, (b) 40, and (d) 60 V, respectively.

It is known that more positive anodization voltages and longer anodization times tend to dissolve nanotube walls at the tips to collapse them together. At 60 V, 5 h gives shorter TiO₂ nanotubes (lengths around 1.9 μm) than that of film prepared at 40 V, 5 h. Note that the nanotube tips collapsed and fused together to give shorter nanotube arrays (Fig. 4.8c).

4.2.1.5 Effect of fluoride ion concentration

TiO₂ nanotubes, grown in glycerol (with ~2-3% water) as medium modifier with varying concentrations of fluoride ions namely, 0.15 M and 0.36 M NH₄F, respectively, yielded distinct appearances as in Fig. 4.9.

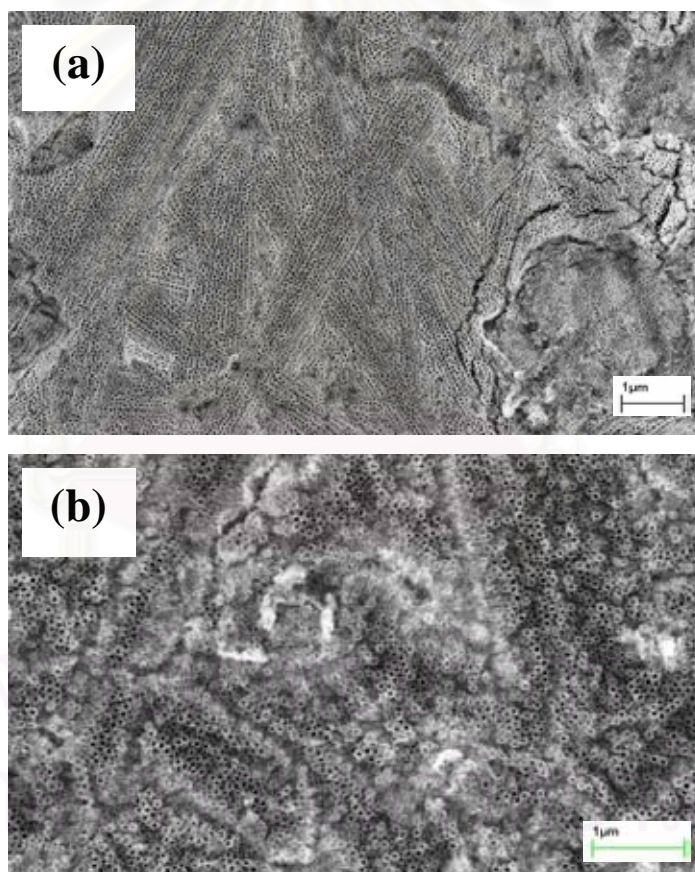


Figure 4.9 Effect of fluoride ion concentration on the morphology of TiO₂ nanotubes as probed by SEM. The films were grown at 20 V for 5 h in (a) 0.15 M NH₄F + glycerol (~2-3% water) and (b) 0.36 M NH₄F + glycerol (~2-3% water).

Interestingly, at a lower fluoride ion concentration (Fig. 4.9a), the TiO_2 nanotube arrays had a drilled in appearance and the tube diameter was around 40 nm while at a higher fluoride ion concentration (Fig. 4.9b), TiO_2 nanotubes grew like a bundle of straws with a tube diameter around 62 nm. This phenomenon may be due to the difference in the etching rate of fluoride ions. Importantly, the effect of fluoride ion concentration on the length of the TiO_2 nanotube arrays can be seen in ethylene glycol as medium modifier (Fig. 4.10). An electrolyte containing 0.15 M NH_4F + ethylene glycol gave shorter TiO_2 nanotubes (approximately 1.1 μm) than in an electrolyte containing 0.36 M NH_4F + ethylene glycol (approximately 1.5 μm) (c.f., Figs. 4.10a and 4.10b).

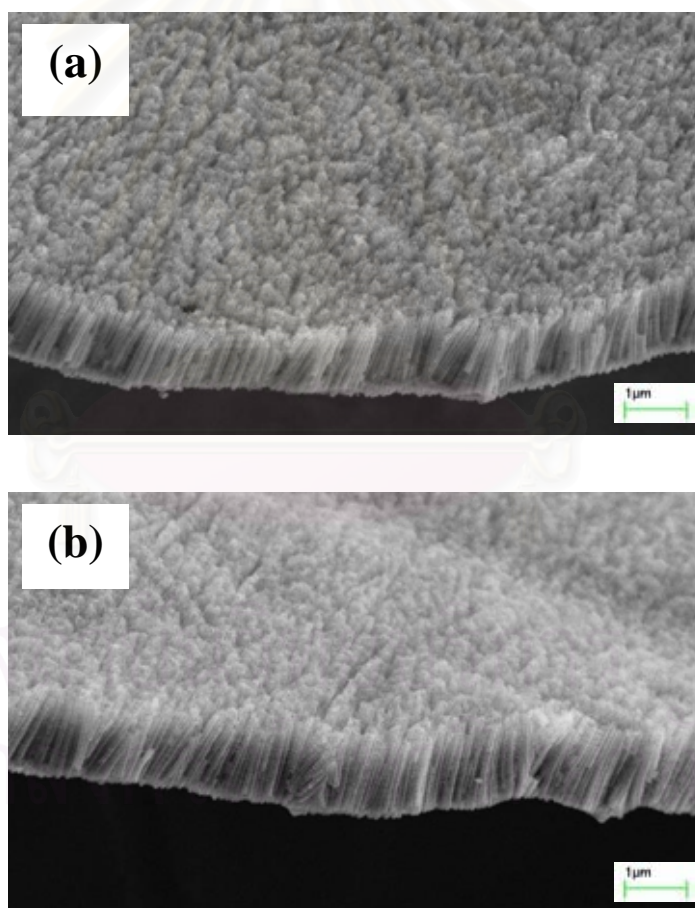


Figure 4.10 Comparison of the lengths of TiO_2 nanotubes as probed by cross-sectional SEM. The nanotube arrays were prepared by anodization of Ti foil at 20 V for 5 h in (a) 0.15 M NH_4F + ethylene glycol: H_2O (90:10) and (b) 0.36 M NH_4F + ethylene glycol: H_2O (90:10).

4.2.2 W/WO₃ prepared by anodization

4.2.2.1. Anodic growth of WO₃ films: variables

Table 4.12 Anodization conditions, photoelectrochemical performance and morphology of nanoporous WO₃ in this study

entry no.	electrolyte, medium modifier	anodization voltage, time	$j_{ph}/\text{mA cm}^{-2}$ ^{a)}	morphology ^{b)}
1	0.15 M NaF	20 V, 3 h	0.99	pre-nanohole
2	„	40 V, 3 h	2.14	nanohole
3	„	60 V, 3 h	2.82	nanoporous
4	„	80 V, 3 h	2.54	nanoporous
5	„	60 V, 1 h	3.21	nanoporous
6	„	60 V, 2 h	3.93	nanoporous
7	„	60 V, 3 h	2.82	nanoporous
8	„	60 V, 4 h	2.70	nanoporous
9	„	60 V, 6 h	2.78	nanoporous
10	0.3 M oxalic acid	20 V, 2 h	1.98	compact film
11	„	40 V, 2 h	2.14	partially eroded
12	„	60 V, 2 h	2.62	totally eroded
13	„	80 V, 2 h	2.62	totally eroded
14	„	60 V, 1 h	2.54	totally eroded
15	„	60 V, 2 h	2.62	totally eroded
16	„	60 V, 3 h	2.94	totally eroded
17	„	60 V, 4 h	3.33	totally eroded
18	„	60 V, 6 h	3.89	totally eroded
19	„	60 V, 10 h	4.13	totally eroded
20	0.15 M NaF/ PEG200:H ₂ O (40:60) ^{c)}	20 V, 3 h	1.57 ^{d)}	aggregated
21	PEG400:H ₂ O (40:60)	20 V, 3 h	1.39 ^{d)}	aggregated
22	PEG600:H ₂ O (40:60)	20 V, 3 h	1.38 ^{d)}	aggregated
23	PEG1000:H ₂ O (40:60)	20 V, 3 h	1.30 ^{d)}	aggregated
24	0.15 M NaF/ EG:H ₂ O (40:60) ^{c)}	20 V, 3 h	1.23	aggregated

^{a)} j_{ph} = photocurrent density in 0.5 M Na₂SO₄ at 2.0 V (c.f., Fig. 1)

^{b)} as assessed by SEM

^{c)} PEG = poly (ethylene glycol); the number pertains to the molecular weight; EG = ethylene glycol

^{d)} average value (see appendix A)

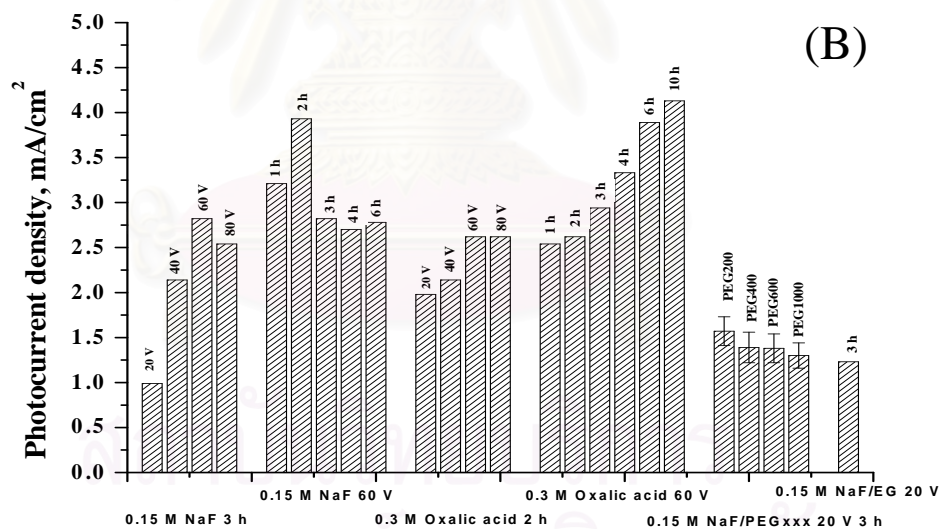
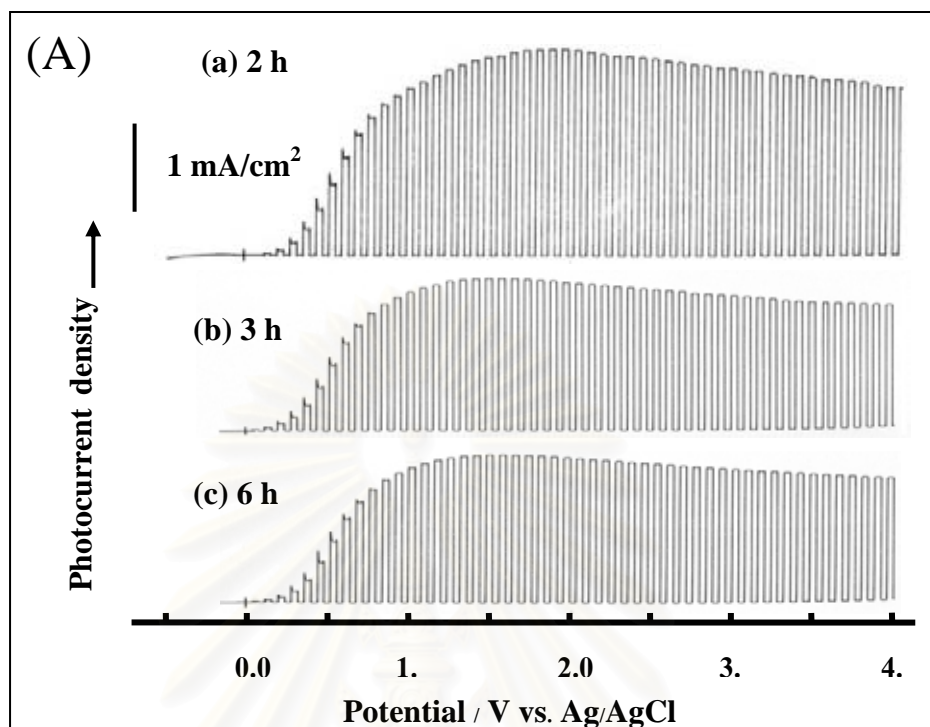


Figure 4.11 (A) Photovoltammograms of nanoporous WO_3 films grown in 0.15 NaF electrolyte at 60 V for (a) 2, (b) 3, and (c) 6 h, respectively. **(B)** Bar diagram comprising of photocurrent density at 2 V for nanoporous WO_3 films grown under various conditions. All the photovoltammograms were obtained in 0.5 M Na_2SO_4 with a scan rate of 2 mV/s using the full output of a 150 W Xe arc lamp.

Table 4.12 summarizes the various conditions used for the W anodization experiments. Thus NaF containing electrolytes were used without (entries 1-9, Table 4.12) and with medium modifiers, namely: poly(ethylene glycol) (PEG) (entries 20-23, Table 4.12) and ethylene glycol (entries 24, Table 4.12). Oxalic acid was also used as the electrolyte in entries 10-19, Table 4.12. Organic additives such as PEG 300 and ethylene glycol have been deployed by Santato *et. al.* (2001) as stabilizers in the preparation of nanoporous WO₃ films by a sol-gel like process.

Figure 4.11 contains representative assessment of the quality of the anodic oxide layers using linear sweep photovoltammetry. Note the excellent rectification quality of the anodic WO₃ layers in this study as diagnosed by the flat baseline response in the “dark” (Fig. 4.11A) over a potential range spanning ~4.0 V. The anodic photocurrents arise from the photooxidation of adsorbed hydroxyl groups or water molecules in the 0.5 M Na₂SO₄ electrolyte.

The photoresponse quality as a function of a given anodization parameter, the photocurrent *density* (photocurrent/surface area of the film) at a fixed potential (2.0 V vs. Ag|AgCl) may be utilized as shown in Fig. 4.11B. Thus, samples grown in 0.15 M NaF for 2 h at 60 V gave excellent photoresponses (approaching 4 mA cm⁻²). Further discussion of these and other data now follows.

4.2.2.2 Effect of anodization voltage

Figure 4.12 shows SEM images of nanoporous WO₂ films prepared in 0.15 M NaF electrolyte for 3 h with anodization voltages of 20 V, 40 V, and 60 V respectively. The oxide film obtained by anodization at 20 V gave a “nanohole” morphology for the oxide surface (Fig. 4.12a) while films obtained from an anodization voltage of 40 V showed the entire surface to be made up of a honeycomb of these nanoholes (Fig 4.12b). On the other hand, the oxide layer obtained from an anodization voltage of 60 V (Fig. 4.12c) gave a very porous structure with high surface area. This change in morphology arises from partial to complete to over-etching of the tungsten surface by the fluoride species. This morphological trend directly correlates with the measured photocurrent density on these WO₃ films as shown in Fig. 4.11B. The photocurrent density increases with increasing anodization

voltage (up to 60 V). The films prepared at 80 V in 0.15 M NaF electrolyte gave a similar nanoporous structure as those prepared at 60 V (SEM image not shown).

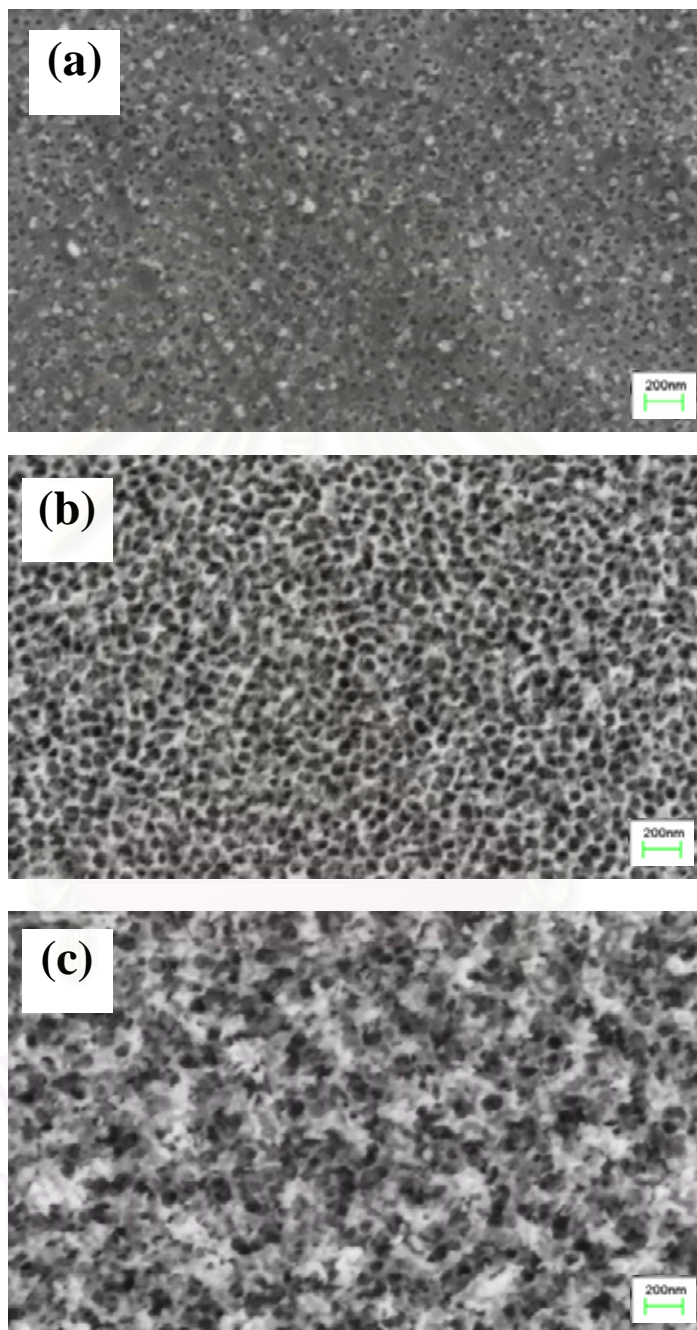


Figure 4.12 Effect of anodization voltage on the morphology of WO₃ nanoporous films as probed by SEM. The films were grown in 0.15 M NaF for 3 h at (a) 20, (b) 40, and (c) 60 V, respectively.

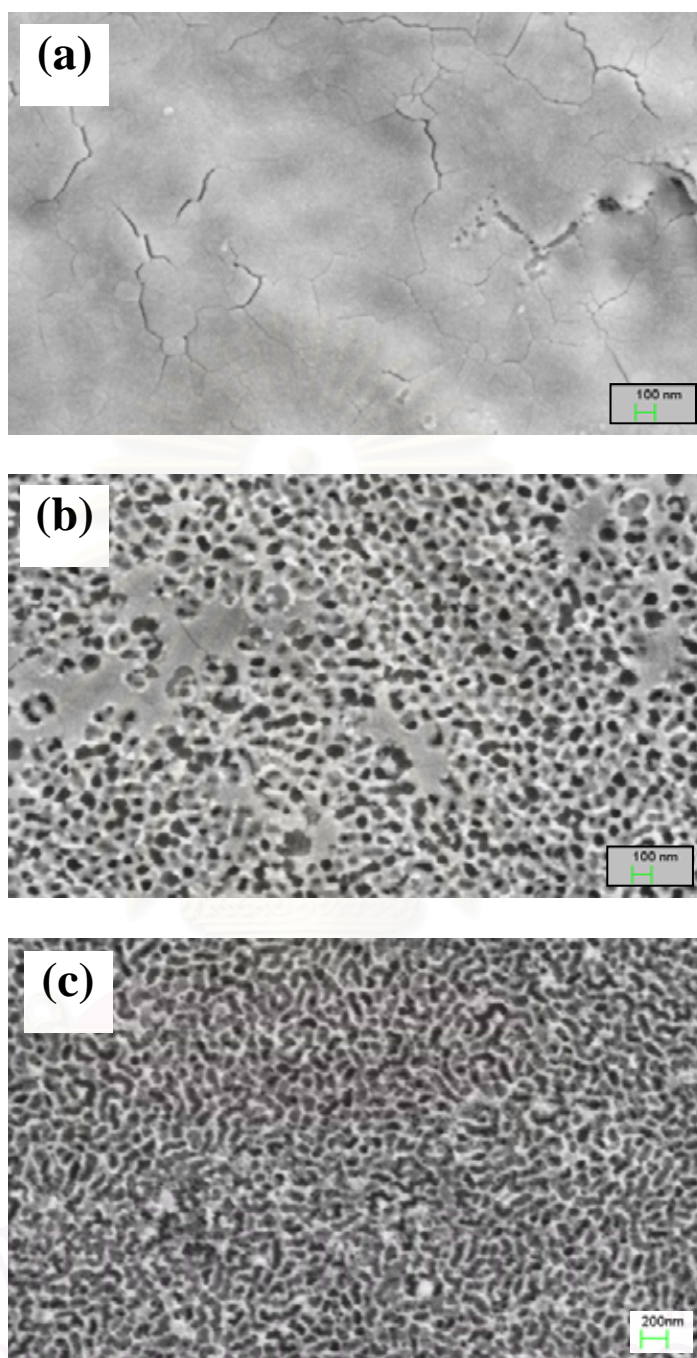


Figure 4.13 Effect of anodization voltage on the morphology of WO_3 nanoporous films as probed by SEM. The films were grown in 0.3 M oxalic acid for 2 h at (a) 20, (b) 40, and (c) 60 V, respectively.

The effect of anodization voltage on the morphology of WO_3 films was also examined in another electrolyte, oxalic acid; the resultant SEM data are shown in Fig. 4.13. At a low anodization voltage of 20 V (Fig. 4.13a) very little etching process can be seen while at a medium anodization voltage of 40 V (Fig. 4.13b) a partially carved oxide layer structure is seen. A higher anodization voltage of 60 V (Fig. 4.13c) yielded a totally etched-in oxide layer with a “brain-like” morphology. Oxide films prepared at 80 V in 0.3 M oxalic acid electrolyte gave the same nanoporous structure as those prepared from 60 V (SEM image not shown). The photocurrent density measured for these films showed a similar trend like the films prepared in NaF electrolyte (c.f., Fig. 4.11B).

4.2.2.3 Effect of anodization time

The tungsten foils were anodized in 0.15 M NaF electrolyte at 60 V (the optimum anodization voltage as established above) for anodization times of 1, 2, 3, 4, and 6 h, respectively (entries 5-9, Table 4.12). The morphologies for the resultant WO_3 films are shown in Fig. 4.14. In all the cases considered, essentially similar nanoporous morphology was seen for a shorter period of anodization (e.g., 2 h, Fig. 4.14a). Such films yielded the best photocurrent density reaching 3.93 mA/cm^2 . On the other hand, samples obtained after longer periods of anodization such as 4 and 6 h (Figs. 4.14b and 4.14c respectively) show extended etching of the initially formed oxide layer to give particle aggregates. This translates to a corresponding decrease in the photocurrent density, as seen in Fig. 4.11B. Moreover, the effect of anodization time on the morphology of WO_3 films was also examined in oxalic acid electrolyte (entries 14-19, Table 4.12). All films gave similar “brain-like” morphology (SEM image not shown). At low anodization time as 1 h is seem enough to form oxide layer but it worth noting that photocurrent increases with increasing the anodization time. Film obtained from long anodization time as 10 h gave the photocurrent reaching 4.13 mA/cm^2 .

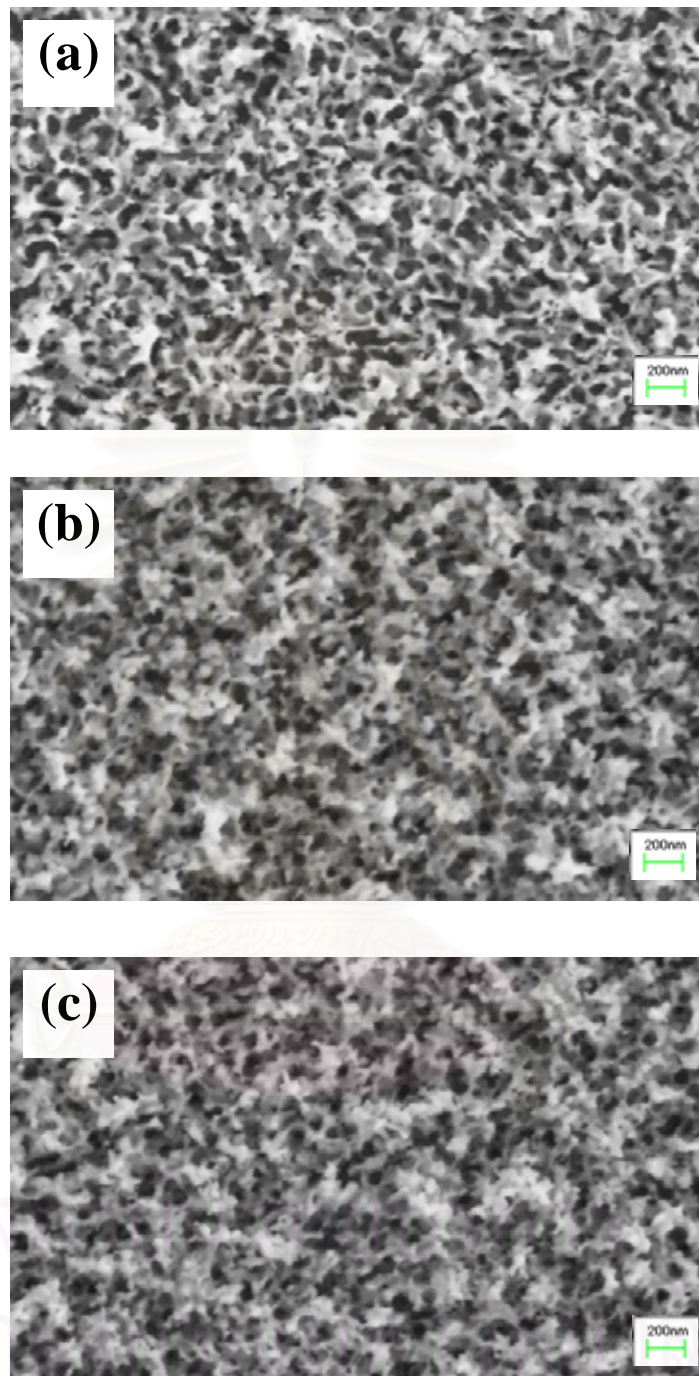


Figure 4.14 Comparison of SEM images of WO_3 nanoporous films obtained by anodization of tungsten foil in 0.15 M NaF at 60 V for (a) 2, (b) 4, and (c) 6 h, respectively.

4.2.2.4 Effect of poly(ethylene glycol) of different molecular weights

Figure 4.15 contains SEM images for WO_3 nanostructures prepared using PEG additive of different molecular weights: PEG 200, 400, 600, or 1000 in 0.15 M NaF electrolyte (60% water plus 40% PEG). In all the cases, the WO_3 films were grown for 3 h at 20 V; the morphology of all these films look similar except for the PEG 1000 case (c.f., Figs. 4.15a-c and Fig. 4.15d)-perhaps a consequence of the slightly higher temperature that was employed for the anodization in this case (Note that PEG 1000 is a solid at room temperature). When the photocurrent densities of these films are compared with a film obtained with those electrosynthesized without the medium modifier (entry 1, Table 4.12), it is seen that the use of PEG as medium modifier enhances the photoelectrochemical response. A similar trend was seen when ethylene glycol (entry 18, Table 4.12) was used as the medium modifier.

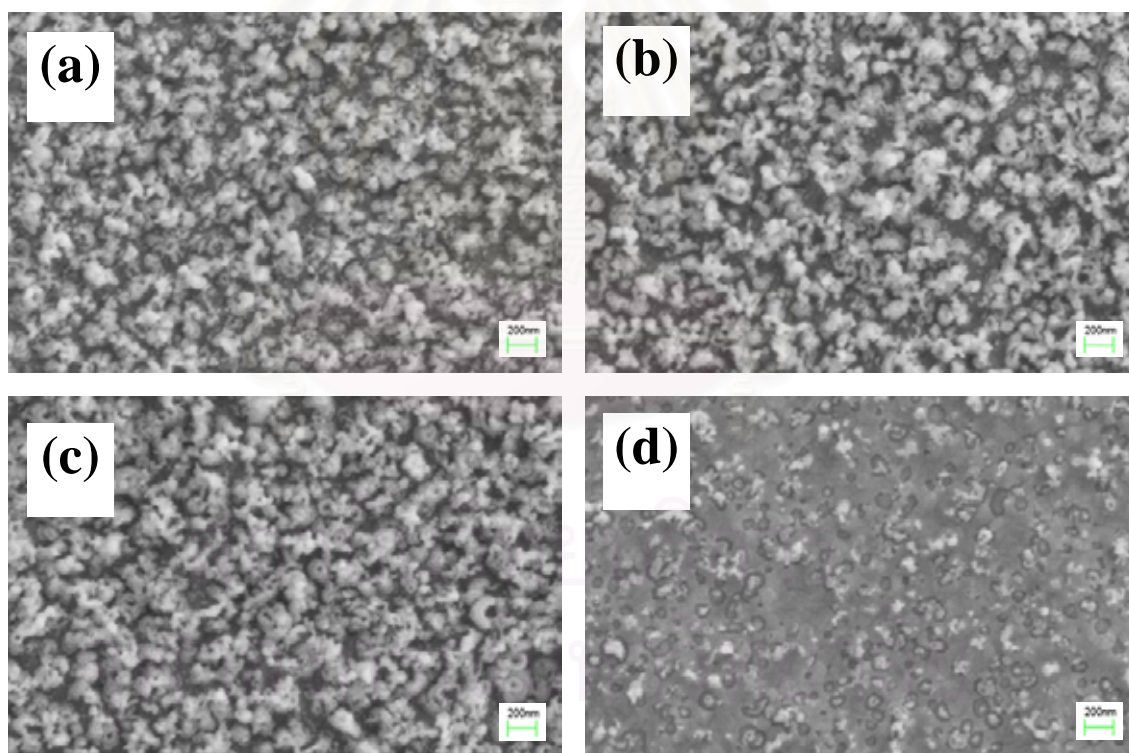


Figure 4.15 Comparison of SEM data for WO_3 nanoporous films obtained by anodization of tungsten foil at 20 V for 3 h in 0.15 M NaF with PEG of different molecular weights: (a) PEG 200, (b) PEG 400, (c) PEG 600, and (d) PEG 1000 with a ratio of PEG: H_2O of 40:60 in each case.

4.2.3 W/WO₃/TiO₂ nanoporous film prepared by pulse anodization

4.2.3.1 Effect of pulsing voltage on morphology of composite W/WO₃/TiO₂ films

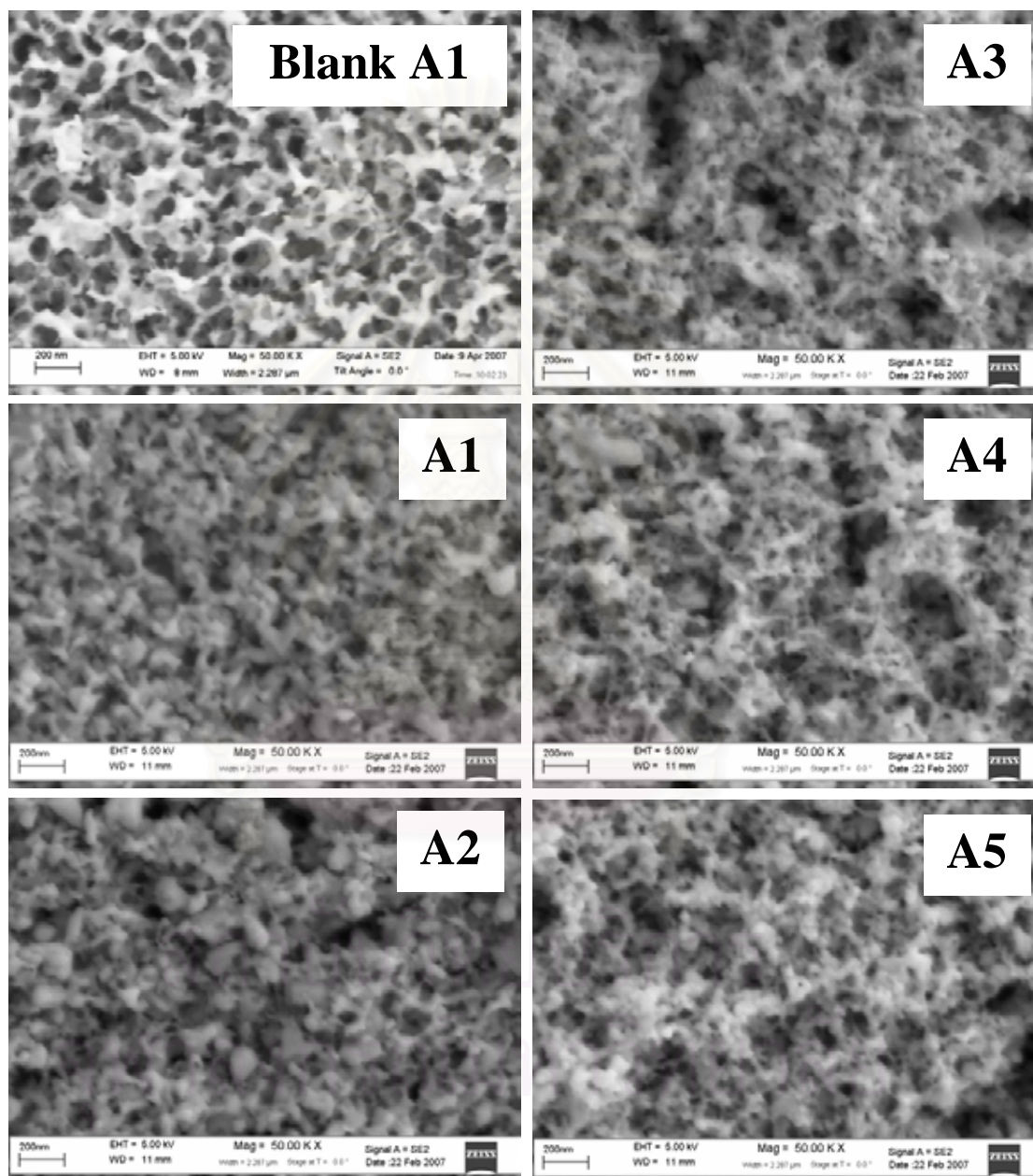


Figure 4.16 SEM images of composite W/WO₃/TiO₂ nanoporous film prepared with initial stage of constant anodization 60 V, 1 h and second stage of pulse waveform (60/-4 V) with different pulsing anodization time (A1) 20 min, (A2) 40 min, (A3) 1 h, (A4) 2 h and (A5) 3 h.

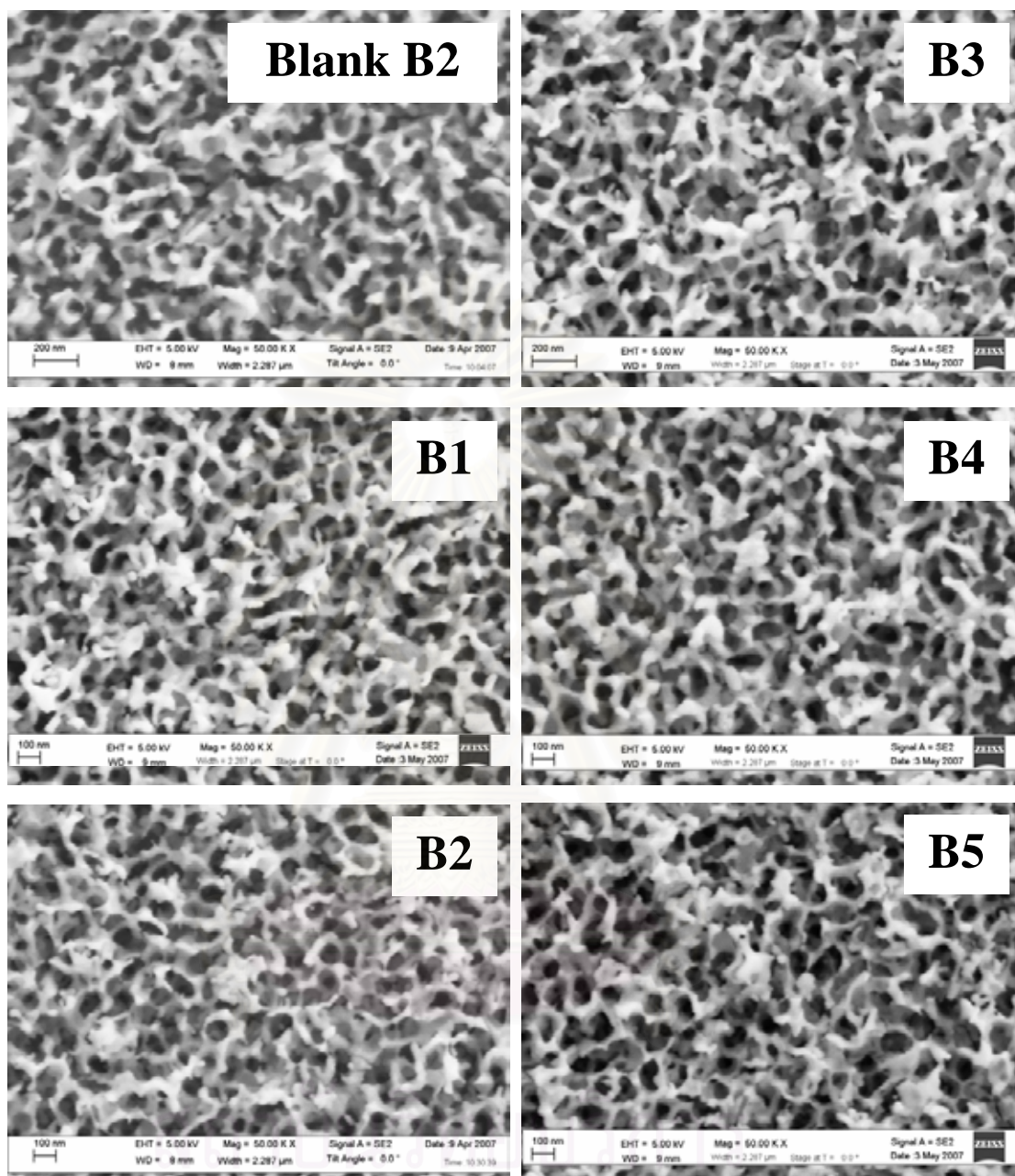


Figure 4.17 SEM images of composite W/WO₃/TiO₂ nanoporous film prepared with initial stage of constant anodization 60 V, 1 h and second stage of pulse waveform (60/0 V) with different pulsing anodization time (B1) 20 min, (B2) 40 min, (B3) 1 h, (B4) 2 h and (B5) 3 h.

Figure 4.16 shows representative SEM images of the top morphology of the W/WO₃/TiO₂ films grown with 60/-4 V waveform perturbation. No highly significant changes are observed on the top morphology although it appears as an increase

roughness due to an overlayer formation consisting of TiO_2 mixed with WO_3 . For the sake of comparison, a WO_3 film (without addition of $\text{TiO}(\text{NO}_3)_2$) was grown with pulsing time of 20 min (Blank A1). The neat WO_3 looks with higher porosity than the composite films.

Figure 4.17 shows SEM of $\text{W}/\text{WO}_3/\text{TiO}_2$ prepared similarly that in Figure 4.16 but with a 60/0 V waveform. The neat WO_3 is also included for a 40 min pulsing time (Blank B2). The surface morphology of these films shows larger pores than in Figure 4.16. The effect of pulsing time is manifested through increase carving with larger and larger holes, likely pointed out to a chemical attack occurring more intensely as the pulsing time increases. In fact during the lower potential of the waveform, the electrochemical growth of WO_3 (occurring at 60 V) is cancelled out and only chemical reaction with F^- and the cathodic electrodeposition of TiO_2 can take place.

4.2.3.2 Effect of pulsing voltage on photoelectrochemical performance of composite $\text{W}/\text{WO}_3/\text{TiO}_2$ films

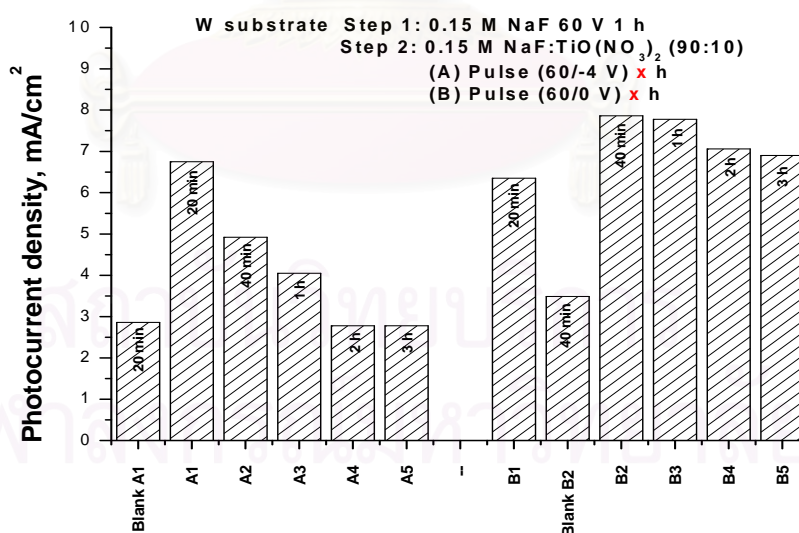


Figure 4.18 Bar diagram comprising of photocurrent density at 2 V for composite $\text{W}/\text{WO}_3/\text{TiO}_2$ films grown under various conditions. All the photovoltammograms were obtained at 0.1 Hz chopped irradiation in 0.5 M Na_2SO_4 with a scan rate of 2 mV/s using the full output of a 150 W Xe lamp.

For the films shown in Figs. 4.16 and 4.17, the photocurrent density in 0.5 M Na_2SO_4 at 2.0 V is shown as a bar plot in Fig. 4.18. For 60/-4 V waveform perturbation, best performance was obtained when applied for 20 min and longer time decreases the photocurrent performance. Importantly, due to the 20 min pulsing time in the present of TiO_2 precursor the photocurrent performance was found to increase for more than double. For the films grown with 60/0 V pulsing waveform the best photocurrent performance was obtained with 40 min pulsing time and longer pulsing times decrease the performance only slightly. A 40 min pulsing for a neat WO_3 gave photocurrent significantly lower (see Fig. 4.18). This behavior contrasts with that of films grown with the 60/-4 V in which longer times decreases the photocurrent performance more dramatically. Apparently, the pulsing at -4 V is associated with the decreased performance. An excessive electroreduction of TiO_2 precursor at -4 V is likely associate with these results.

During the pulsing waveform at the lower potential limit the growing films becomes dark blue which indicated the formation of a tungsten bronze (Na_xWO_3) in which Na^+ is intercalated in the oxide film. In fact the intensity of the blue coloration is higher when using pulses at -4 V than at 0 V. During the pulses at -4 V the hydrogen evolution reaction is clearly observed as bubbles coming out of the film. Contrast at 0 V, hydrogen evolution is not visually observed. As a consequence of the hydrogen evolution reaction the pH at film/electrolyte interface increases and therefore a decrease in the acidity attack is expected in films prepared with pulsing at -4 V. The H_2 evolution at -4 V is expected also to contribute to the film roughness as observe in Fig. 4.16.

It's worth to mention that as the conduction band position of WO_3 is located at ca. 0 V (vs. Ag/AgCl) at neutral pH, in the pulse anodization procedure, the pulsing at 0 V would make the WO_3 conductive in dark (direct polarization), but when pulsing is at -4 V, the WO_3 is not only in direct polarization but also able to intercalate Na^+ and be electroreduced to its related bronze structure.

Photocurrent potential profiles for selected W/ WO_3 / TiO_2 grown under the two pulsing waveforms are compared in Fig. 4.19. Observe that the photocurrent onset is dominated by the WO_3 component in the film.

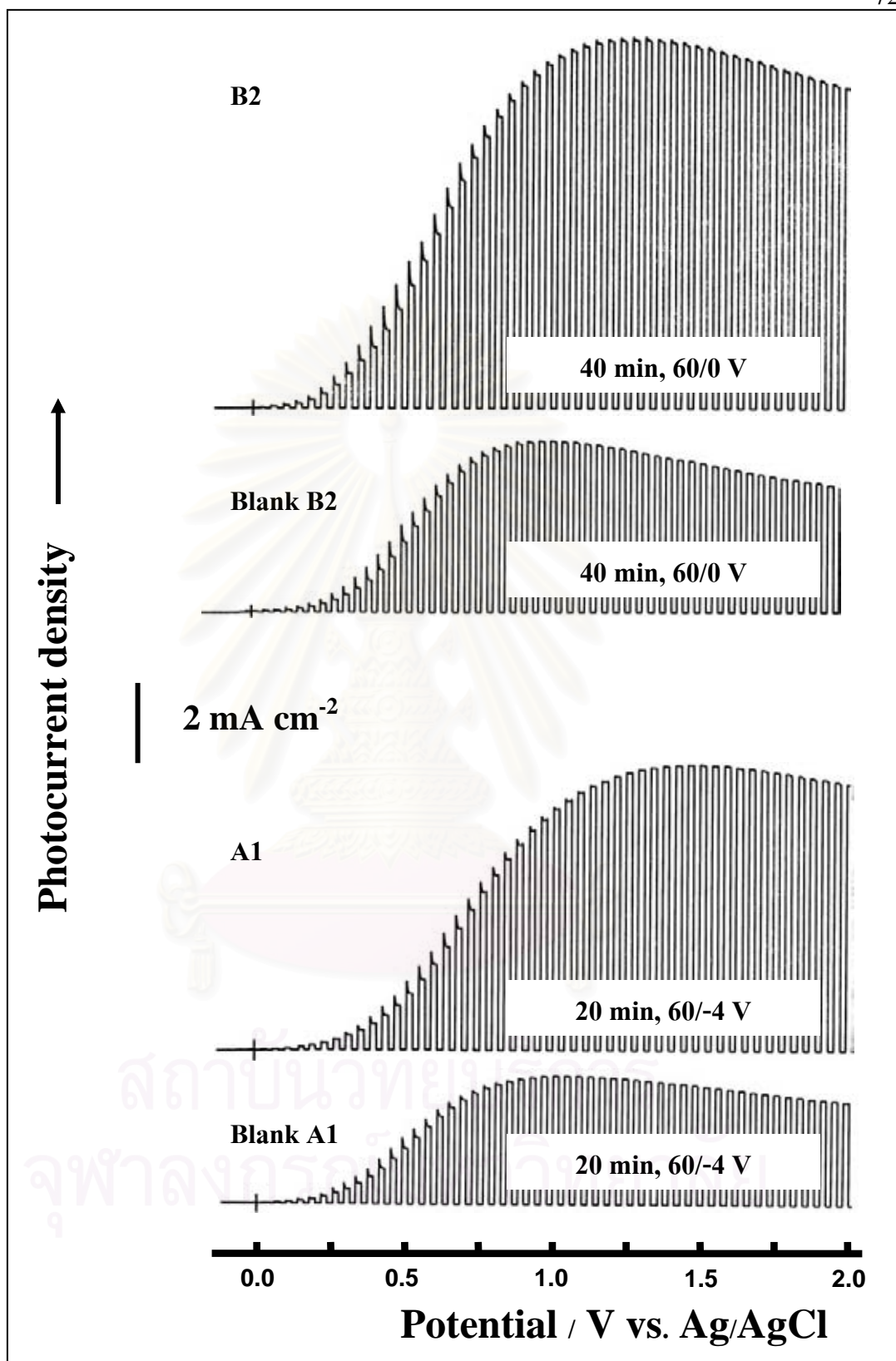


Figure 4.19 Photovoltammograms for selected $\text{W}/\text{WO}_3/\text{TiO}_2$ grown under the two pulsing waveforms (60/-4 V and 60/0 V) compare with neat WO_3 .

The two best photocurrent performance in Fig. 4.18 were found to contain a W:Ti % atom ratio of 96.6:3.4 for film A1 and 94.5:5.5 for film B2 as determined by XPS quantitative analysis . The solution for film preparation contained a 10 % of the TiO₂ precursor in both cases.

It is surprising how a lower percent of TiO₂ is bringing about a ca. 100 % increase in the photocurrent but keep in mind that XPS analyzes only the film surface and more TiO₂ could be at internal parts of the films. We ascribe the better performance to a very efficient e⁻-h⁺ separation that inhibits surface recombination. It is also very interesting the comparison of photocurrent potential profiles of films prepared with the two pulsing waveforms. While the W/WO₃/TiO₂ film obtained with 60/-4 V behave practically emulating the pristine WO₃ film at potential 0.75 V, at higher potential the photocurrent increases to almost the double. This behavior is different that for films prepared with 60/0 V in which a neat increased of the photocurrent of W/WO₃/TiO₂ film is observed at all the potentials when compared to the respective WO₃ films.

4.2.4 Ti/TiO₂/WO₃ nanoporous film prepared by pulse anodization

4.2.4.1 Effect of pulsing voltage on morphology of composite

Ti/TiO₂/WO₃ films

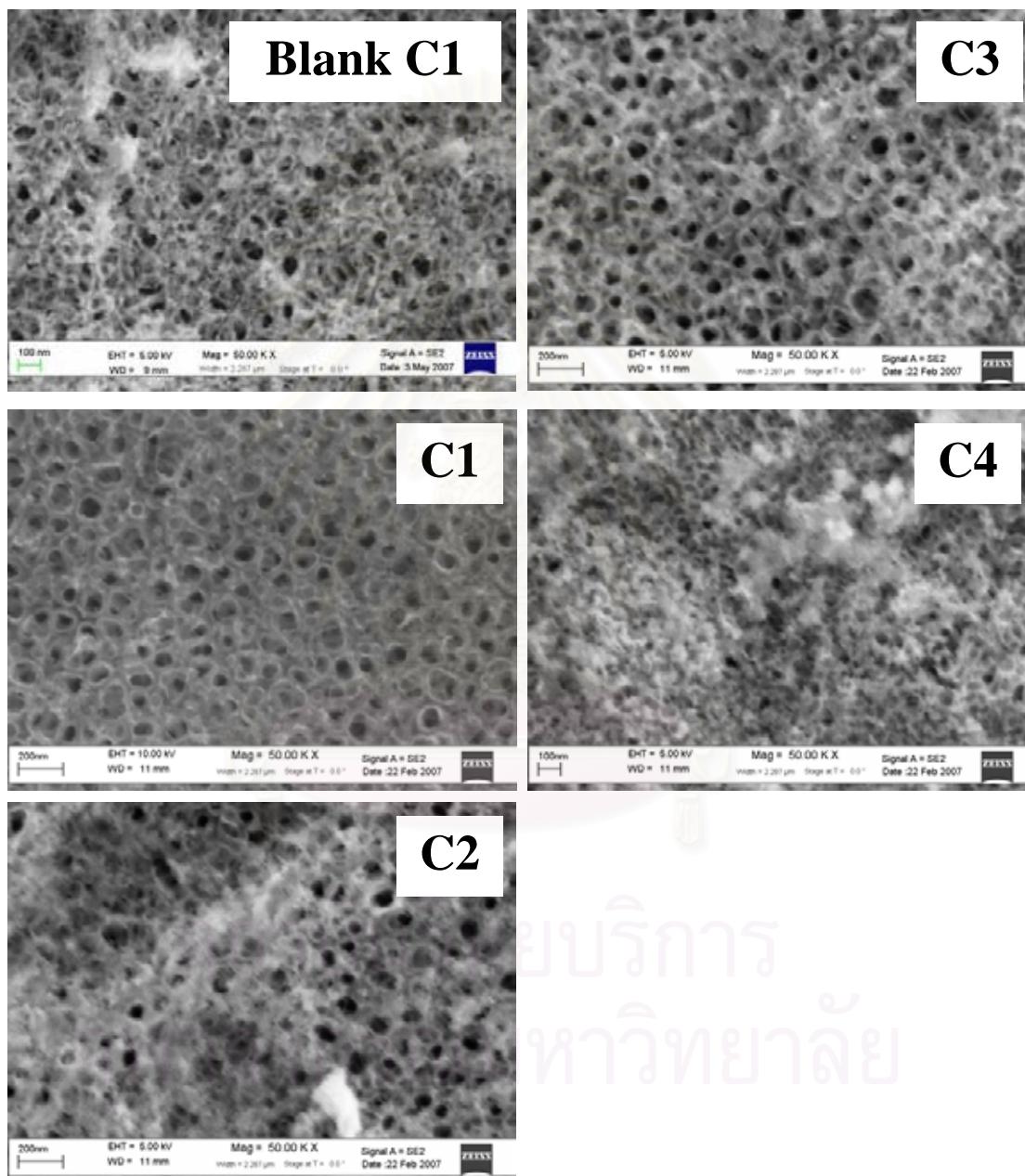


Figure 4.20 SEM images of composite Ti/TiO₂/WO₃ nanoporous film prepared with initial stage of constant anodization 20 V, 30 min and second stage of pulse waveform (20/-4 V) with different pulsing anodization time (C1) 30 min, (C2) 1 h, (C3) 2 h and (C4) 3 h.

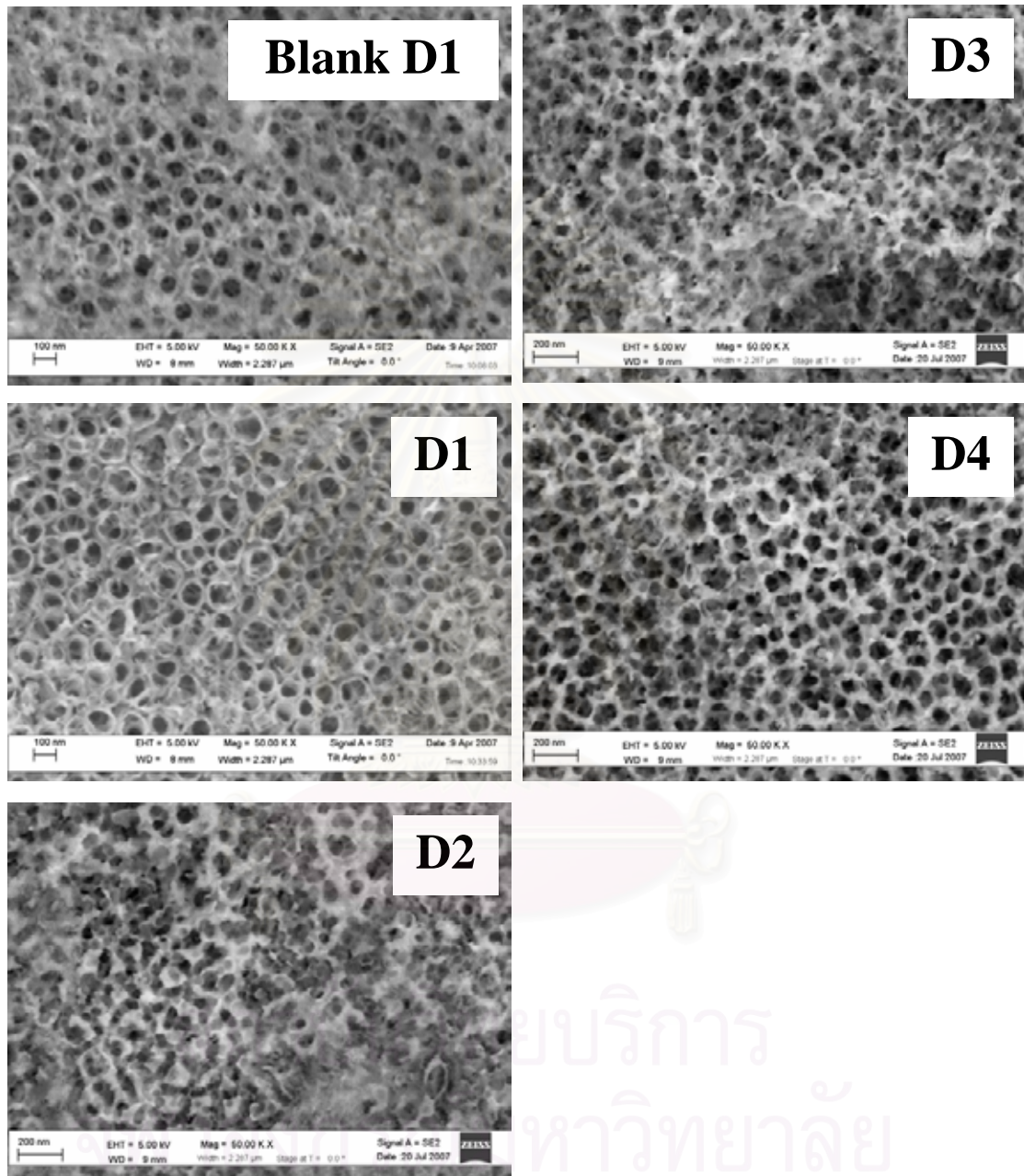


Figure 4.21 SEM images of composite Ti/TiO₂/WO₃ nanoporous film prepared with initial stage of constant anodization 20 V, 30 min and second stage of pulse waveform (20/0 V) with different pulsing anodization time (D1) 30 min, (D2) 1 h, (D3) 2 h and (D4) 3 h.

In this part, TiO₂ nanoporous films were formed at 20 V during 30 min in 0.15 M NH₄F and then the films were subjected to a pulsing waveform of 20/-4 V or 20/0 V for pre-selected times in a solution containing a 10% by volume of WO₃ precursor. The perturbation waveform consisted as in the previous case of 3 min at the positive potential and 15 s at the lower one. At variance with the growth of WO₃ the resulting morphology for TiO₂ (Fig. 4.20) is more ordered showing self organized nanotubes. The duration of the pulsing waveform affect the top morphology of the film. For 20/-4 V pulsing, longer times showed a more complete overlayer on a top of the TiO₂ nanotubes. For 30 min pulsing, the nanotubes are almost empty at their top but at 1 h and 2 h more filling is observed. Finally at 3 h a completely covered surface is observed in which the nanotubes are not visible anymore.

For 20/0 V pulsing (Fig. 4.21) the duration of the pulsing changes the morphology from that of the typical TiO₂ nanotubes (For instance, as seen in the film prepared with 30 min pulsing) to that of an overlayer with the characteristic morphology of WO₃ (at 3 h pulsing). In fact comparing the SEM for 3 h pulsing with that of Fig. 4.17 for WO₃ without TiO₂ precursor, the similarity is clear. The evolution of the surface morphology is indicating that at the lower potential of the pulsing WO₃ is electrodeposited at least at the external part of the film. Besides at the higher potential (20 V) the growth of TiO₂ occurs internally at Ti/TiO₂ interface and thus the TiO₂ growth could not be visible from top images of films.

4.2.4.2 Effect of pulsing voltage on photoelectrochemical performance of composite Ti/TiO₂/WO₃ films

Figure 4.22 compares in a bar plot the photocurrent performance for the films shown in Figures 4.20 and 4.21. The left side of the plot corresponds to 20/-4 V and the right end to 20/0 V. In each group a blank sample obtained under the same experimental conditions of the best performance for the Ti/TiO₂/WO₃ composite but prepared without the WO₃ precursor is also included. The effect of the pulse duration is observed to bring about a decrease in the photocurrent performance in both pulsing waveforms. Besides, the benefit of the uptake of WO₃ by the TiO₂ nanotubes is not quite significant in relation to the enhancement in photocurrent performance and contrasting with the results obtained for Ti/TiO₂/WO₃ composite (see Fig. 4.22).

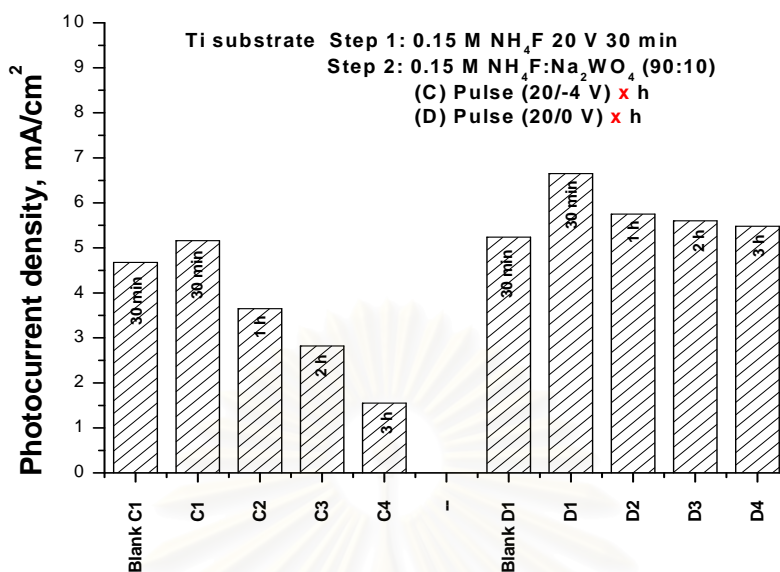


Figure 4.22 Bar diagram comprising of photocurrent density at 2 V for composite $\text{Ti}/\text{TiO}_2/\text{WO}_3$ films grown under various conditions. All the photovoltammograms were obtained at 0.1 Hz chopped irradiation in 0.5 M Na_2SO_4 with a scan rate of 2 mV/s using the full output of a 150 W Xe lamp.

The fact that the internal part of the films is made of a TiO_2 barrier layer is manifested in the photocurrent potential profiles of the $\text{Ti}/\text{TiO}_2/\text{WO}_3$ composite films where the photocurrent onset occurs at ca. -0.4 V (i.e. characteristic of pristine TiO_2 film). Photocurrent potential profiles for selected $\text{Ti}/\text{TiO}_2/\text{WO}_3$ grown under the two pulsing waveforms are compared in Fig. 4.23.

The photocurrent enhancement due to pulsing in the presence of the WO_3 precursor is only ~15 % for 20/-4 V and 22% for 20/0 V. Both enhancement are obtained by comparison with films prepared similarly but without the WO_3 precursor and with a pulsing duration of 30 min. XPS analysis of these $\text{Ti}/\text{TiO}_2/\text{WO}_3$ films gave a Ti:W ratio of 97.8:2.2 for 20/-4 V and 96.8:3.2 for 20/0 V. The better performance of the film with 20/0 V scales with the higher amount of WO_3 .

With respect to the photocurrent performance with Ti/TiO₂/WO₃ films prepared with 20/0 V pulsing, the slightly lower performance at longer times of pulsing might be related to light absorption at the external WO₃ layer (see Fig. 4.21 D4, 3h) that decreases the photoelectron formation at more internal TiO₂ regions. As WO₃ cannot inject the photoelectrons in its TiO₂ companion, the film remains negatively charged (charge storage) but with lower photocurrent performance.

Why Ti/TiO₂/WO₃ composites are less efficient in photocurrent vs. their W/WO₃/TiO₂ counterparts? We expostulated that the behavior is due to the conduction band positions of the two semiconductor components in the composite. As indicated in Fig. 4.24 photogenerated electrons on the TiO₂ are able to be drained to WO₃ but the opposite is not possible, and therefore when the internal part of the film is made of WO₃, all the photoelectrons (be generated on TiO₂ or WO₃) will be able to reach the back contact (W). Contrariety when the internal part is TiO₂, the electrons generated on WO₃ are not able to reach the back contact due to the barrier imposed by the TiO₂. It is for this reason that the photocurrent performance in Ti/TiO₂/WO₃ composites is not significantly different that the TiO₂ itself. Even more, the photocurrent efficiency is seen decreasing with the pulsing duration, more in the case of 20/-4 V than for 20/0 V. It was reported that TiO₂ films decrease their photoactivity by polarization at negative potentials of the flat band potential (conduction band edge) and it is likely that this is the reason for the lower performance of those films formed with 20/-4 V pulsing.

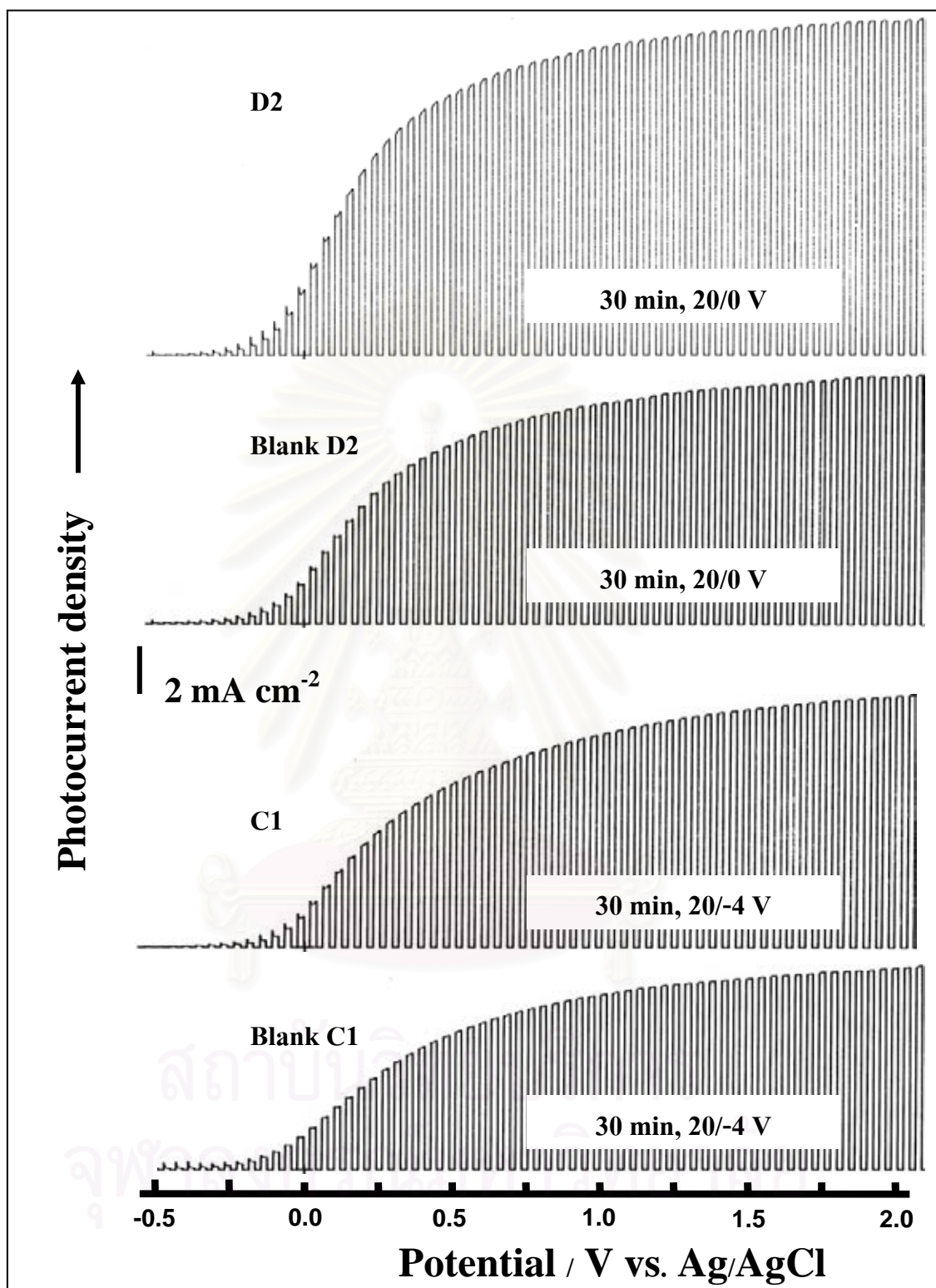


Figure 4.23 Photovoltammograms for selected Ti/TiO₂/WO₃ grown under the two pulsing waveforms (20/-4 V and 20/0 V) compare with neat TiO₂.

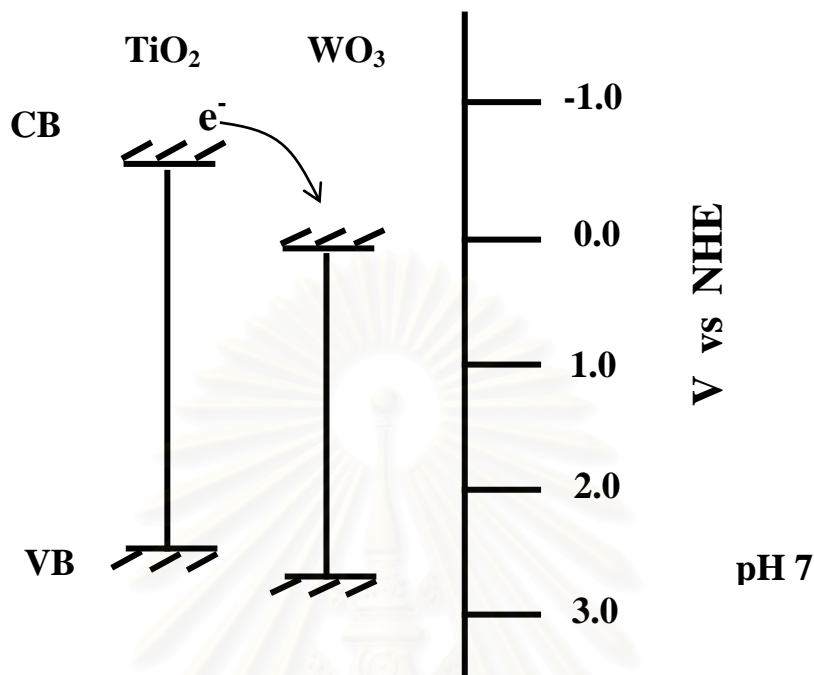


Figure 4.24 Band positions of TiO₂ and WO₃ in solution pH 7.

4.2.5 Effect of electrolyte composition on the resulting W/WO₃/TiO₂ and Ti/TiO₂/WO₃ composites prepared by pulse anodization

4.2.5.1 Effect of electrolyte composition on morphology of W/WO₃/TiO₂ and Ti/TiO₂/WO₃ composites

In this part, different volume ratios of added semiconductor precursors for cathodic electrodeposition of one of them on the other which is simultaneously grown by anodic polarization were studied. Figures.4.25-4.28 show W/WO₃/TiO₂ and Ti/TiO₂/WO₃ prepared with different volume ratio of the anodization electrolyte (NaF for W and NH₄F for Ti) and the corresponding TiO₂ or WO₃ precursor solution for cathodic electrodeposition. Quantitative XPS analysis for the films was shown in Table 4.13.

Table 4.13 Ti:W composition for composite W/WO₃/TiO₂ and Ti/TiO₂/WO₃ films analyzed by XPS analysis

Films	Substrate	Pulsing waveform	Electrolyte composition	% Atom concentration
0.15 M NaF : Ti				
			precursor solution	Ti : W
Fig.4.25 (a)	W	60/-4 V 20 min	100:0	0 : 100
Fig.4.25 (b)	W	„	90:10	3.4 : 96.6
Fig.4.25 (c)	W	„	70:30	4.7 : 95.3
Fig.4.25 (d)	W	„	50:50	0.9 : 99.1
Fig.4.26 (a)	W	60/0 V 40 min	100:0	0 : 100
Fig.4.26 (b)	W	„	90:10	5.5 : 94.5
Fig.4.26 (c)	W	„	70:30	4.2 : 95.8
Fig.4.26 (d)	W	„	50:50	0.1 : 99.9
0.15 M NH₄F : W				
			precursor solution	Ti : W
Fig.4.27 (a)	Ti	20/-4 V 30 min	100:0	100 : 0
Fig.4.27 (b)	Ti	„	90:10	97.8 : 2.2
Fig.4.27 (c)	Ti	„	70:30	92.6 : 7.4
Fig.4.27 (d)	Ti	„	50:50	93.2 : 6.8
Fig.4.28 (a)	Ti	20/0 V 30 min	100:0	100 : 0
Fig.4.28 (b)	Ti	„	90:10	96.8 : 3.2
Fig.4.28 (c)	Ti	„	70:30	95.3 : 4.7
Fig.4.28 (d)	Ti	„	50:50	95.0 : 5.0

สถาบันวิทยบริการ
จุฬาลงกรณ์มหาวิทยาลัย

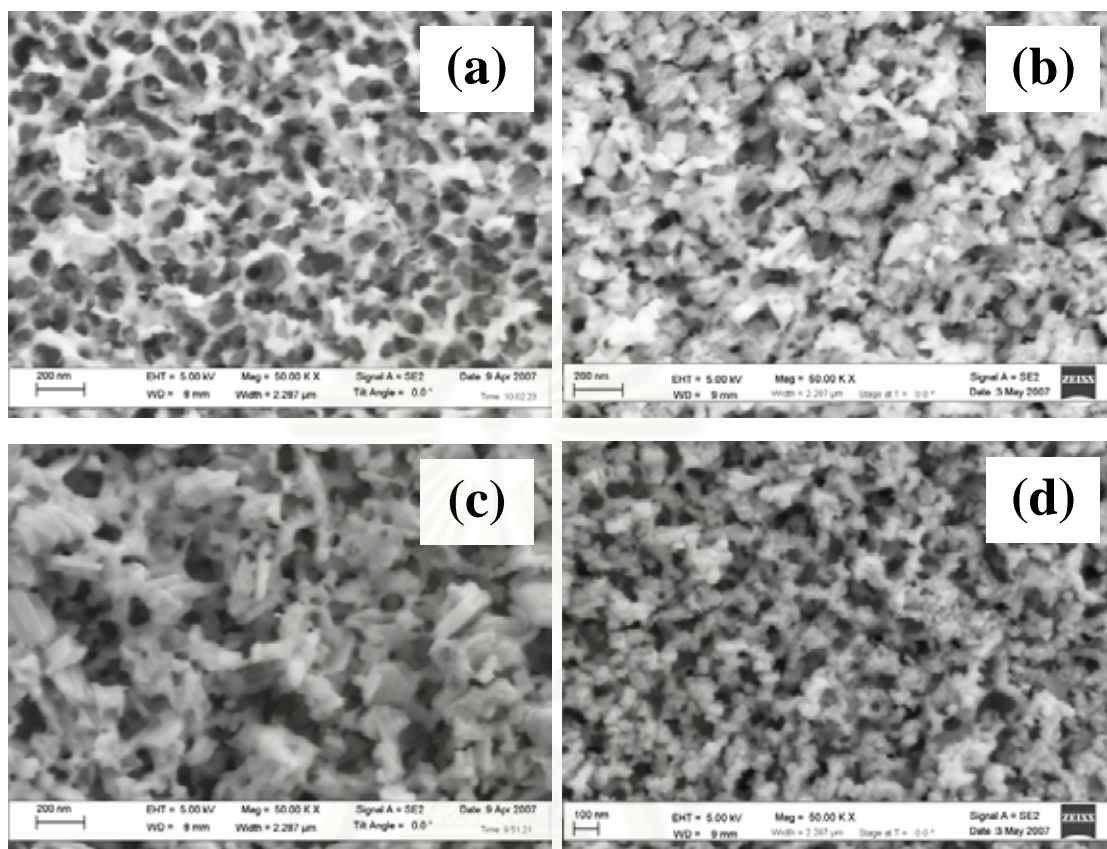


Figure 4.25 Comparison of SEM images of W/WO₃/TiO₂ films grown with initial stage of constant anodization 60 V, 1 h and second stage of pulse waveform 60/-4 V 20 min with different volume ratios of 0.15 M NaF and TiO₂ precursor solution, (a) 100:0, (b) 90:10, (c) 70:30 and (d) 50:50.

Figure 4.25 shows SEM top morphologies of W/WO₃/TiO₂ films grown with 60/-4 V 20 min and four different volume ratios of 0.15 M NaF and TiO₂ precursor solution, that is 100:0, 90:10, 70:30 and 50:50. It is very clear that as the ratio of the titanium solution increases, the surface morphology gets a higher roughness atop the characteristic morphology of the WO₃ films. In fact from 90:10 to 70:30 the ratio Ti:W changes from 3.4:96.6 to 4.7:95.3 as obtained by quantitative XPS analysis.

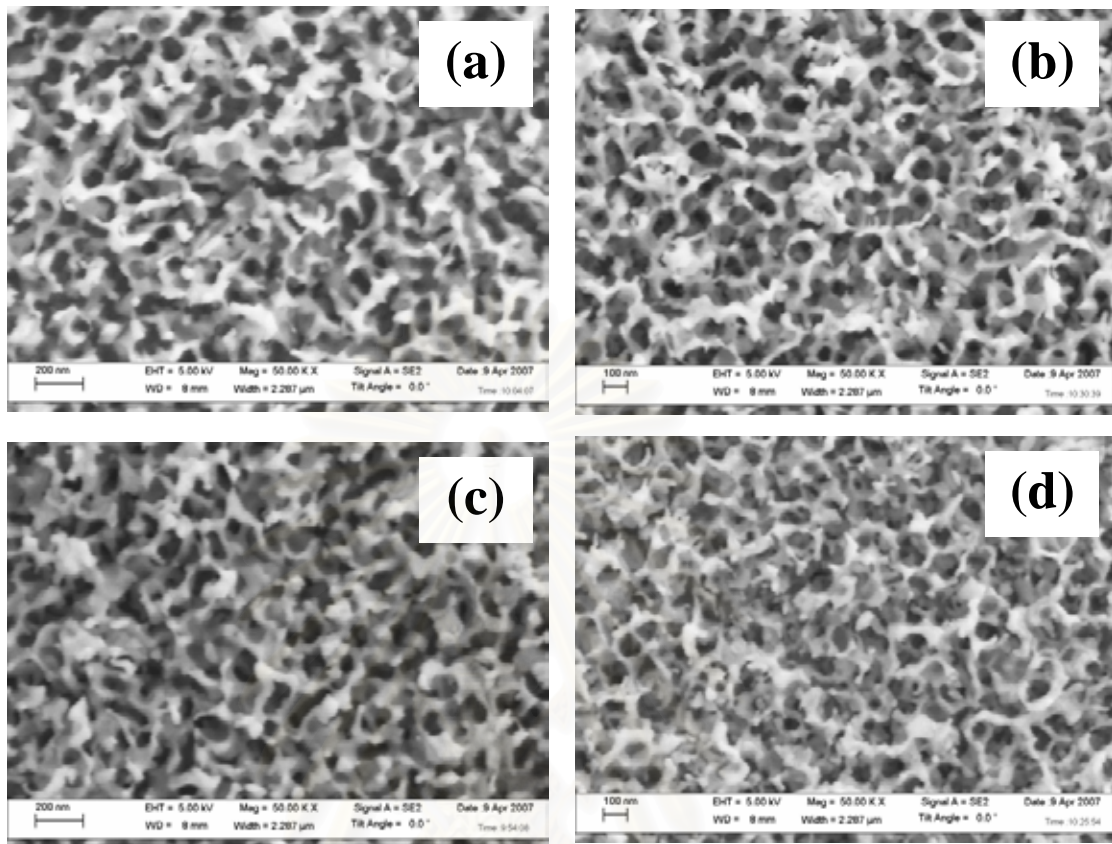


Figure 4.26 Comparison of SEM images of W/WO₃/TiO₂ films grown with initial stage of constant anodization 60 V, 1 h and second stage of pulse waveform 60/0 V 40 min with different volume ratios of 0.15 M NaF and TiO₂ precursor solution, (a) 100:0, (b) 90:10, (c) 70:30 and (d) 50:50.

Figure 4.26 relates to the morphology changes due to cathodic electrodeposition of TiO₂ on WO₃ anodically grown films under different ratio of added titanyl precursor solution and with 60/0 V pulsing for 40 min. The morphology changes due to the solution ratios are less dramatic than that in films shown in Fig. 4.25.

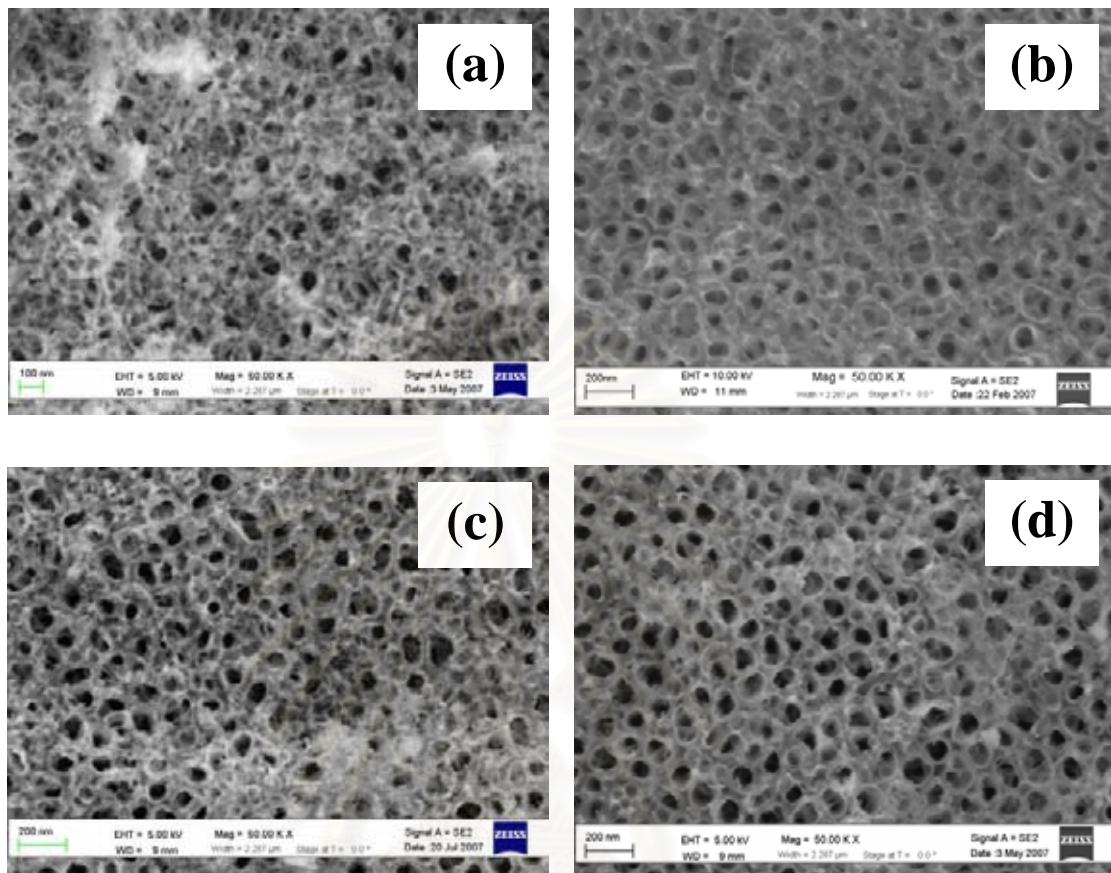


Figure 4.27 Comparison of SEM images of Ti/TiO₂/WO₃ films grown with initial stage of constant anodization 20 V, 30 min and second stage of pulse waveform 20/-4 V 30 min with different volume ratios of 0.15 M NH₄F and WO₃ precursor solution, (a) 100:0, (b) 90:10, (c) 70:30 and (d) 50:50.

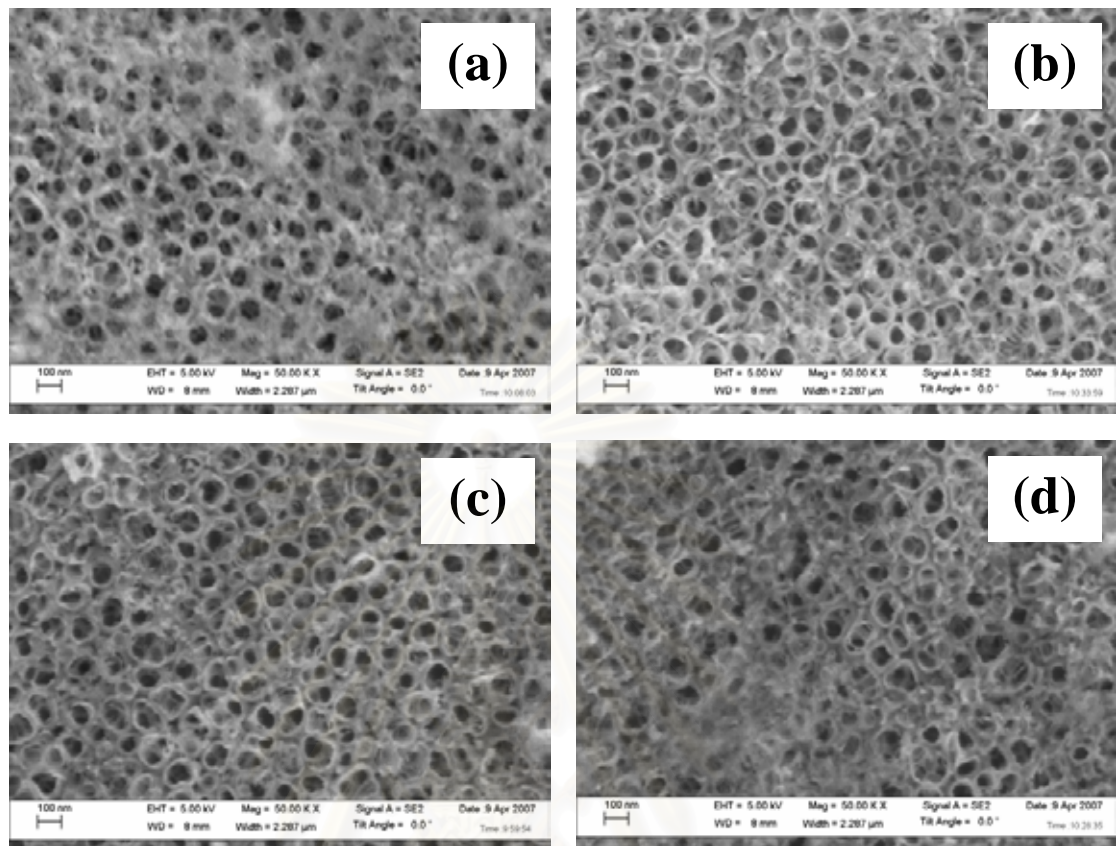


Figure 4.28 Comparison of SEM images of Ti/TiO₂/WO₃ films grown with initial stage of constant anodization 20 V, 30 min and second stage of pulse waveform 20/0 V 30 min with different volume ratios of 0.15 M NH₄F and WO₃ precursor solution, (a) 100:0, (b) 90:10, (c) 70:30 and (d) 50:50.

Figures 4.27 and 4.28 give the evolution of the TiO₂ nanotubes when the same different ratios as in Figs. 4.25 and 4.26 but now with the WO₃ precursor is used in the film preparation. Partially filling of TiO₂ nanotubes are observed in some areas of the films.

4.2.5.2 Effect of electrolyte composition on photocurrent performance of W/WO₃/TiO₂ and Ti/TiO₂/WO₃ composites

A comparison of the effect of electrolyte ratio on the photocurrent performance for the 4 scenarios, i.e. W/WO₃/TiO₂ and Ti/TiO₂/WO₃ at the two pulsing waveform is presented in Fig. 4.29. In the four cases, best performances are obtained with a 90:10 ratio. These performances are always enhanced vs. the pristine case (be WO₃ or TiO₂). Observe that the pulsing time is not the same for the 4 types of films. In fact, the electrolyte ratio was varied after optimizing the pulsing time for best photocurrent performance. Definitely the winner is a W/WO₃/TiO₂ film that was formed with 40 min at 60/0 V giving photocurrents of ca. 220 % higher than a WO₃ film alone. For a 90:10 electrolyte ratio, the W/WO₃/TiO₂ formed with 60/0 V performed better in photocurrent than that formed with 60/-4 V. Similarly, the Ti/TiO₂/WO₃ formed with 20/0 V is better than its counterpart grown with 20/-4 V.

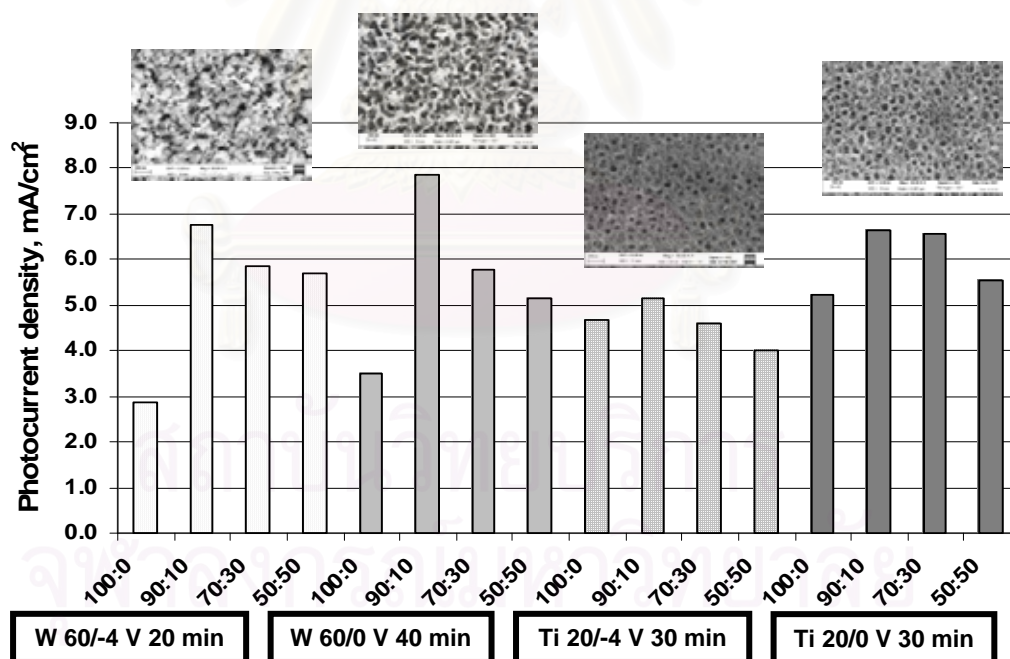


Figure 4.29 Comparison of the effect of electrolyte ratio on the photocurrent performance for W/WO₃/TiO₂ and Ti/TiO₂/WO₃ at the two pulsing waveform.

4.2.6 Ti/TiO₂/WO₃ nanotubes prepared by pulse anodization

4.2.6.1 Effect of constant polarization time and pulsing time on morphology and photoelectrochemical performance of nanotubes Ti/TiO₂/WO₃ films

Ti/TiO₂/WO₃ nanotubes prepared by a 2 step method. The initial growth of TiO₂ nanotubes is performed at constant anodization at 20 V in a PEG400:water mixture (90:10) containing 0.15 M NH₄F. This growth stage was performed for different times from 10 min to 3 h. After this stage was completed a 10 % v/v of WO₃, precursor was added to the electrolytic bath and a pulse waveform of 20/0V was applied for different time from 10 min to 3 h. The total potential perturbation is shown in Figure 3.3. Quantitative XPS analysis for Ti/TiO₂/WO₃ nanotubes films was showed in Table 4.14.

Table 4.14 Ti:W composition for composite nanotubes Ti/TiO₂/WO₃ films analyzed by XPS analysis

Film	Constant anodization	Pulse anodization	% Atom concentration
	20 V	20/0 V	Ti : W
CT1	10 min	10 min	99.75 : 0.25
CT2	„	30 min	99.49 : 0.51
CT3	„	1 h	99.46 : 0.54
CT4	30 min	10 min	99.58 : 0.42
CT5	„	30 min	99.71 : 0.29
CT6	„	1 h	99.65 : 0.35
CT7	1 h	10 min	99.86 : 0.14
CT8	„	30 min	99.62 : 0.38
CT9	„	1 h	99.80 : 0.20
CT10	2 h	30 min	99.74 : 0.26
CT11	„	1 h	99.30 : .070
CT12	„	2 h	98.57 : 1.43
CT13	„	3 h	98.97 : 1.03
CT14	3 h	30 min	99.12 : 0.88
CT15	„	1 h	99.34 : 0.66
CT16	„	2 h	99.26 : 0.74
CT17	„	3 h	98.91 : 1.09

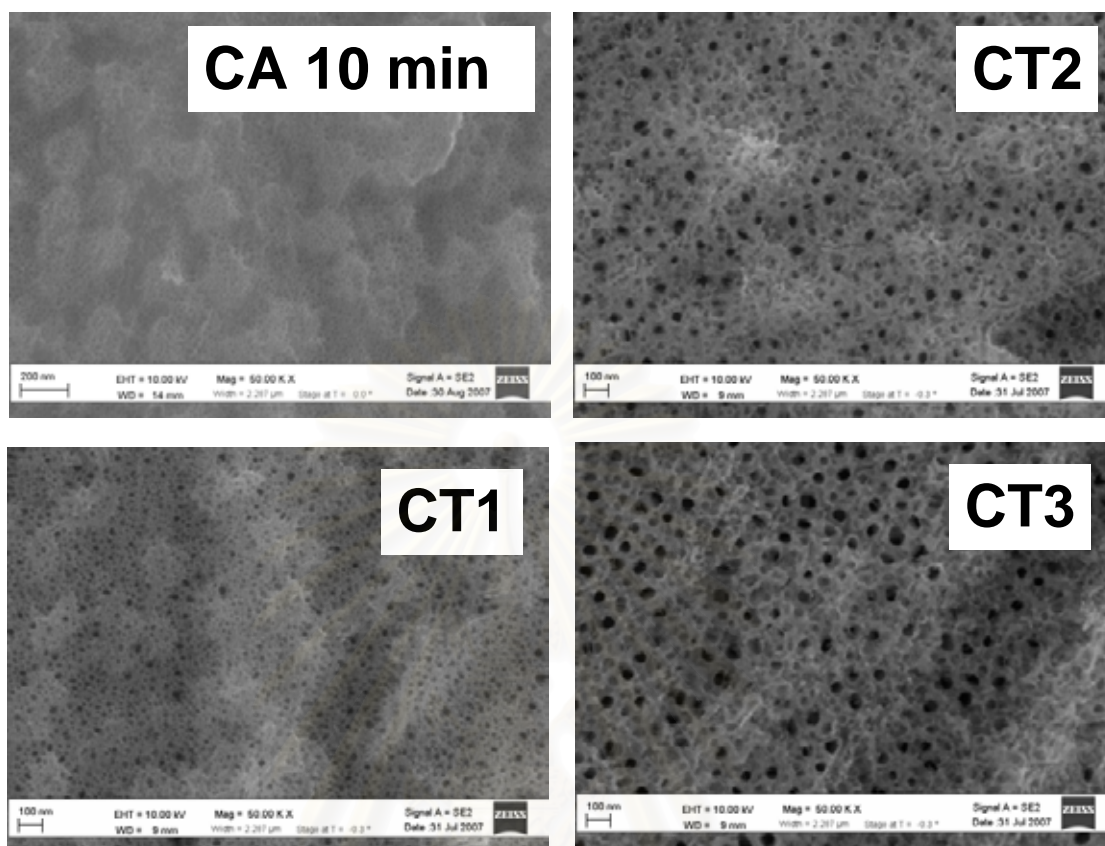


Figure 4.30 Comparison of SEM images of Ti/TiO₂/WO₃ films grown with initial stage of constant anodization 20 V, 10 min (CA 10 min) and second stage of pulse waveform (20/0V) with different pulsing anodization time (CT1) 10 min, (CT2) 30 min, and (CT3) 1 h.

It is very relevant the time at constant potential that brought about the growth of TiO₂ on the Ti substrate. Short times, 10 min (CT1), form a barrier layer of TiO₂ with very small pores (compared with the film grown with only initial stage of constant anodization 20 V, 10 min (CA 10 min)) at the surface of the film that are filled with WO₃ during the pulsing procedure (Fig. 4.30). The pulsing time increases the upper diameter of the pores increases while some areas are seen partially filled (Fig. 4.30 (CT2), (CT3)). This short time growth of TiO₂ does not bring about the formation of TiO₂ nanotubes arrays but allow the uptake of WO₃ in increasing amounts as the pulsing times increases. In fact XPS analysis showed that the percent of W at the top of the films increases from 0.25 to 0.51 and to 0.54 for pulsing times of 10 min, 30 min and 1 h, respectively.

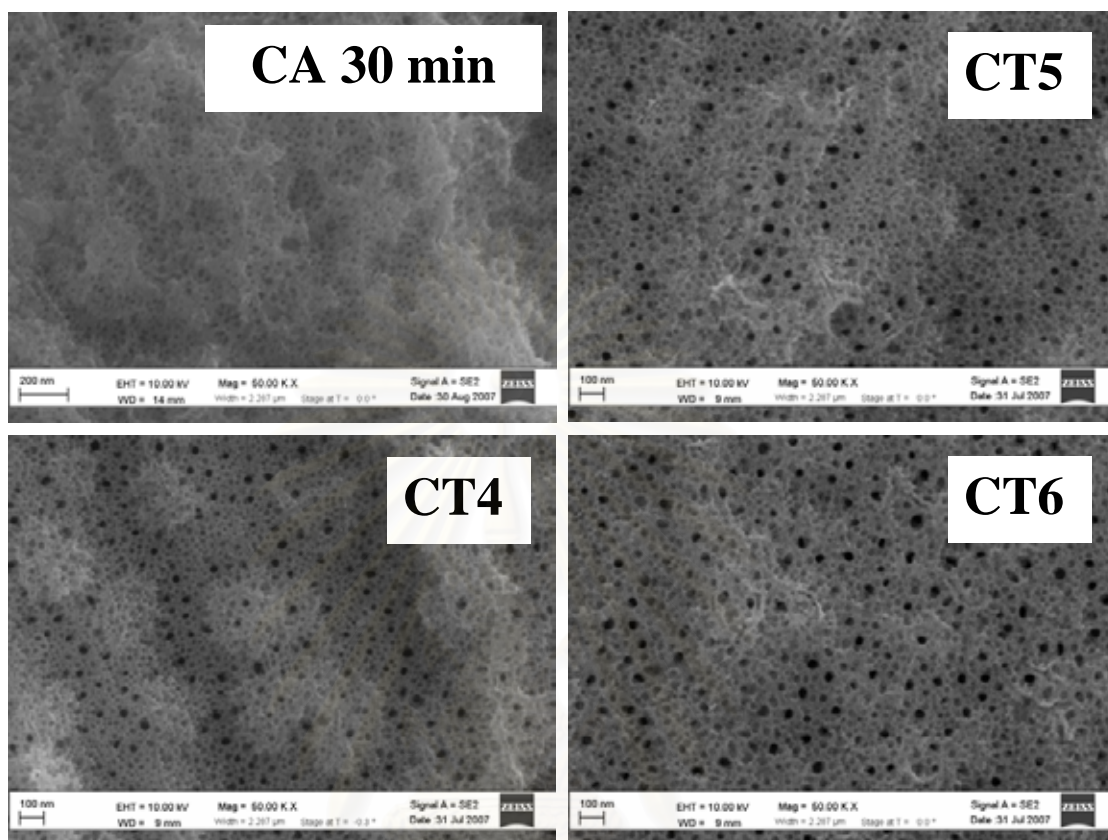


Figure 4.31 Comparison of SEM images of Ti/TiO₂/WO₃ films grown with initial stage of constant anodization 20 V, 30 min (CA 30 min) and second stage of pulse waveform 20/0 V with different pulsing anodization time (CT4) 10 min, (CT5) 30 min, and (CT6) 1 h.

สถาบันวิทยบริการ
จุฬาลงกรณ์มหาวิทยาลัย

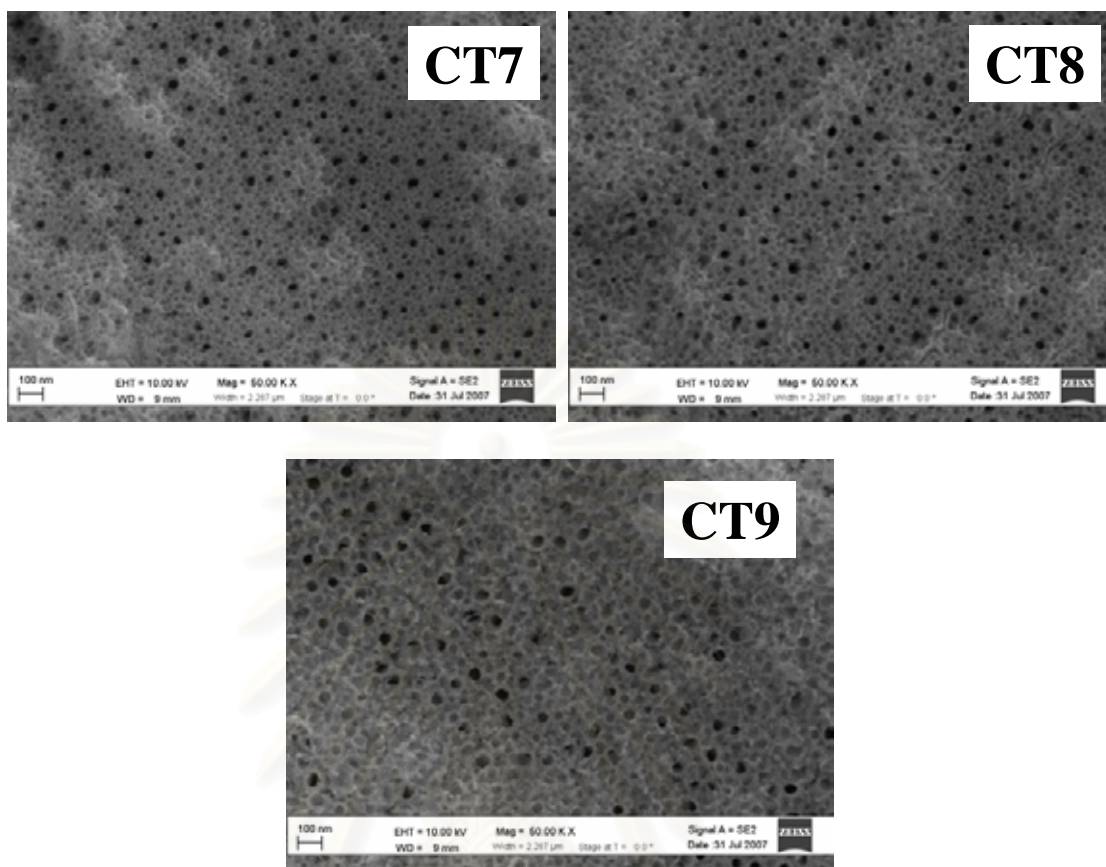


Figure 4.32 Comparison of SEM images of Ti/TiO₂/WO₃ films grown with initial stage of constant anodization 20 V, 1 h and second stage of pulse waveform 20/0 V with different pulsing anodization time (CT7) 10 min, (CT8) 30 min, and (CT9) 1 h.

Figures 4.31 and 4.32 show top morphologies of films prepared with same protocol as in Fig. 4.30 but with longer times of the initial growth of TiO₂. In fact Fig. 4.31 is for 30 min at 20 V and Fig. 4.32 is for 1 h at 20 V. It is very clear that the initial growth time affect the top morphology of the film. For instance, a comparison of images in Figs. 4.30 (CT1), 4.31 (CT4) and 4.32 (CT7) shows that the pore size increases with the constant polarization time. Although films in Figs. 4.31 and 4.32 were grown for longer time than in Fig. 4.30, the percent of W was not increase significantly and in some films even were smaller than in Fig. 4.30. More specifically, film in Fig. 4.32 (CT7) has 0.14 % of W. Higher TiO₂ barrier layer in films prepare with 1 h constant anodization is likely responsible for a lower uptake of WO₃ when

compared to that of 10 min constant anodization. As the lower potential is 0 V, the TiO_2 is not expected to be highly conductive in dark and thus a thicker barrier films will be in detriment of the amount of WO_3 cathodically electrodeposited.

The photocurrent/potential profiles of these $\text{Ti/TiO}_2/\text{WO}_3$ nanotubes (not shown) are very similar to those of pristine TiO_2 nanotubes. The photocurrent onset is at ca. 0.4 V and increasing with a sigmoidal shape reaching a plateau value at ca. 1 V, and keeping at rather constant photocurrent at more anodic potential. This behavior contrasts with that of $\text{W/WO}_3/\text{TiO}_2$ films which were found to define a maximum in the plateau potential region. The photocurrent performance at 2 V for these $\text{Ti/TiO}_2/\text{WO}_3$ films was taken as a figure-of-merit for the film photoconversion efficiency.

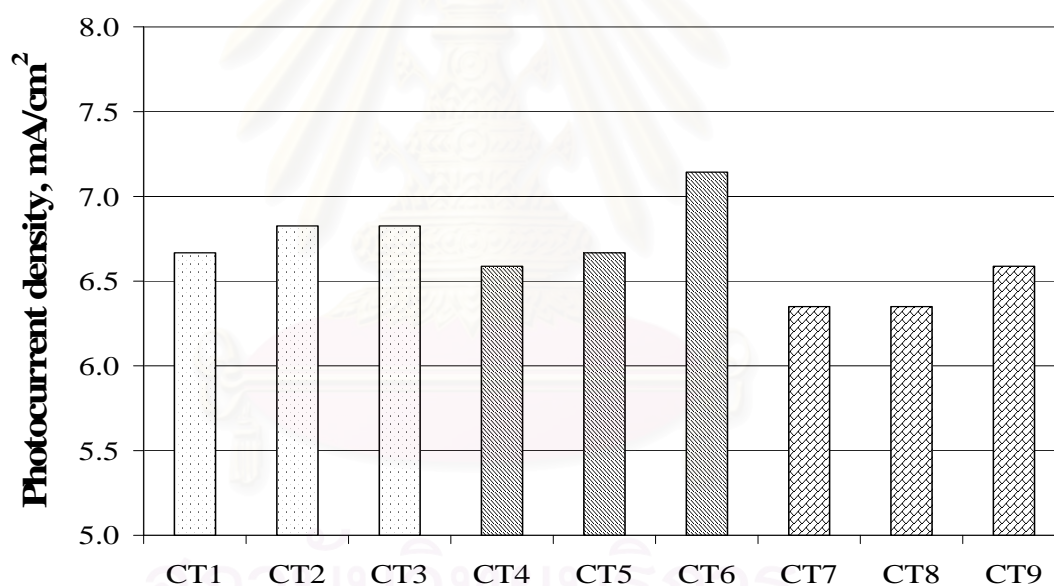


Figure 4.33 Compares photocurrent performance for the films shown in Figures 4.30, 4.31 and 4.32.

Figure 4.33 shows photocurrent performance for the films shown in Figs. 4.30, 4.31 and 4.32. For films prepared with constant anodization of 10 min (films CT1, CT2 and CT3) the photocurrent increases (although slightly) when the pulsing time increases. This behavior also correlates with an increased amount of WO_3 that is likely doping the TiO_2 nanotubes films.

For films prepared with constant anodization of 30 min (films CT4, CT5 and CT6) and 1 h (films CT 7, CT8 and CT9) the photocurrent increases with pulsing time although the amount of WO_3 on the film surface was not found to increase proportionally (see Table 4.14). The rationale for the photocurrent increase should be related to a better film morphology (better order) that promote better $e^- - h^+$ separation and improve directionality of the photoelectron towards the back contact. In summary, a combination of better development of nanotubes and a doping with WO_3 , both processes occurring during the pulsing potential perturbation seems to be responsible for the photocurrent performance which is slightly better than in films prepared without PEG400.

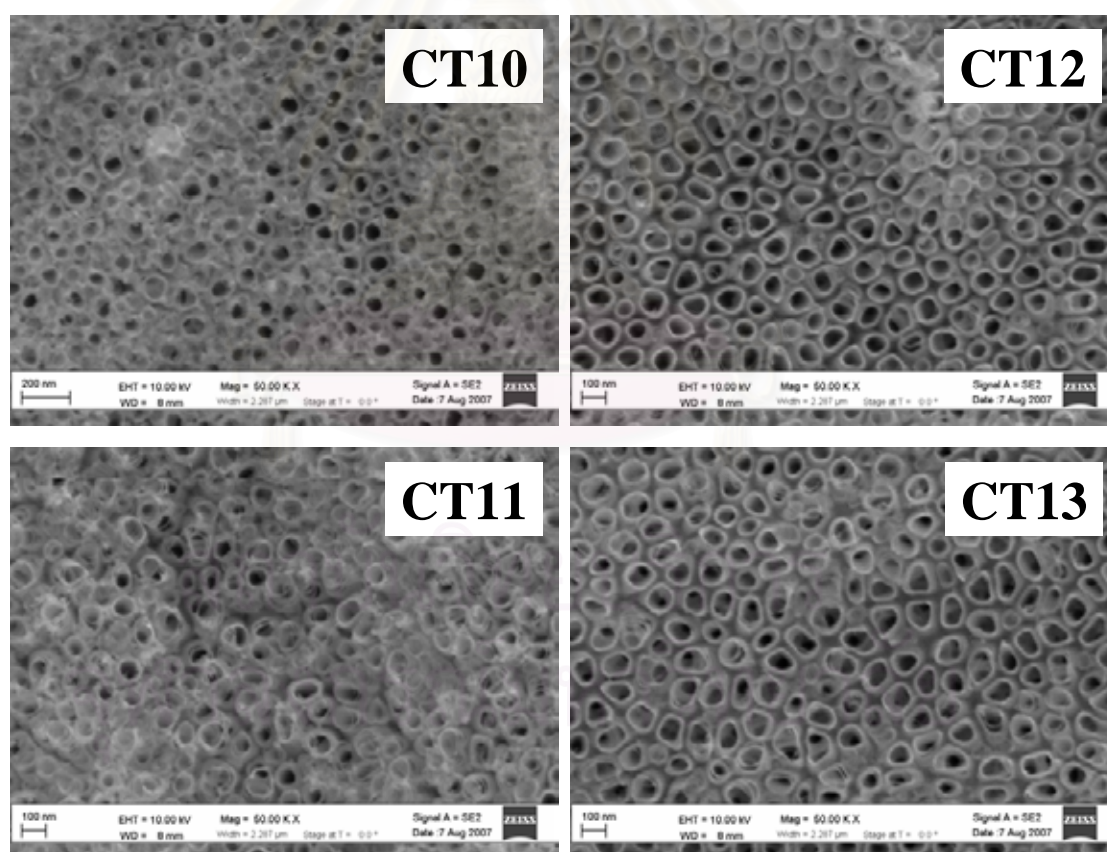


Figure 4.34 Comparison of SEM images of $\text{Ti}/\text{TiO}_2/\text{WO}_3$ films grown with initial stage of constant anodization 20 V, 2 h and second stage of pulse waveform 20/0 V with different pulsing anodization time (CT10) 30 min, (CT11) 1 h, (CT12) 2 h and (CT13) 3 h.

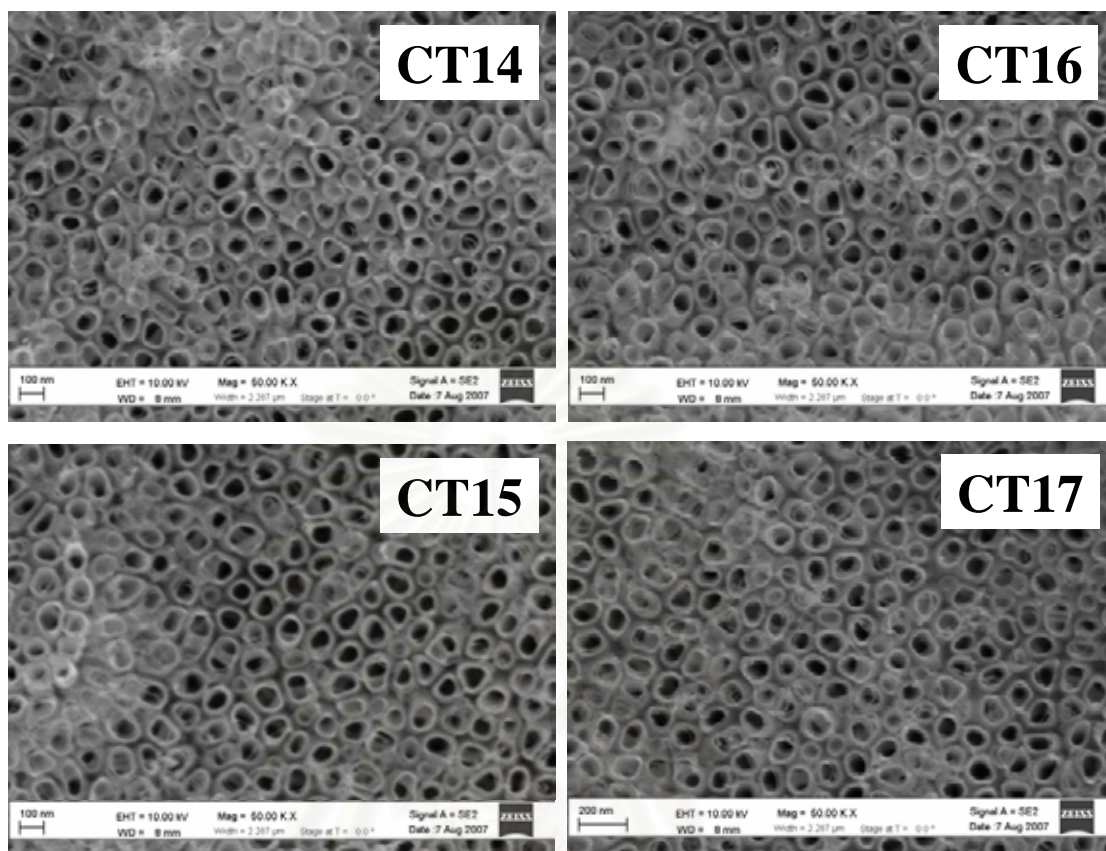


Figure 4.35 Comparison of SEM images of Ti/TiO₂/WO₃ films grown with initial stage of constant anodization 20 V, 3 h and second stage of pulse waveform 20/0 V with different pulsing anodization time (CT14) 30 min, (CT15) 1 h, (CT16) 2 h and (CT17) 3 h.

In order to see more developed TiO₂ nanotubes, increasing of the constant anodization time that is applied previous to the pulsing waveform was studied. Figures 4.34 and 4.35 show top morphology of films prepared with constant anodization time 2 h (films CT10 through CT13) and 3 h (films CT14 through CT17) at 20 V, respectively. In fact the typical nanotube array obtained with PEG400 is now clearly observed and some films areas are showing TiO₂ nanotubes partially or almost totally filled. Film CT11 in Fig. 4.34 is significantly covered in a way that the top of the nanotubes are less clearly distinguished. In none of these images, the nanotubes are fully filled because of the low TiO₂ conductivity at 0 V. However these films performance in photocurrent are better than those in Figs. 4.30, 4.31 and 4.32. This

trend is shown in Fig. 4.36 which contains the photocurrent performance for the eight films presented in Figs. 4.34 and 4.35.

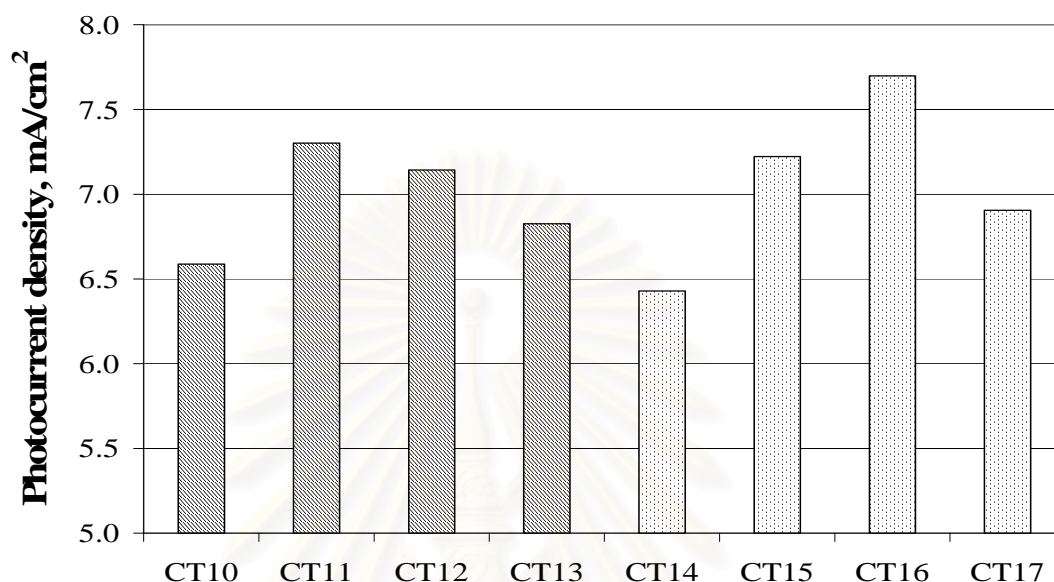


Figure 4.36 Comparison of photocurrent performance for the films shown in Figures 4.34 and 4.35.

The two best films of this series are CT11 and CT16, the latter being better than the former. This finding could present us to conclude that the better efficiency is related to the longer time at 20 V that would bring about longer TiO₂ nanotubes. However, this conclusion is not in agreement with the relative photocurrent behavior of other films that share same pulsing times but different constant anodization times. For instant, films CT10 and CT14 behave as if a longer constant anodization times is not contributing to the photocurrent performance. That would point out that 2 h constant polarization seems enough for photocurrent performance and the pulsing waveform and time is the one determining the performance. Apparently the pulsing waveform should be applied for periods no longer than the constant anodization. In previous studies we have found that TiO₂ nanotubes grown by pulsing polarization (Wilaiwan *et al.*, 2007) are shorter but better self-organized than those grown under constant polarization. Thus, during the 0 V pulse the TiO₂ nanotubes undergoes two reactions: 1) dissolution by chemical attack with the Fion and 2) cathodic

electrodeposition of WO_3 . It might occur that long pulsing times dissolves excessively the TiO_2 nanotubes.

However the XPS analysis for films CT10 through CT13 and films CT14 through CT 17 indicates that the percent of W tend to increase as the pulsing times increase. Although percent of W in films CT13 and CT14 show contrasting in series CT10 through CT13 and CT14 through CT 17, respectively. But keep in mind that XPS analyzes only the film surface and more W could be at internal parts of the tubes.

4.3 Photocatalysis application for TiO_2 , WO_3 , and composite film preparation by anodization

From the results of film fabrication using electrodeposition and anodization techniques, the films obtaining from electrodeposition technique have shown low adhesion, discontinuity, and non-uniformity properties while those obtaining from anodization technique present high quality film with high stability, continuity, uniformity and provide high photocurrent density. Consequently, the photocatalysis experiments were investigated using the selected films from anodization technique only. Hexavalent chromium, Cr(VI) and methylene blue, MB were used as pollutant models in this experiment.

4.3.1 Ultraviolet (UV) light photocatalysis of Hexavalent Chromium, Cr(VI) by TiO_2 , WO_3 , and composite films prepared by anodization

In photocatalysis process, photogenerated electron-hole pairs occur when semiconductor obtains appropriate energy to excite electrons from valence band (VB) to conduction band (CB) of the semiconductor and leave the hole (h^+) in valence band.

The reduction of hexavalent chromium, Cr(VI), by photogenerated electrons in acidic aqueous solution basically follows the following reactions (Ku and Jung, 2001):



Kinetics of hexavalent chromium, Cr(VI), photoreduction was determined. The reaction orders of all investigated reactions were best described by zero order pattern as straight lines from all experiments were obtained from plot of concentration (C) versus time rather than the plot of $\ln(C/C_0)$ versus time. The apparent rate constant (k_{app}) is equivalent to initial reaction rate ($r_{initial}$) calculating from slope of the straight line multiply by initial concentration (C_0) of Cr(VI). Unit of k_{app} and $r_{initial}$ are $\mu\text{M}/\text{min}$. For zero order reaction, half-life of the reaction ($t_{1/2}$) can be calculated from the equation below:

$$t_{1/2} = \frac{C_0}{2k_{app}} \quad (4.2)$$

In these photocatalytic studies, the apparent quantum yield (Φ_{app}) of the reaction can be defined as the initial degradation rate of hexavalent chromium, $r_{initial}$ (photon/s) divided by the photon flux, P (photon/s).

$$\Phi_{app} = \frac{r_{initial}}{P} \quad (4.3)$$

(For the photon flux measurement and quantum yield calculations see appendix B).

- *Effect of modifier in Ti/TiO₂ film fabrication on photocatalytic reduction of Cr(VI)*

Results of photocatalytic reduction of Cr(VI) using Ti/TiO₂ film fabricated by different modifiers are shown in Fig. 4.37. Zero order plots of photocatalytic reactions also exhibited in Fig. 4.38. In addition, Table 4.15 contains the kinetic constant, initial rate and half-life of chromium relevant to the investigated reactions.

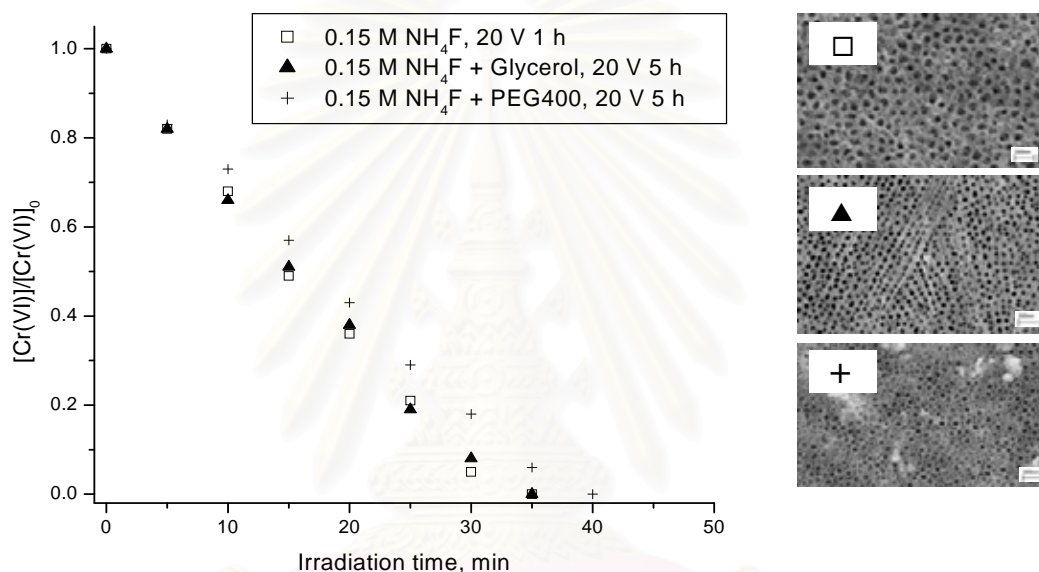


Figure 4.37 Effect of modifier in Ti/TiO₂ film fabrication on photocatalytic reduction of Cr(VI).

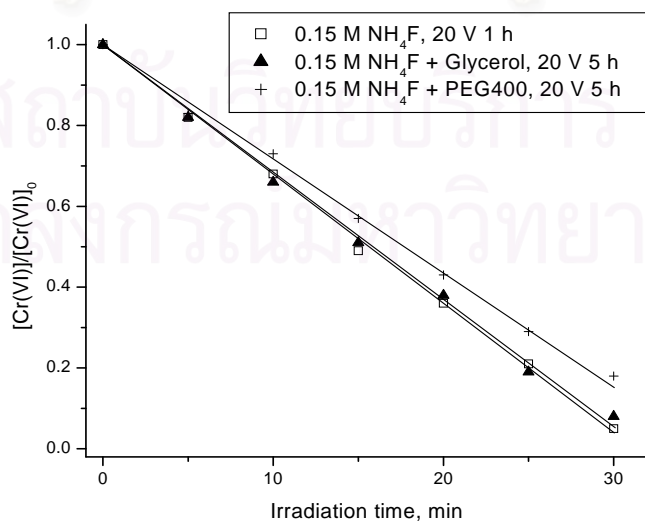


Figure 4.38 Zero order plot of photocatalytic reduction of Cr(VI) by Ti/TiO₂ films.

Table 4.15 Photoelectrochemical performance and kinetic parameters on photocatalytic reduction of Cr(VI) for Ti/TiO₂ films prepared by anodization technique

Ti/TiO ₂	j_{ph} (mA/cm ²)	k_{app} (μ M/min)	$r_{initial}$ (μ M/min)	$t_{1/2}$ (min)	Φ_{app} ($\times 10^{-2}$)
0.15 M NH ₄ F, 20 V 1 h	2.10	3.25	3.25	15.63	0.60
0.15 M NH ₄ F + Glycerol, 20 V 5 h	2.58	3.12	3.12	15.82	0.57
0.15 M NH ₄ F + PEG400, 20 V 5 h	2.74	2.84	2.84	17.86	0.52

For this experiment, photocatalytic reduction of Cr(VI) by the anodized Ti/TiO₂ shows zero order kinetic reaction rate. For films prepared without medium modifier at 20 V, 1 h gave low photocurrent density than those prepared with medium modifiers (glycerol and PEG400). These films show big open hole with nanoporous morphology while those prepared with glycerol and PEG400 show small hole and well organized nanotube morphology, respectively. This should be explained that in well organized nanotube morphology, electron should move faster than in nanoporous morphology. Thus the trapped electrons to be used for photocatalytic reduction of Cr(VI) in nanoporous morphology are much higher than that in nanotube morphology. Consequently, nanoporous morphology can provide higher photoreduction efficiency than the well organized nanotube morphology. In this work, as nanoporous film has higher amount of electrons on the surface, reduction of hexavalent chromium should be better than nanotube film. For films prepared with medium modifier, glycerol gave better photoreduction performance than PEG400 which should be explained by the difference in morphology as well. Films obtained by glycerol as medium modifier has smaller nanohole, thus it has more active surface electrons and has higher area of catalyst/liquid interface than the film obtained from PEG400 which has bigger TiO₂ nanotube. Consequently, Cr(VI) reduction rate of the former film is better than the latter film. For appearance quantum yield (Φ_{app}) calculation, it was found that films

prepared without medium modifier at 20 V, 1 h gave higher Φ_{app} (0.60×10^{-2}) than those prepared with medium modifiers glycerol and PEG400 (0.57×10^{-2} and 0.52×10^{-2} , respectively).

- Comparison of composite W/WO₃/TiO₂ films on photocatalytic reduction of Cr(VI)

Results of photocatalytic reduction of Cr(VI) using W/WO₃/TiO₂ film fabricated by different pulsing waveform (60/-4 V and 60/0 V) are shown in Fig. 4.39. Zero order plots of photocatalytic reactions also exhibited in Fig. 4.40. In addition, Table 4.16 contains the kinetic constant, initial rate and half-life of chromium relevant to the investigated reactions.

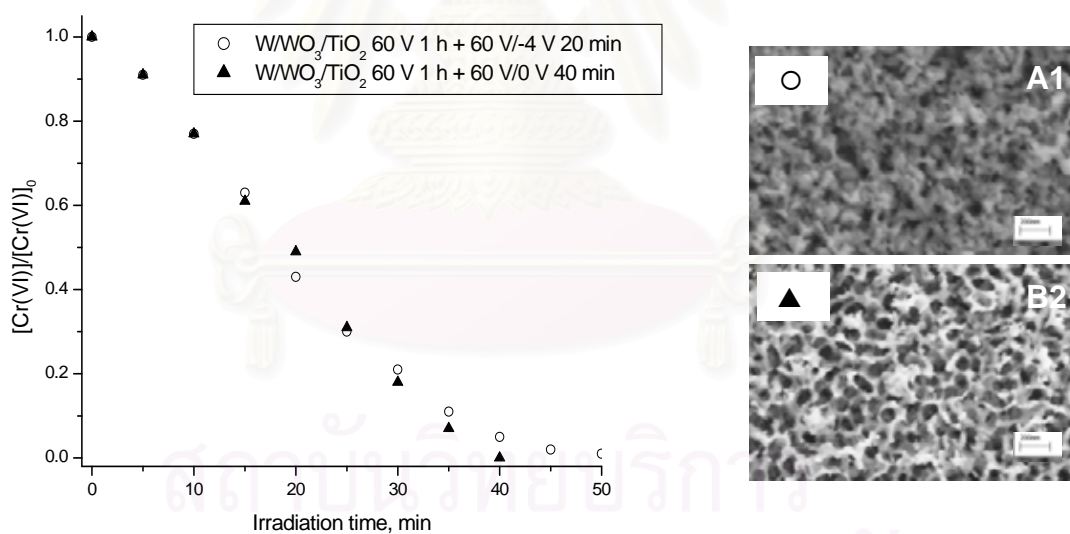


Figure 4.39 Comparison of composite W/WO₃/TiO₂ films on photocatalytic reduction of Cr(VI).

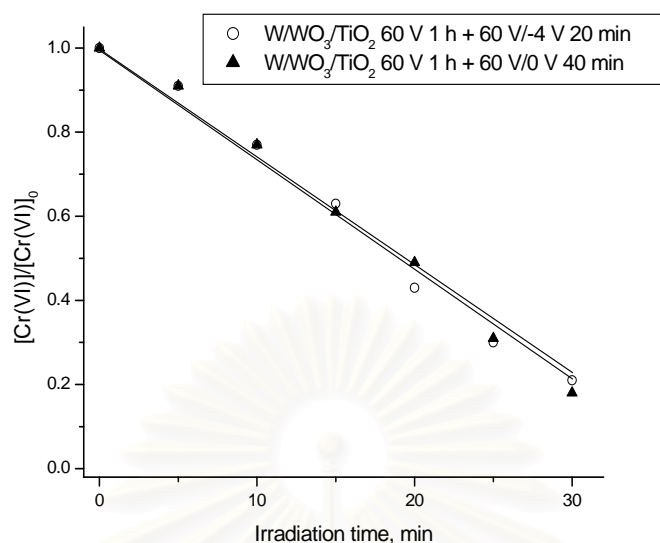


Figure 4.40 Zero order plot of photocatalytic reduction of Cr(VI) by composite W/WO₃/TiO₂ films.

Table 4.16 Photoelectrochemical performance and kinetic parameters on photocatalytic reduction of Cr(VI) for composite W/WO₃/TiO₂ films prepared by anodization technique

Films	j_{ph} (mA/cm ²)	k_{app} (μ M/min)	$r_{initial}$ (μ M/min)	$t_{1/2}$ (min)	Φ_{app} ($\times 10^{-2}$)
W/WO ₃ /TiO ₂ 60 V 1 h + 60 V/-4 V 20 min	6.75	2.69	2.69	18.66	0.49
W/WO ₃ /TiO ₂ 60 V 1 h + 60 V/0 V 40 min	7.86	2.64	2.64	18.73	0.49

When considering the photocurrent performance of these two films, the two composite films have higher photocurrent density than film W/WO₃ (see Table 4.16). It is relevant to the theory that when outer part of the film is TiO₂ and inner part is WO₃, the electrons from conduction band of TiO₂ can drain to conduction band of WO₃, the electrons from conduction band of TiO₂ can drain to conduction band of WO₃ and all the photoelectrons (be generated on TiO₂ or WO₃) will be able to reach the back contact (W). Film W/WO₃/TiO₂ obtained from 60/-4 V pulsing waveform has TiO₂ on the top morphology covering the surface of the film. Apparently, the

original morphology of WO_3 cannot be seen owing to the fact that at -4 V polarizations Ti was more deposited than at 0 V polarizations. Thus film obtained from $60/0$ V pulsing wave form has less TiO_2 on the surface of the film. Interestingly, the film obtained from $60/0$ V has higher photocurrent performance than the film obtained from $60/-4$ V due to the former film has more photoelectrons that can reach the back contact while top surface of the latter film has excess TiO_2 . Consequently, photoelectrons from the inner layer (WO_3) in this case are less than the former.

For this experiment, photocatalytic reduction of Cr(VI) by the composite $\text{W/WO}_3/\text{TiO}_2$ films show zero order kinetic reaction rate. It is worth to mention that both composite $\text{W/WO}_3/\text{TiO}_2$ films (obtained from both pulsing waveform, $60/-4$ V and $60/0$ V) have slightly different in photocurrent density, but they are nearly same in photocatalytic reduction rate of Cr(VI) . This result indicates that the photocatalytic performance is not a direct proportional to the photocurrent density. Other parameters such as film morphology and catalyst surface area play the important role here. Active surface electron is an important key to indicate the Cr(VI) photoreduction performance of the film. This experiment shows that the appearance quantum yield (Φ_{app}) of both composite $\text{W/WO}_3/\text{TiO}_2$ films are equivalent at 0.49×10^{-2} .

- Comparison of composite $\text{Ti/TiO}_2/\text{WO}_3$ films on photocatalytic reduction of Cr(VI)

Results of photocatalytic reduction of Cr(VI) using $\text{Ti/TiO}_2/\text{WO}_3$ film fabricated by different pulsing waveform ($20/-4$ V and $20/0$ V) are shown in Fig. 4.41. Zero order plots of photocatalytic reactions also exhibited in Fig. 4.42. In addition, Table 4.17 contains the kinetic constant, initial rate and half-life of chromium relevant to the investigated reactions.

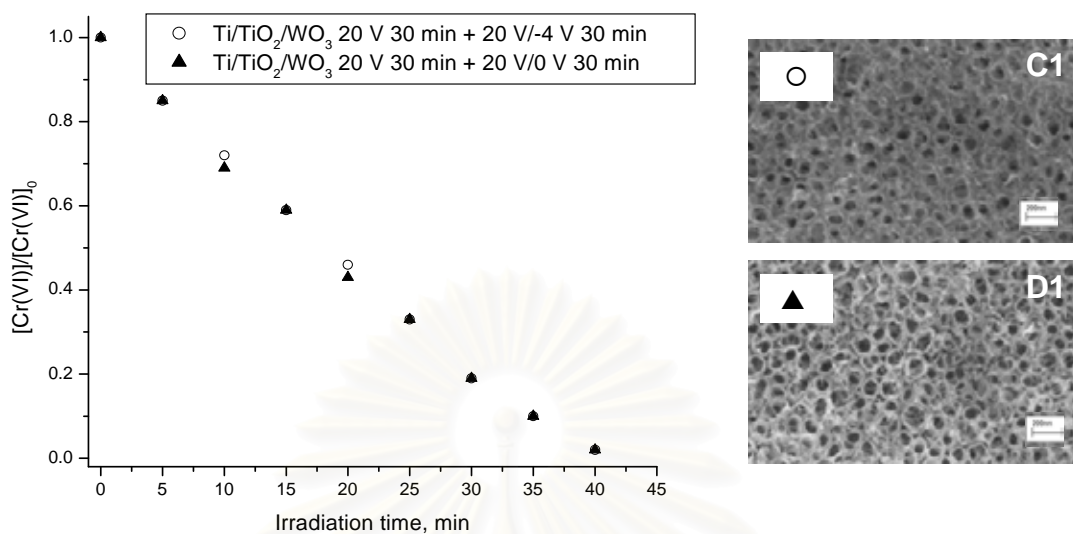


Figure 4.41 Comparison of composite Ti/TiO₂/WO₃ films on photocatalytic reduction of Cr(VI).

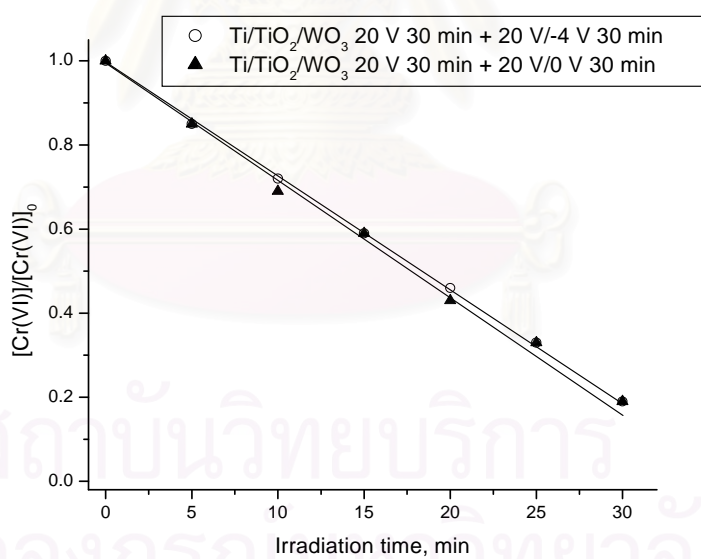


Figure 4.42 Zero order plot of photocatalytic reduction of Cr(VI) by composite Ti/TiO₂/WO₃ films.

Table 4.17 Photoelectrochemical performance and kinetic parameters on photocatalytic reduction of Cr(VI) for composite Ti/TiO₂/WO₃ films prepared by anodization technique

Films	j_{ph} (mA/cm ²)	k_{app} (μ M/min)	$r_{initial}$ (μ M/min)	$t_{1/2}$ (min)	Φ_{app} ($\times 10^{-2}$)
Ti/TiO ₂ /WO ₃ , 20 V 30 min + 20 V/-4 V 30 min	5.16	2.77	2.77	18.45	0.51
Ti/TiO ₂ /WO ₃ , 20 V 30 min + 20 V/0 V 30 min	6.65	2.65	2.65	18.18	0.49

In theory, for the composite film if outer part of the film is WO₃ and inner part is TiO₂, the electron from conduction band of WO₃ (more positive reduction potential) cannot drain to conduction band of TiO₂ (more negative reduction potential) so only the photoelectrons which be generated from TiO₂ will be able to reach the back contact (Ti). However, these composite Ti/TiO₂/WO₃ films from the anodization technique gave higher photocurrent performance than the pure Ti/TiO₂ film (see Table 4.15) because these composite films are not comprised of an ideal layer of TiO₂ and WO₃ but the WO₃ is intercalated in the TiO₂ nanotubes. Thus photoelectrons which are generated from TiO₂ can drain to the back contact and run faster in the nanotubes film than in pure Ti/TiO₂ porous film. Considering photocurrent performance of the composite film obtained from different pulsing waveform, film Ti/TiO₂/WO₃ obtained from 20/-4 V pulsing waveform has more WO₃ filled in nanotubes than in the film Ti/TiO₂/WO₃ obtained from 20/0 V pulsing waveform. Thus the former film has less photoelectron (generated from TiO₂) than the latter film due to the irradiated area of TiO₂ was blocked by WO₃.

From this experiment, photocatalytic reduction of Cr(VI) by the composite Ti/TiO₂/WO₃ films show zero order kinetic reaction rate. Even though, film Ti/TiO₂/WO₃ obtained from 20/-4 V pulsing waveform has less photocurrent density than that obtained from 20/0 V pulsing waveform, the former film has slightly better in photoreduction of Cr(VI). This result can be explained that composite film obtained from 20/-4 V pulsing waveform has more photogenerated electrons at the film surface

(from both WO_3 and TiO_2) while the film obtained from 20/0 V pulsing waveform has less photogenerated electron at the film surface due to has less WO_3 covered on the TiO_2 . This experiment provided appearance quantum yield (Φ_{app}) as shown in Table 4.17. The composite $\text{Ti}/\text{TiO}_2/\text{WO}_3$ film obtained from 20/-4 V pulsing waveform has higher value of Φ_{app} than that obtained from 20/0 V pulsing waveform.

- Comparison of Ti/TiO_2 nanotube film and $\text{Ti}/\text{TiO}_2/\text{WO}_3$ nanotube film on photocatalytic reduction of Cr(VI)

Results of photocatalytic reduction of Cr(VI) using Ti/TiO_2 nanotube film fabricated with constant anodization potential 20 V and $\text{Ti}/\text{TiO}_2/\text{WO}_3$ nanotube film fabricated with pulsing waveform (20/0 V) are shown in Fig. 4.43. Zero order plots of photocatalytic reactions also exhibited in Fig. 4.44. In addition, Table 4.18 contains the kinetic constant, initial rate and half-life of chromium relevant to the investigated reactions.

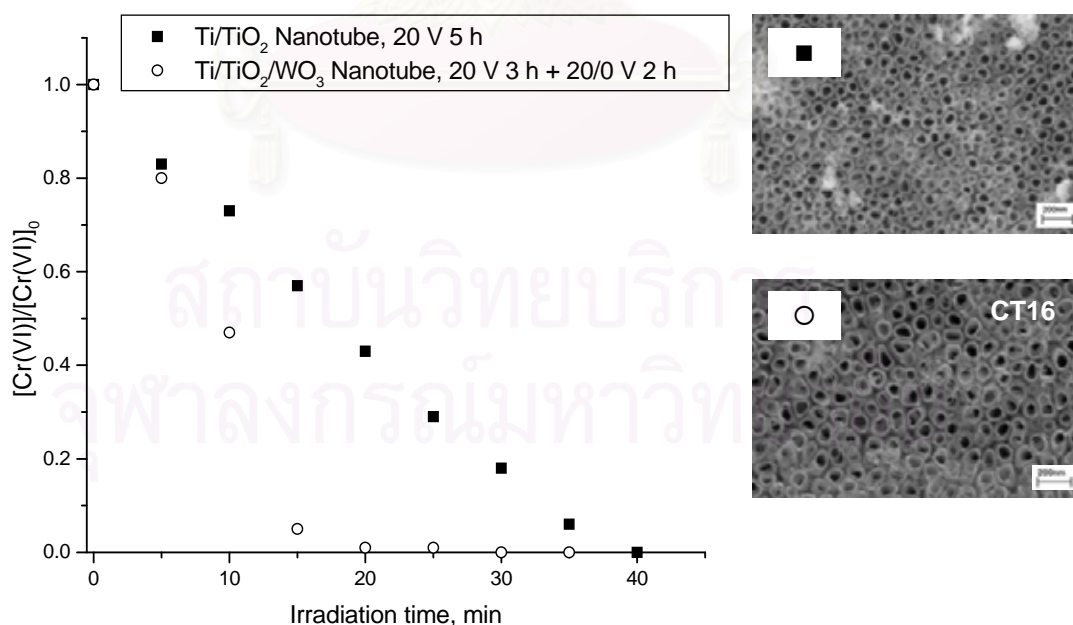


Figure 4.43 Comparison of Ti/TiO_2 nanotube film and $\text{Ti}/\text{TiO}_2/\text{WO}_3$ nanotube film on photocatalytic reduction of Cr(VI) .

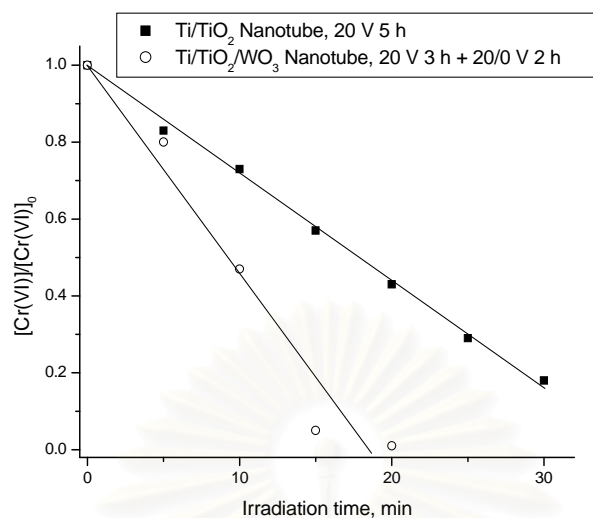


Figure 4.44 Zero order plot of photocatalytic reduction of Cr(VI) by Ti/TiO₂ nanotube film and composite Ti/TiO₂/WO₃ nanotube film.

Table 4.18 Photoelectrochemical performance and kinetic parameters on photocatalytic reduction of Cr(VI) for Ti/TiO₂ nanotube film and Ti/TiO₂/WO₃ nanotube film prepared by anodization technique

Films nanotube	j_{ph} (mA/cm ²)	k_{app} (μ M/min)	$r_{initial}$ (μ M/min)	$t_{1/2}$ (min)	Φ_{app} ($\times 10^{-2}$)
Ti/TiO ₂ 0.15 M NH ₄ F + PEG400, 20 V 5 h	2.74	2.84	2.84	17.86	0.52
Ti/TiO ₂ /WO ₃ 0.15 M NH ₄ F + PEG400, 20 V 3 h + 20/0 V 2 h	7.70	5.43	5.43	9.26	1.00

From this experiment, photocatalytic reduction of Cr(VI) by the anodized Ti/TiO₂ film and Ti/TiO₂/WO₃ film follow zero order kinetic reaction. It is worth mentioning that photocurrent density (Table 4.19) of the composite nanotube Ti/TiO₂/WO₃ has reached 7.7 mA/cm² and higher than the pure Ti/TiO₂ nanotube film (2.74 mA/cm²). In addition, photocatalytic reduction of Cr(VI) on the composite nanotube Ti/TiO₂/WO₃ is better than pure Ti/TiO₂ nanotube film. Photogenerated electrons (from TiO₂ and WO₃) which reduce Cr(VI) are likely associated with these

results. In considering of the morphology of the composite nanotube Ti/TiO₂/WO₃, the TiO₂ nanotube was filled with WO₃, thus photoelectrons at the surface are from both TiO₂ and WO₃. While pure Ti/TiO₂ nanotubes film has photoelectrons are from only TiO₂ which we expected that the rate of electron transfer in the nanotube of these two films are not significantly different due to the similarity of their nanotube morphologies. For appearance quantum yield (Φ_{app}) calculation, it was found that composite Ti/TiO₂/WO₃ film prepared with 20/0 V pulsing wave form gave higher Φ_{app} (1×10^{-2}) than Ti/TiO₂ film prepared with constant anodization 20 V (0.52×10^{-2}).

- Quantum efficiencies on photocatalytic reduction of hexavalent chromium, Cr(VI)

Generally quantum yield has value less than 1 or 100 %. The equation above implied that how much of photogenerated electron or hole can be used to degrade the pollutant. The apparent quantum yield, Φ_{app} for photocatalytic reduction of hexavalent chromium from this work has value in the range of $0.40 \times 10^{-2} - 1.00 \times 10^{-2}$ (Table 4.15 through Table 4.18). This range is similar to the previous research of Mills and Le Hunte in 1997, which reported Φ_{app} values for photocatalytic systems are ca. 1 %.

Importantly, the most photogenerated electron (e⁻) could not be used in the photoreduction of Cr(VI), but only some of them were used. The photogenerated electron which can be used to reduce Cr(VI) are only the trapped electron on the surface of catalyst (see Fig. 4.45).

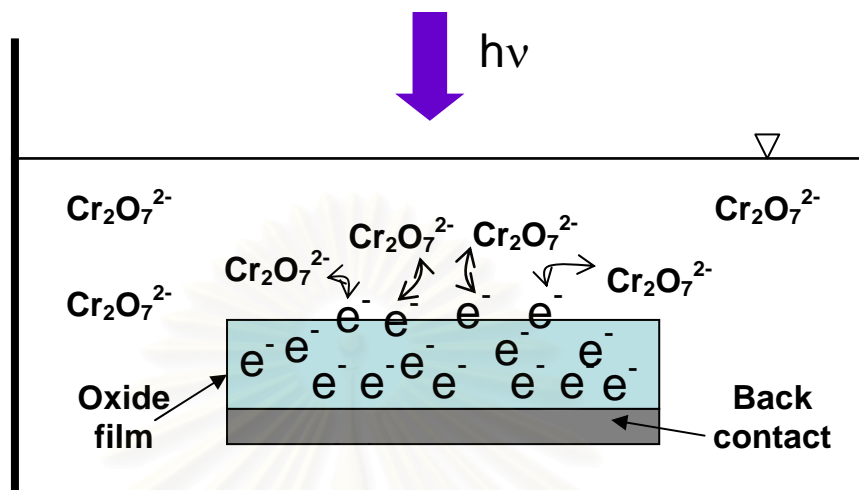


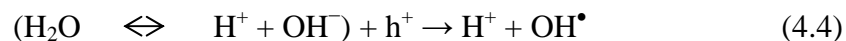
Figure 4.45 Photogenerated electrons (e^-) at the surface of oxide layer reacted with chromium species.

4.3.2 Ultraviolet (UV) light photocatalysis of Methylene blue by TiO_2 , WO_3 , and composite films prepared by anodization

In photocatalysis process, photogenerated electron-hole pairs occur when semiconductor obtain appropriate energy to excite electrons from valence band (VB) to conduction band (CB) of the semiconductor and leave the hole (h^+) in valence band.

For degradation of methylene blue by photocatalysis process, photogenerated hole (h^+) (mainly involved in the decarboxylation reaction) and hydroxyl radical (OH^\bullet) at the surface of each film are oxidizing agents which can oxidize methylene blue. Hydroxyl radicals are known as strongly active species but non-selective agents and can be generated by the following reactions (Houas *et al.*, 2001):

1. Oxidation of water by holes



2. Transient formation of hydroperoxide radicals



Houas *et al.* in 2001 reported photocatalytic degradation pathway of methylene blue as shown in Fig. 4.46 and suggested that photo-holes (h^+) are certainly not concerned by the initial step since the reactant is cationic and not electron donor. By contrast, the OH^\bullet radicals can attack the $\text{C}-\text{S}^+=\text{C}$ functional group in methylene blue. Therefore, the initial step of methylene blue degradation can be ascribed to the cleavage of the bonds of the $\text{C}-\text{S}^+=\text{C}$ functional group in methylene blue.

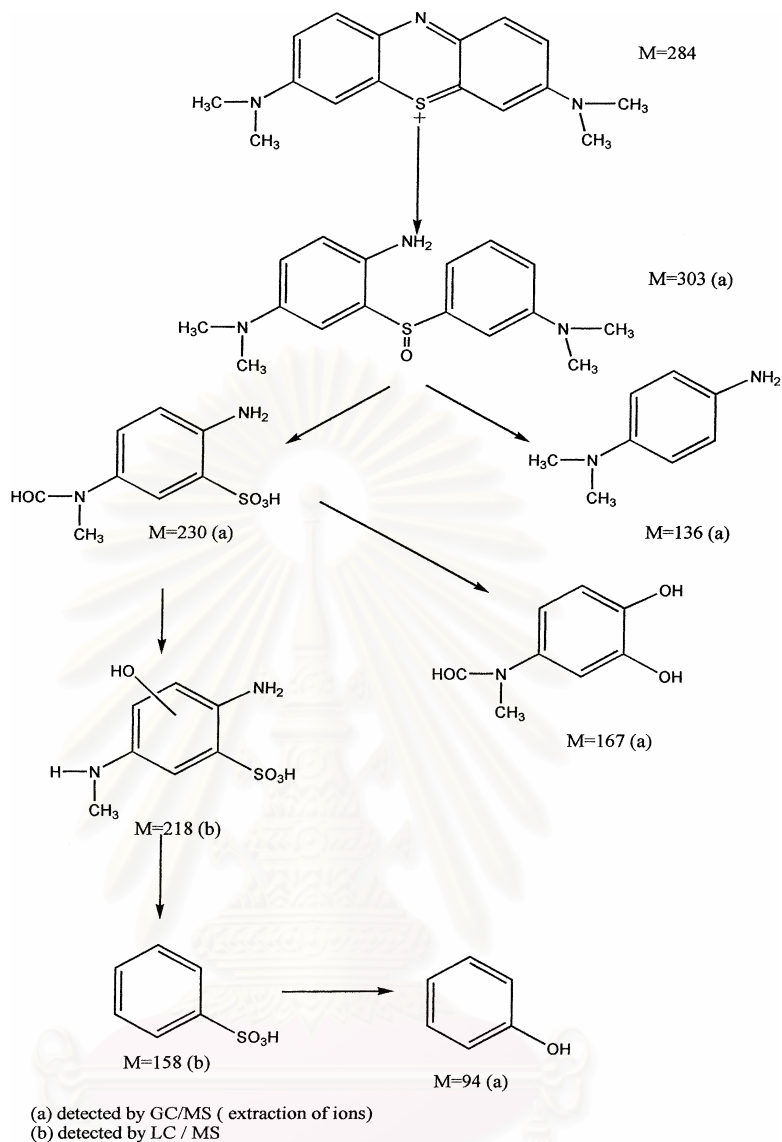


Figure 4.46 Photocatalytic degradation pathway of methylene blue.

(Houas *et al.*, 2001)

In this research work kinetic of methylene blue, MB, photooxidation was investigated. The reaction order of this experiment was found to be pseudo-first order which was represented by the straight lines obtained from the plot of $\ln(C/C_0)$ versus time. The apparent rate constant (k_{app}) is slope of the straight line from previous plot and has unit of min^{-1} . Initial reaction rate ($r_{initial}$) was calculated from k_{app} multiply by initial concentration (C_0) of MB. Unit of $r_{initial}$ are $\mu\text{M}/\text{min}$. For first order reaction, half-life of the reaction ($t_{1/2}$) can be calculated from the equation below:

$$t_{1/2} = \frac{\ln 2}{k_{app}} \quad (4.9)$$

In these photocatalytic studies, the apparent quantum yield (Φ_{app}) of the reaction can be defined as the initial degradation rate of methylene blue, $r_{initial}$ (photon/s) divided by the photon flux, P (photon/s)

$$\Phi_{app} = \frac{r_{initial}}{P} \quad (4.3)$$

(For the photon flux measurement and quantum yield calculations see appendix B).

- Effect of modifier in Ti/TiO₂ film fabrication on photocatalytic oxidation of MB

Results of photocatalytic oxidation of MB using Ti/TiO₂ film fabricated by different modifiers are shown in Fig. 4.47. First order plots of photocatalytic reactions also exhibited in Fig. 4.48. In addition, Table 4.19 contains the kinetic constant, initial rate and half-life of MB relevant to the investigated reactions.

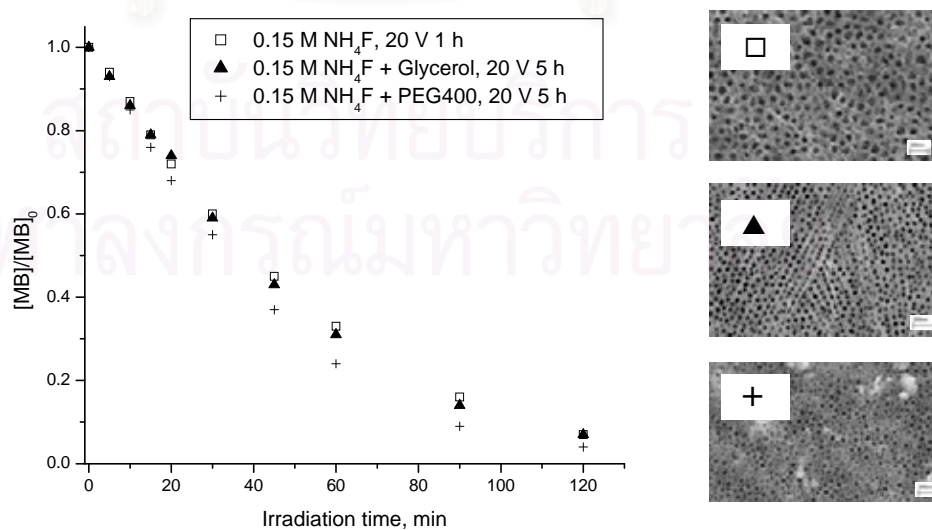


Figure 4.47 Effect of modifier in Ti/TiO₂ film fabrication on photocatalytic oxidation of MB.

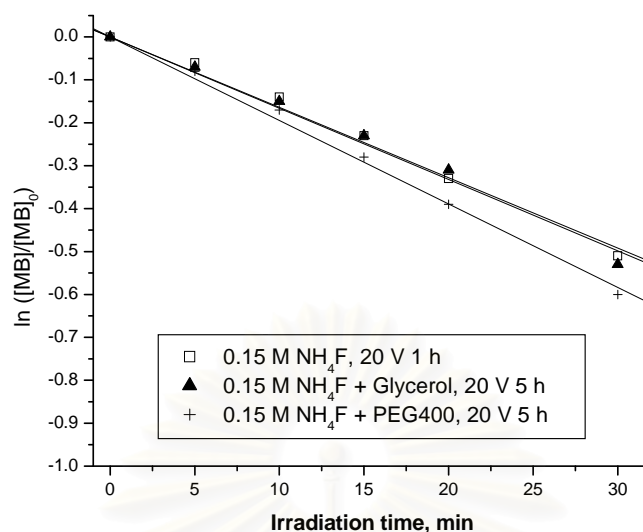


Figure 4.48 Pseudo first-order plot of photocatalytic oxidation of MB by Ti/TiO₂ films.

Table 4.19 Photoelectrochemical performance and kinetic parameters on photocatalytic reduction of MB for Ti/TiO₂ films prepared by anodization technique

Ti/TiO ₂	j_{ph} (mA/cm ²)	k_{app} (min ⁻¹)	$r_{initial}$ (μM/min)	$t_{1/2}$ (min)	Φ_{app} (× 10 ⁻²)
0.15 M NH ₄ F, 20 V 1 h	2.10	0.017	0.56	42.00	0.10
0.15 M NH ₄ F + Glycerol, 20 V 5 h	2.58	0.017	0.56	42.00	0.10
0.15 M NH ₄ F + PEG400, 20 V 5 h	2.74	0.019	0.66	35.72	0.12

From this experiment, photocatalytic oxidation of methylene blue, MB by the anodized Ti/TiO₂ shows pseudo-first order kinetic reaction rate. The kinetic parameters were shown in Table 4.20. Apparently, the photocatalytic performances on the oxidation of methylene blue of Ti/TiO₂ films obtained from PEG400 as medium modifier is better than those obtained from glycerol and without medium modifier. This trend in opposite direction with the result of photocatalytic reduction of Cr(VI). Result should be associated with the photogenerated hole (h⁺) and hydroxyl radical

(OH[•]) at the surface of each film which can oxidize with methylene blue. Owing to high amount of electron-hole pairs generated in well organized nanotube film (obtained from PEG400) and the rapid moving of electrons to the back contact of the film, thus high amount of photogenerated holes (h⁺) were left at the film surface for photocatalytic oxidation of methylene blue. This experiment provided appearance quantum yield (Φ_{app}) as shown in Table 4.19. The Ti/TiO₂ film obtained from PEG400 as medium modifier has slightly higher value of Φ_{app} than those obtained from glycerol and without medium modifier.

- Comparison of composite W/WO₃/TiO₂ films on photocatalytic oxidation of MB

Results of photocatalytic oxidation of MB using W/WO₃/TiO₂ films fabricated by different pulsing waveform (60/-4 V and 60/0 V) are shown in Fig. 4.49. First order plots of photocatalytic reactions also exhibited in Fig. 4.50. In addition, Table 4.20 contains the kinetic constant, initial rate and half-life of MB relevant to the investigated reactions.

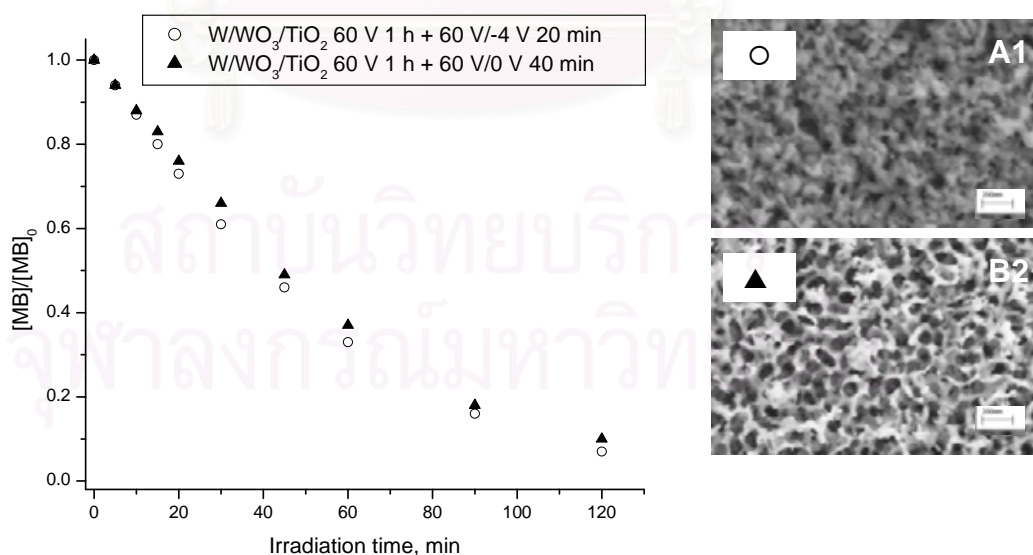


Figure 4.49 Comparison of composite W/WO₃/TiO₂ films on photocatalytic oxidation of MB.

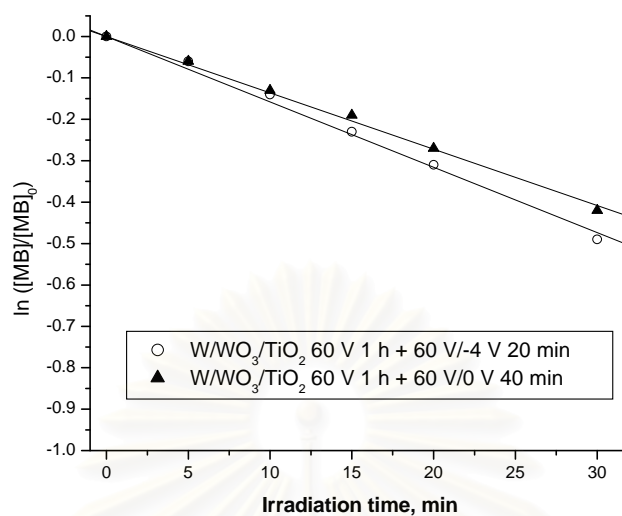


Figure 4.50 Pseudo first-order plot of photocatalytic oxidation of MB by composite W/WO₃/TiO₂ films.

Table 4.20 Photoelectrochemical performance and kinetic parameters on photocatalytic oxidation of MB for composite W/WO₃/TiO₂ films prepared by anodization technique

Films	j_{ph} (mA/cm ²)	k_{app} (min ⁻¹)	$r_{initial}$ (μM/min)	$t_{1/2}$ (min)	Φ_{app} (× 10 ⁻²)
W/WO ₃ /TiO ₂ 60 V 1 h + 60 V/-4 V 20 min	6.75	0.016	0.54	43.86	0.10
W/WO ₃ /TiO ₂ 60 V 1 h + 60 V/0 V 40 min	7.86	0.014	0.47	51.33	0.09

For this experiment, photocatalytic oxidation of methylene blue by the composite W/WO₃/TiO₂ films showed pseudo-first order kinetic reaction rate. It is worth mentioning that the overload TiO₂ covered the WO₃ surface (60/-4 V pulsing waveform) tends to decrease the photocurrent density, however, the photogenerated holes (h⁺) and hydroxyl radicals (OH[•]) which be generated from the overload TiO₂ covered the WO₃ surface improved the photocatalytic oxidation of methylene blue.

The appearance quantum yield (Φ_{app}) from both composite W/WO₃/TiO₂ films are slightly different.

- Comparison of composite Ti/TiO₂/WO₃ films on photocatalytic oxidation of MB

Results of photocatalytic oxidation of MB using Ti/TiO₂/WO₃ film fabricated by different pulsing waveform (20/-4 V and 20/0 V) are shown in Fig. 4.51. First order plots of photocatalytic reactions also exhibited in Fig. 4.52. In addition, Table 4.21 contains the kinetic constant, initial rate and half-life of MB relevant to the investigated reactions.

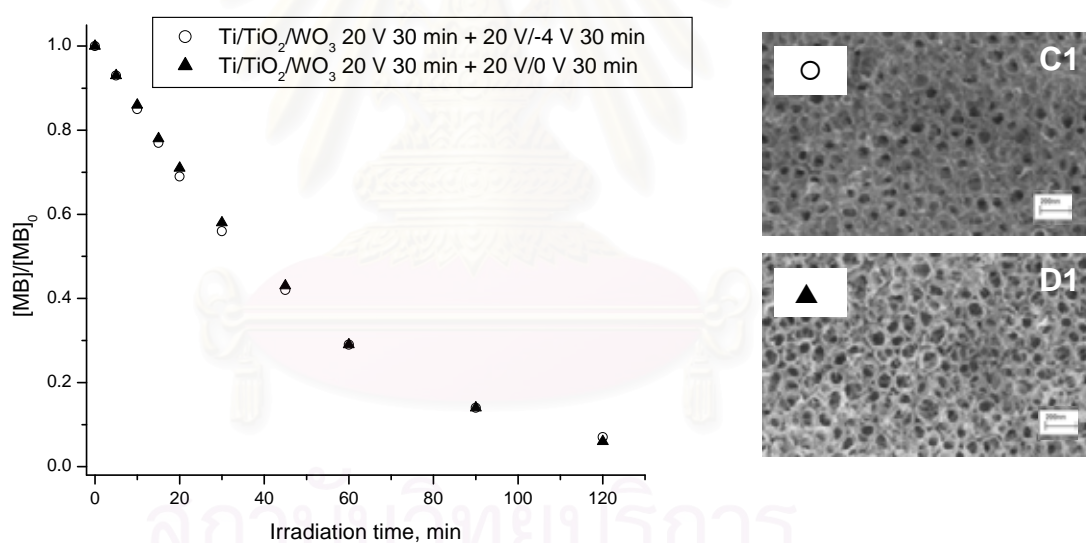


Figure 4.51 Comparison of composite Ti/TiO₂/WO₃ films on photocatalytic oxidation of MB.

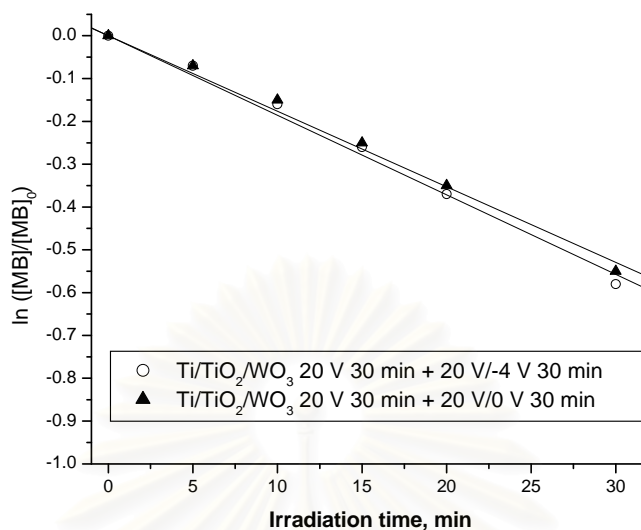


Figure 4.52 Pseudo first-order plot of photocatalytic oxidation of MB by composite Ti/TiO₂/WO₃ films.

Table 4.21 Photoelectrochemical performance and kinetic parameters on photocatalytic oxidation of MB for composite Ti/TiO₂/WO₃ films prepared by anodization technique

Films	j_{ph} (mA/cm ²)	k_{app} (min ⁻¹)	$r_{initial}$ (μM/min)	$t_{1/2}$ (min)	Φ_{app} ($\times 10^{-2}$)
Ti/TiO ₂ /WO ₃ , 20 V 30 min + 20 V/-4 V 30 min	5.16	0.019	0.64	37.26	0.12
Ti/TiO ₂ /WO ₃ , 20 V 30 min + 20 V/0 V 30 min	6.65	0.018	0.60	39.38	0.11

As mentioned before, the ideal composite Ti/TiO₂/WO₃ film, outer part is WO₃ and inner part is TiO₂, the electron from conduction band of WO₃ (more positive reduction potential) cannot drain to conduction band of TiO₂ (more negative reduction potential) so only the photoelectrons which are generated from TiO₂ will be able to reach the back contact (Ti). However, composite Ti/TiO₂/WO₃ films from these anodization technique gave higher photocurrent performance than the pure Ti/TiO₂ film (see Table 4.15) because these composite films are not comprise of an ideal

layer of TiO₂ and WO₃ but the WO₃ is intercalated in the TiO₂ nanotubes. Thus photoelectrons which are generated from TiO₂ can drain to the back contact and run faster in the nanotubes film than in pure Ti/TiO₂ porous film. Considering photocurrent performance of the composite film obtained from different pulsing waveform, film Ti/TiO₂/WO₃ obtained from 20/-4 V pulsing waveform has more WO₃ filled in nanotubes than in the film Ti/TiO₂/WO₃ obtained from 20/0 V pulsing waveform. Thus the former film has less photoelectron (generated from TiO₂) than the latter film due to the irradiated area of TiO₂ was blocked by WO₃.

For this experiment, photocatalytic oxidation of methylene blue by the composite Ti/TiO₂/WO₃ films showed pseudo-first order kinetic reaction rate. Remarkably, composite Ti/TiO₂/WO₃ films obtained from 20/-4 V pulsing waveform has less photocurrent density than that obtained from 20/0 V pulsing waveform. The opposite trend of photocatalytic efficiency can be seen in the photocatalytic oxidation rate of methylene blue as the Ti/TiO₂/WO₃ films obtained from 20/-4 V provide slightly higher in kinetic constant than that of 20/0 V. This should be explained that film Ti/TiO₂/WO₃ obtained from 20/-4 V pulsing waveform has more WO₃ filled in nanotubes than the film obtained from 20/0 V pulsing waveform thus photogenerated holes (h⁺) and hydroxyl radical (OH[•]) at film surface (which reacted with methylene blue) from the former film are from both TiO₂ and WO₃ while the latter film has less. From the appearance quantum yield (Φ_{app}) calculation, it was found that the composite Ti/TiO₂/WO₃ film obtained from 20/-4 V pulsing waveform has slightly higher value of Φ_{app} (0.12×10^{-2}) than that obtained from 20/0 V pulsing waveform (0.11×10^{-2}).

- Comparison of Ti/TiO₂ nanotube film and Ti/TiO₂/WO₃ nanotube films on photocatalytic oxidation of MB

Results of photocatalytic oxidation of MB using Ti/TiO₂ nanotube film fabricated with constant anodization potential 20 V and Ti/TiO₂/WO₃ nanotube film fabricated with pulsing waveform (20/0 V) are shown in Fig. 4.53. First order plots of photocatalytic reactions also exhibited in Fig. 4.54. In addition, Table 4.22 contains

the kinetic constant, initial rate and half-life of MB relevant to the investigated reactions.

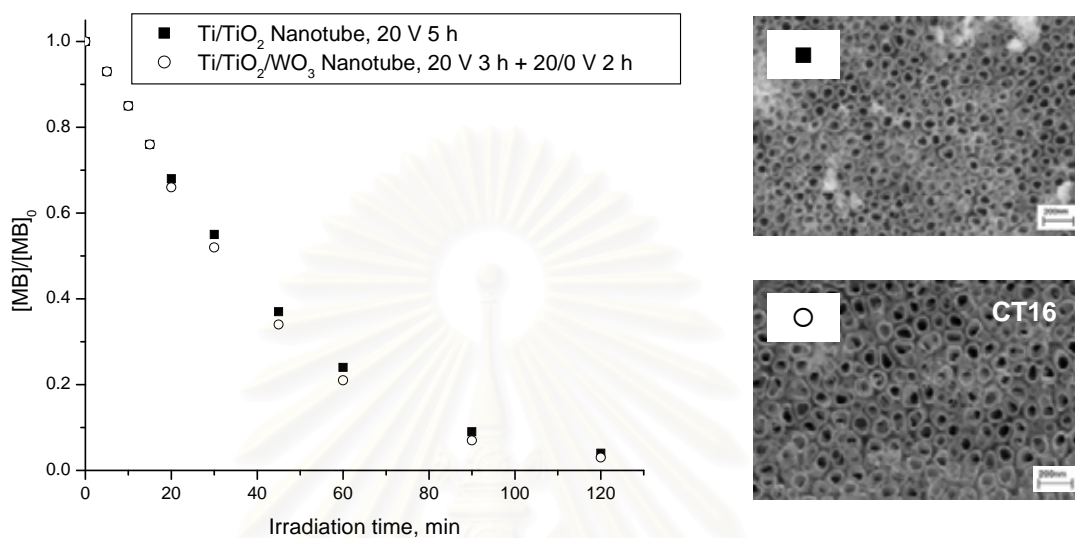


Figure 4.53 Comparison of Ti/TiO₂ nanotube film and Ti/TiO₂/WO₃ nanotube film on photocatalytic oxidation of MB.

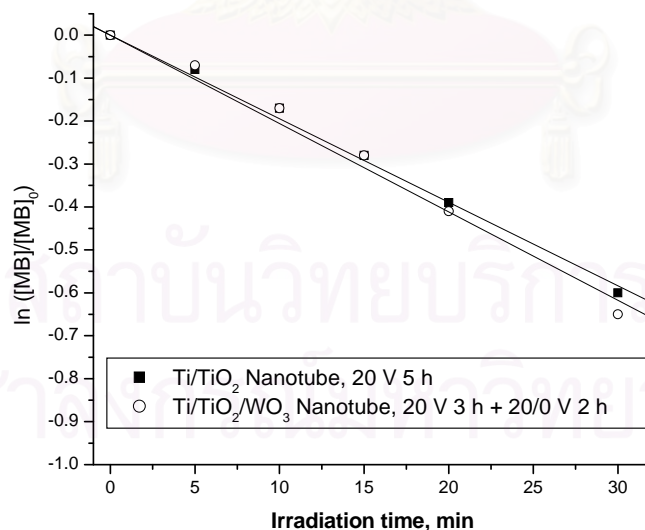


Figure 4.54 Pseudo first-order plot of photocatalytic oxidation of MB by Ti/TiO₂ nanotube film and composite Ti/TiO₂/WO₃ film.

Table 4.22 Photoelectrochemical performance and kinetic parameters on photocatalytic oxidation of MB for Ti/TiO₂ nanotube film and Ti/TiO₂/WO₃ nanotube film prepared by anodization technique

Films nanotube	j_{ph} (mA/cm ²)	k_{app} (min ⁻¹)	$r_{initial}$ (μM/min)	$t_{1/2}$ (min)	Φ_{app} ($\times 10^{-2}$)
Ti/TiO ₂ 0.15 M NH ₄ F + PEG400, 20 V 5 h	2.74	0.019	0.66	35.72	0.12
Ti/TiO ₂ /WO ₃ 0.15 M NH ₄ F + PEG400, 20 V 3 h + 20/0 V 2 h	7.70	0.021	0.69	33.64	0.13

From this experiment, photocatalytic oxidation of methylene blue by the anodized Ti/TiO₂ film and Ti/TiO₂/WO₃ films show pseudo-first order kinetic reaction rate. It is worth mentioning that photocurrent density (Table 4.24) of the composite nanotube Ti/TiO₂/WO₃ has reached 7.7 mA/cm² which is dramatically higher than the pure Ti/TiO₂ nanotube film (2.74 mA/cm²). In addition, photocatalytic oxidation of methylene blue on the composite nanotube Ti/TiO₂/WO₃ is better than pure Ti/TiO₂ nanotube film. Photogenerated holes (h⁺) and hydroxyl radical (OH[•]) (from TiO₂ and WO₃) are likely associated with these results. On morphology of the composite nanotube Ti/TiO₂/WO₃, the TiO₂ nanotube was filled with WO₃ so photogenerated holes (h⁺) and hydroxyl radical (OH[•]) at the surface are from both TiO₂ and WO₃. While pure Ti/TiO₂ nanotubes film has photogenerated holes (h⁺) and hydroxyl radical (OH[•]) are from only TiO₂. The appearance quantum yield, Φ_{app} of composite Ti/TiO₂/WO₃ film obtained from 20/0 V pulsing waveform has slightly higher value than Ti/TiO₂ film obtained from constant anodization at 20 V (see Table 4.22).

- Quantum efficiencies on photocatalytic oxidation of methylene blue, MB

Generally quantum yield has value less than 1 or 100 %. The equation above implied that how much photogenerated electron or hole can be used to degrade the pollutant. The apparent quantum yield, Φ_{app} for photocatalytic oxidation of methylene blue from this work has value in the range of $0.09 \times 10^{-2} - 0.13 \times 10^{-2}$ (Table 4.19 through Table 4.22). This range is different from the work of McMurray *et al.* in 2004 which reported the Φ_{app} value for the photocatalytic degradation of organic pollutant was 5 % for oxalic acid and 10 % for formic acid.

Hydroxyl radicals (OH^\bullet) generated from equations (4.4) and (4.8) are the most important key in the photooxidation of MB. The degradation of MB is only at the surface of catalyst (see Fig. 4.55).

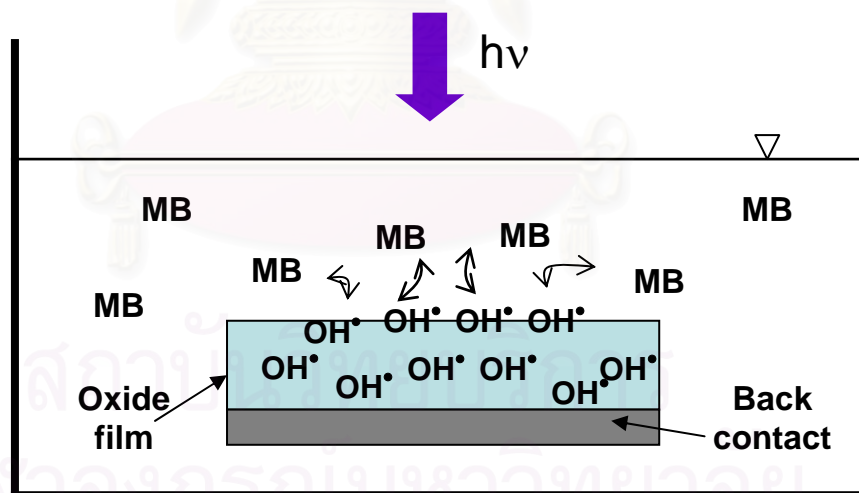


Figure 4.55 Hydroxyl radical (OH^\bullet) at the surface of oxide layer reacted with methylene blue, MB.

4.3.3 Visible light photocatalysis oxidation of Methylene blue, MB by W/WO₃ film preparation by anodization

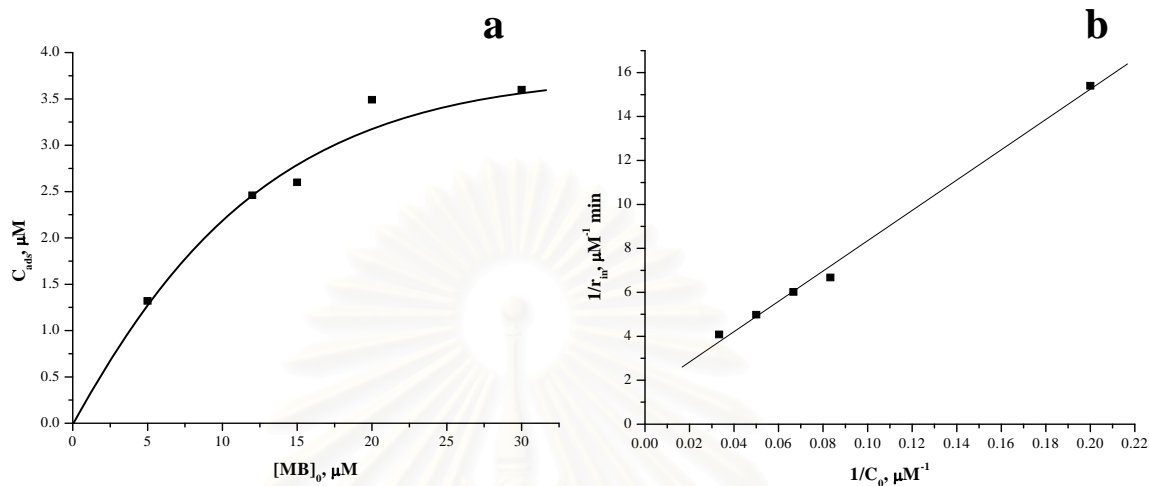


Figure 4.56 (a) Langmuir adsorption plot of methylene blue with different initial solution concentrations on nanoporous WO₃ film obtained by anodization of W foil at 60 V for 2 h in 0.15M NaF electrolyte. The line was simply drawn through the data points. (b) Variation of initial rate (R_{initial}) with initial methylene blue (MB) concentration. The line is a least-squares fit.

Figure 4.56(a) shows an adsorption isotherm plot for methylene blue on W/WO₃ nanoporous films obtained from 0.15 M NaF electrolyte and anodization potential of 60 V for 2 h. To generate these data, the WO₃ film (geometric area: 0.63 cm²) was equilibrated with 10 mL of the methylene blue solution (pH 9) at a given concentration for 30 min. At low initial concentrations (5, 12 and 15 μM) the amount of dye adsorbed on the WO₃ film surface increases proportionally to the bulk concentration but at higher concentrations than 20 μM the extent of methylene blue adsorption reaches a plateau because of surface (adsorption) site saturation (Matthews, 1989).

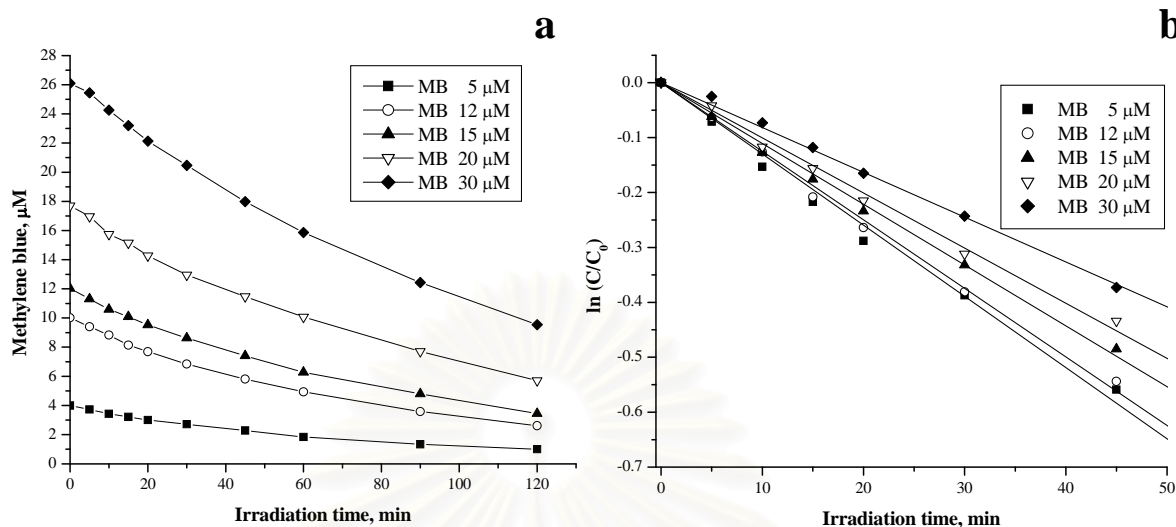


Figure 4.57 (a) Visible light ($k > 400 \text{ nm}$) decomposition of methylene blue at different initial concentrations by nanoporous WO_3 films obtained by anodization of tungsten foil at 60 V for 2 h in 0.15M NaF electrolyte. The lines are simply drawn through the data points. (b) Corresponding pseudo first-order plot of these data. The line is a least-squares fit.

Kinetics data for the photodecomposition of methylene blue are presented in Fig. 4.57(a) with the initial concentration of the dye as a parameter. Plots of $\ln(C/C_0)$ versus irradiation time, constructed from these data, are contained in Fig. 4.57(b). Values for the apparent first-order rate constant (k_{app}), culled from these plots, decreased with an increase of the initial dye concentration as shown in Table 4.23 – a trend reminiscent of similar data on methylene blue in contact with near UV-illuminated TiO_2 films (Matthews, 1989). This is accommodated within the framework of the Langmuir–Hinshelwood model (Eq. (4.10)) (Ollis, 2005). This model then affords an expression for the initial rate (r_{initial}) (Ollis, 2005)

$$1/r_{\text{initial}} = 1/k + 1/kKC_0 \quad (4.10)$$

where C_0 is the initial concentration of the dye, K is the Langmuir adsorption constant, and k is a reactivity constant, providing a measure of the reactivity of the

surface of the catalyst with the dye. According to Eq. (4.10), a plot of the reciprocal of initial rate against the reciprocal of initial concentration would be linear (Fig. 4.56(b)) and yields $k = 0.687 \mu\text{M min}^{-1}$ and $K = 0.021 \mu\text{M}^{-1}$ from the intercept and slope, respectively. As also pointed out by a reviewer, values of K obtained from such kinetics analyses may be at variance with estimates from adsorption data (Fig. 4.56(a)) because of the importance of additional factors in the kinetics data (Ollis, 2005).

Table 4.23 Effect of initial methylene blue (MB) concentration on the kinetics parameters

Initial MB concentration, C_0 (μM)	$C_{\text{ads, 30 min}}$ (μM)	Apparent rate constant, k_{app} (min^{-1})	Initial reaction rate, r_{initial} ($\mu\text{M min}^{-1}$) $r_{\text{initial}} = k_{\text{app}} \times C_0$	$t_{1/2}$ (min)	$t^*_{1/2}$ (min)
5	1.32	0.013	0.065	53.43	51.41
12	2.46	0.012	0.150	55.48	56.51
15	2.60	0.011	0.166	62.60	58.69
20	3.49	0.010	0.201	69.02	62.33
30	3.60	0.008	0.245	84.93	69.62

The initial reaction rate increases with the initial concentration of methylene blue (Table 4.23). Because of the very short lifetime of hydroxyl radicals (only a few nanoseconds, Sauer *et al.*, 2002), they are consumed at or very near the location where they are generated. Thus the initial rate of methylene blue decomposition increases with increasing initial dye concentrations because of the higher probability of reaction partner encounters at the interface.

Figure 4.58 compares plots of the half-life parameters ($t_{1/2}$ and $t^*_{1/2}$) versus the initial dye concentration for W/WO_3 samples where $t_{1/2}$ and $t^*_{1/2}$, respectively are given by Eqs. (4.11) and (4.12) (Sadik *et al.*, 2007):

$$t_{1/2} = 0.693/k_{\text{app}} \quad (4.11)$$

$$t^*_{1/2} = 0.5C_0/k + \ln 2/kK \quad (4.12)$$

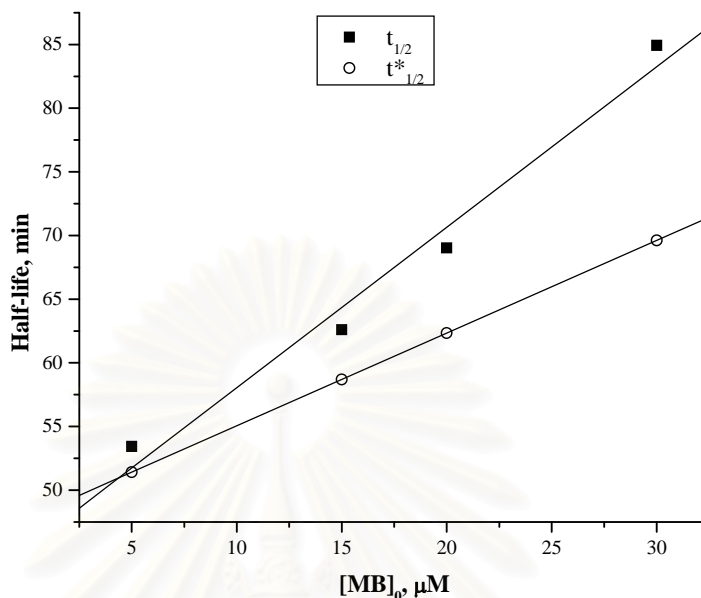


Figure 4.58 Plots of $t_{1/2}$ and $t^*_{1/2}$ values versus initial methylene blue concentration for the nanoporous WO_3 films in this study. The lines are least-squares fits.

Interestingly, at low methylene blue concentrations (e.g., 5 μM), the difference between $t_{1/2}$ and $t^*_{1/2}$ is small as seen in Table 4.23 and Fig. 4.58 ($t_{1/2} = 53.43$ min and $t^*_{1/2} = 51.41$ min). This may be explained as follows: at low methylene blue concentrations, the concentration of the intermediate products formed during the dye breakdown is concomitantly low. On the other hand, the difference between $t_{1/2}$ and $t^*_{1/2}$ increases with an increase in the initial dye concentration (in the 5–30 μM range) (Fig. 4.58) owing to an increase in the concentration of the intermediates which in turn inhibit the decomposition of methylene blue. Light screening by methylene blue itself can also reduce the efficiency of the photocatalytic reaction at these dye levels (Sadik *et al.*, 2007).

CHAPTER V

CONCLUSIONS AND SUGGESTIONS FOR FUTURE WORKS

5.1 Conclusions

5.1.1 WO₃, TiO₂, and composite film preparation by cathodic electrodeposition on stainless steel (SS) AISI 304

In this work the best conditions for composite film of two semiconductors WO₃ and TiO₂ are as follow.

- For WO₃ cathodic electrodeposition on stainless steel (SS) AISI 304, the best electrodeposition time and electrodeposition potential studied in this work are 10 min and -400 mV, respectively which gave photocurrent density up to 546.7 $\mu\text{A}/\text{cm}^2$.

- For TiO₂ cathodic electrodeposition on stainless steel (SS) AISI 304, the best electrodeposition time and electrodeposition potential studied in this work are 30 min and -950 mV, respectively which gave photocurrent density up to 28.0 $\mu\text{A}/\text{cm}^2$.

The effect of multilayer films of electrodeposition on photocurrent performance was also study. Interestingly, both types of semiconductors show the same result that only one layer of film on stainless steel (SS) AISI 304 show better photocurrent performances than multilayer film.

For composite film preparations, SS/WO₃/TiO₂ films were prepared in different electrodeposition steps. The result shows that film SS/WO₃/TiO₂ in the type of SS/5/15min (2 layers) gave the highest photocurrent density up to 229.3 $\mu\text{A}/\text{cm}^2$. For SS/TiO₂/WO₃ films, the SS/30/10 min (1 layer) gave the highest photocurrent density up to 66.7 $\mu\text{A}/\text{cm}^2$. In comparison, film SS/WO₃/TiO₂ show better photocurrent performance than film SS/TiO₂/WO₃. The composite film SS/WO₃/TiO₂ is relevant to the theory of composite film WO₃/TiO₂ which TiO₂ should be outer part and WO₃ should be inner part. Conduction band of TiO₂ has more negative reduction potential than that of WO₃, so photogenerated electron in conduction band of TiO₂ can move down to conduction band of WO₃. This reduces recombination of e⁻ - h⁺

pair in the composite semiconductor thus film SS/WO₃/TiO₂ show better performance.

These cathodic electrodeposition films fabricated in this thesis had less continuity, uniformity and had less stability as well.

5.1.2 TiO₂, WO₃, and composite film preparation by anodization

For this study, TiO₂, WO₃ and composite films were fabricated using anodization technique which oxide layers were anodically growth on Ti or W substrates relies on the controlled balance between oxide formation and chemical/electrochemical dissolution phenomena. It is summarized that Ti/TiO₂ films grown in 0.15 M NH₄F/glycerol for 10 h at 20 V or in 0.15 M NH₄F/PEG 400 for 5 h at 20 V gave excellent photocurrent density approaching 2.82 and 2.74 mA cm⁻², respectively. Modifier (glycerol or PEG) improved the surface morphology of oxide layer by formed self-organized nanotubes arrays. For good photoelectrochemical performance, it is necessary to have long nanotubes with a continuous, extended morphology.

W/WO₃ films grown in 0.15 M NaF for 2 h at 60 V or in 0.3 M oxalic acid for 10 h at 60 V gave excellent photocurrent density approaching 3.93 and 4.13 mA cm⁻², respectively. Modifier (PEG or EG) in this W/WO₃ film fabrication decreased the photocurrent performance when compared with W/WO₃ film obtained without medium modifier.

Composite W/WO₃/TiO₂ obtained from 60/-4 V pulsing waveform for 20 min gave the best photocurrent density around 6.75 mA cm⁻² while the counterpart obtained from 60/0 V pulsing waveform for 40 min gave the best photocurrent density around 7.86 mA cm⁻². For opposite side, composite Ti/TiO₂/WO₃ obtained from 20/-4 V pulsing waveform for 30 min gave the best photocurrent density around 5.16 mA cm⁻² while the counterpart obtained from 20/0 V pulsing waveform for 30 min gave the best photocurrent density around 6.65 mA cm⁻². Importantly, both type of composite films obtained from 0 V lower limit gave better photocurrent performance than that obtained from -4 V. From the study of electrolyte composition on the both type of composite films, 90:10 ratio show better photocurrent performance than 70:30 and 50:50 ratios (see Fig. 4.29).

For the fabrications of Ti/TiO₂/WO₃ nanotubes the initial stage with short time growth (10 min, 30 min and 1 h) of TiO₂ does not bring about the formation of TiO₂ nanotubes arrays but allows the uptake of WO₃ in increasing amounts as the pulsing times increases. However, the typical nanotube arrays were observed when grown with longer time (2 h and 3 h) of constant anodization. Film Ti/TiO₂/WO₃ nanotubes grown with constant anodization at 20 V for 3 h and continued with 20/0 V pulsing waveform for 2 h (CT16) gave the best photocurrent performance up to 7.70 mA cm⁻².

5.1.3 Photocatalysis application for TiO₂, WO₃, and composite film preparation by anodization

For UV light photocatalytic reduction of hexavalent chromium, Cr(VI) (initial concentration of 100 μM) using TiO₂, WO₃, and composite film, zero order kinetic reaction rate was observed. Initial rate of Cr(VI) reduction varied from 2.20 - 5.43 μM/min. Film Ti/TiO₂/WO₃ nanotubes (CT16) show an excellent photocatalytic reduction of Cr(VI) with an initial rate of 5.43 μM/min.

For UV light photocatalytic oxidation of methylene blue, MB (initial concentration of 30 μM) using TiO₂, WO₃, and composite film, first order kinetic reaction rate was observed. Initial rate of methylene blue oxidation varied from 0.43 - 0.69 μM/min. Film Ti/TiO₂/WO₃ nanotubes (CT16) also show the best photocatalytic oxidation of methylene blue with an initial rate of 0.69 μM/min. Photocatalytic oxidation of methylene blue by W/WO₃ films was also possible by using visible light (wavelength > 400 nm). Values for the apparent first-order rate constant (k_{app}), decreased with an increase of the initial dye concentration.

5.2 Suggestions for future work

TiO₂ or WO₃ prepared from cathodic electrodeposition on stainless steel substrate gave non-continuous film surface thus gave less photocurrent performance. The additive may be added into electrodeposition bath in order to improve the film morphology. The study of effect of additive on film morphology is should be investigated further.

From the study of electrolyte composition on morphology of W/WO₃/TiO₂ films obtained from pulse waveform of 60/-4 V, obviously, the morphologies were different when prepared films with different ratio. The rectangular form of oxide was observed when used 70:30 ratio. Deep detail experiment for this aspect is the suggestion for a future work.



สถาบันวิทยบริการ
จุฬาลงกรณ์มหาวิทยาลัย

REFERENCES

- Agency for Toxic Substances and Disease Registry (ATSDR). 1998. Toxicological Profile for Chromium. U.S. Public Health Service, U.S. Department of Health and Human Services, Atlanta, GA.
- Anderson, R.A. 2000. Chromium in the prevention and control of diabetes. Diabetes Metab. 26: 22–27.
- Attenborough, K., Boeve, H., de Boeck, J., Borghs, G. and Celis, J-P. 2000. Ultra-sensitive spin-valve structures grown on n-GaAs by single bath electrodeposition. Sensors and Actuators 81: 9–12.
- Beranek, R., Hildebrand, H. and Schmuki, P. 2003. Self-Organized porous titanium oxide prepared in H₂SO₄/HF electrolytes. Electrochemical and Solid-State Letters 6: B12-B14.
- Beranek, R., Tsuchiya, H., Sugishima, T., Macak, J. M., Taveira, L., Fujimoto, S., Kisch, H. and Schmuki, P. 2005. Enhancement and limits of the photoelectrochemical response from anodic TiO₂ nanotubes. Applied Physics Letters 87, 243114.
- Bianco-Prevot, A., Baiocchi, C., Brussino, M. C., Pramauro, E., Savarino, P., Augugliaro, V., Marci, G. and Palmisano, L. 2001. Photocatalytic degradation of Acid Blue 80 in aqueous solutions containing TiO₂ suspensions, Environmental Science and Technology 35: 971–976.
- Bickley, R. I., Gonzales-Carreno, T., Lees, J. S., Palmisano, L. and Tilley, R. J. D. 1991. A structural investigation of titanium dioxide photocatalysts. Journal of Solid State Chemistry 92: 178-190.
- Bockmeyer, M. and Löbmann, P. 2007. Crack formation in TiO₂ films prepared by sol-gel processing: Quantification and characterization. Thin Solid Films 515: 5212-5219.
- Braun, A. M., Maurette, M.-T., Oliveros, E. 1991. Photochemical Technology, John Wiley & Sons Ltd, New York.

- Cai, Q., Paulose, M., Varghese, O. K. and Grimes, C. A. 2005. The effect of electrolyte composition on the fabrication of self-organized titanium oxide nanotube arrays by anodic oxidation. Journal of Materials Research 20: 230.
- Chenthamarakshan, C. R., de Tacconi, N. R., Xu, L. and Rajeshwar, K. 2004. Photoelectrochromism in Tungsten Trioxide Colloidal Solutions. Journal of Chemical Education 81: 1790-1793.
- Damme, H. V., 1989. Photocatalysis-Fundamentals and Applications. (N. Serpone and E. Pelizzetti, Eds.), Chap. 7, Wiley, New York.
- Demas, J. N., Bowman, W. D., Zalewski, E. F. and Veiapoidl, R. A. 1981. Determination of the quantum yield of the ferrioxalate actinometer with electrically calibrated radiometers. Journal of physical chemistry 85: 2766-2771.
- de Tacconi, N. R., Chenthamarakshan, C. R., Rajeshwar, K., Pauporté, T. and Lincot, D. 2003. Pulsed electrodeposition of $\text{WO}_3\text{-TiO}_2$ composite films. Electrochemistry Communications 5: 220-224.
- de Tacconi, N. R., Chenthamarakshan, C. R., Wouters, K. L., MacDonnell, F. M. and Rajeshwar, K. 2004. Composite $\text{WO}_3\text{-TiO}_2$ films prepared by pulsed electrodeposition: morphological aspects and electrochromic behavior. Journal of Electroanalytical Chemistry 566: 249-256.
- de Tacconi, N. R., Chenthamarakshan, C. R., Yogeeswaran, G., Watcharenwong, A., de Zoysa, R. S., Basit, N. A. and Rajeshwar, K. 2006. Nanoporous TiO_2 and WO_3 films by anodization of titanium and tungsten substrates: Influence of process variables on morphology and photoelectrochemical response. Journal of Physical Chemistry B 110: 25347.
- Diggle, J. W., Downie, T. C. and Goulding, C. W. 1969. Anodic Oxide Films on Aluminum. Chemical Reviews 69: 365-405.
- Do, Y. R., Lee, W., Dwight, K. and Wold, A. 1994. The effect of WO_3 on the photocatalytic activity of TiO_2 . Journal of Solid State Chemistry. 108: 198-201.
- Domenech, J. and Munoz, J. 1987. Photocatalytic reduction of Cr(VI) over ZnO powder. Electrochimica Acta 32: 1383-1386.

- Galindo, C., Jacques, P. and Kalt, A. 2001. Photochemical and photocatalytic degradation of an indigoid dye: a case study of Acid Blue 74 (AB74). Journal of Photochemistry and Photobiology A: Chemistry 141: 47–56.
- Georgieva, J., Armyanov, S., Valova, E., Tsacheva, Ts., Poulis, I. and Sotiropoulos, S. 2005. Photoelectrochemical behavior of electrodeposited tungsten trioxide and electrosynthesised titanium dioxide single component and bilayer coatings on stainless steel substrates. Journal of Electroanalytical Chemistry 585: 35–43.
- Gong, D., Grimes, C. A., Varghese, O. K., Hu, W., Singh, R. S., Chen, Z. and Dickey, E. C. 2001. Titanium oxide nanotube arrays prepared by anodic oxidation. Journal of Materials Research 16: 3331-3334.
- Grimes, C. A. 2007. Synthesis and application of highly ordered arrays of TiO₂ nanotubes. Journal of Materials Chemistry 17: 1451-1457.
- Harada, H. and Ueda, T. 1984. Photocatalytic activity of ultra-fine rutile in methanol-water solution and dependence of activity on particle size. Chemical Physics Letters. 106: 229-231.
- Hasnat, M. A., Siddiquey, I. A. and Nuruddin, A. 2005. Comparative photocatalytic studies of degradation of a cationic and an anionic dye. Dyes and Pigments 66:185–188.
- Hatchard, C. G. and Parker, C. A. 1956. A new sensitive chemical actinometer. II. Potassium ferrioxalate as a standard chemical actinometer. Proceedings of the Royal Society of London, Series A 235:518-568.
- He, Y., Wu, Z., Fu, L., Li, C., Miao, Y., Cao, L., Fan, H. and Zou, B. 2003. Photochromism and size effect of WO₃ and WO₃-TiO₂ aqueous sol. Chemistry of Materials 15: 4039-4045.
- Herrmann, J. M. 1999. Heterogeneous photocatalysis: fundamentals and applications to the removal of various types of aqueous pollutants. Catalysis Today 53: 115-129.
- Houas, A., Lachheb, H., Ksibi, M., Elaloui, E., Guillard, C. and Hermann, J. M. 2001. Photocatalytic degradation pathway of methylene blue in water. Applied Catalysis B: Environmental 31: 145–157.

- Kajitvichyanukul, P. and Amornchat, P. 2005. Effects of diethylene glycol on TiO₂ thin film properties prepared by sol-gel process. Science and Technology of Advanced Materials 6: 344-347.
- Kajitvichyanukul, P. and Vatcharenwong, A. 2005. Role of pH, organic and inorganic anions on photocatalytic reduction of chromium(VI) with titania Powders. Asean Journal on Science and Technology for Development 22(1&2): 169-179.
- Keller, V., Bernhardt, P. and Garin, F. 2003. Photocatalytic oxidation of butyl acetate in vapor phase on TiO₂, Pt/TiO₂ and WO₃/TiO₂ catalysts. Journal of Catalysis 215: 129-138.
- Kennedy, J. H. (1990) Analytical chemistry: principles. Saunders, New York, USA.
- Kuhn, H. J., Braslavsky, S. E. and Schmidt, R. 2004. Chemical actinometry (IUPAC Technical report). Pure Applied Chemistry 76: 2105-2146.
- Ku, Y. and Jung, I. L. 2001. Photocatalytic reduction of Cr(VI) in aqueous solutions by UV irradiation with the presence of titanium dioxide. Water Research 35: 135-142.
- Kwon, Y. T., Song, K. Y., Lee, W. I., Choi, G. J. and Do, Y. R. 2000. Photocatalytic Behavior of WO₃-Loaded TiO₂ in an Oxidation Reaction. Journal of Catalysis 191: 192-199.
- Lee, B-Y., Park, S-H., Kang, M., Lee, S-C. and Choung, S-J. 2003. Preparation of Al/TiO₂ nanometer photo-catalyst film and the effect of H₂O addition on photo-catalytic performance for benzene removal. Applied Catalysis A: General 253: 371-380.
- Lincot, D. 2005. Electrodeposition of semiconductors. Thin Solid Films 487: 40-48.
- Linsebigler, A. L., Lu, G., and Yates, Jr., J. T. 1995. Photocatalysis on TiO₂ Surfaces: Principles, Mechanisms, and Selected Results. Chemical Review 95: 735-758.
- Liu, X-Z., Xu, M-X., Tian, Y-M., Shang, M. and Zhang, P. (2006) Regularity control of porous anodic alumina and photodegradation activity of highly ordered titania nanostructures. Transactions of Nonferrous Metals Society of China 16: s341-s344.

- Macak, J. M., Tsuchiya, H. and Schmuki, P. 2005. High-aspect-ratio TiO₂ nanotubes by anodization of titanium. Angewandte Chemie International Edition 44: 2100.
- Macak, J. M. and Schmuki, P. 2006. Anodic growth of self-organized TiO₂ nanotubes in viscous electrolytes. Electrochimica Acta 52: 1258.
- McMurray, T. A., Byrne, J. A., Dunlop, P. S. M., Winkelman, J. G. M., Eggins, B. R. and McAdams, E. T. 2004. Intrinsic kinetics of photocatalytic oxidation of formic and oxalic acid on immobilized TiO₂ films. Applied Catalysis A: General 262: 105-110.
- Miki, T., Nishizawa, K., Suzuki, K. and Kato, K. 2004. Preparation of thick TiO₂ film with large surface area using aqueous sol with poly(ethylene glycol). Journal of materials science 39: 699-701.
- Mills, A., and Le Hunte, S. 1997. An overview of semiconductor photocatalysis. Journal of Photochemistry and Photobiology A: Chemistry 108: 1–35.
- Mishra, K. K. and Rajeshwar, K. 1989. A re-examination of the mechanisms of electrodeposition of CdX and ZnX (X = Se, Te) semiconductors by the cyclic photovoltammetric technique. Journal of Electroanalytical Chemistry 273:169.
- Mor, G. K., Varghese, O. K., Paulose, M., Shankar, K. and Grimes, C. A. 2006. A review on highly ordered, vertically oriented TiO₂ nanotube arrays: Fabrication, material properties, and solar energy applications. Solar Energy Materials and Solar Cells 90: 2011-2075.
- Natarajan, C. and Nogami, G. 1996. Cathodic Electrodeposition of Nanocrystalline Titanium Dioxide Thin Films. Journal of Electrochemical Society 143: 1547-1550.
- Navo, J. A., Colon, G., Trillas, M., Peral, J., Domenech, X., Testa, J. J., Padron, J., Rodriguez, D. and Litter, M. 1998. Heterogeneous photocatalytic reactions of nitrite oxidation and Cr(VI) reduction on iron-doped titania prepared by the wet impregnation method. Applied Catalysis B: Environment 16: 187-196.
- Oppenlander, T. (2003) Photochemical purification of water and air. Wiley-VCH, Weinheim, Germany.

- Park, J. H., Choi, E. and Gill, K. I. 2003. Removal of reactive dye using UV/TiO₂ in circular type reactor. Journal of Environmental Science and Health Part A 38: 1389–1399.
- Prairie, M. R., Evans, L. R., Stange, B. M. and Martinez, S. L. 1993. An investigation of photocatalysis for the treatment of water contaminated with metals and organic chemicals. Environmental Science Technology 27:1776-1782.
- Potter, E. C. (1956) Electrochemistry: Principles & Applications. Cleaver-Hume, London.
- Rajeshwar, K. (2001) Electron Transfer at Semiconductor-Electrolyte Interfaces," in Electron Transfer in Chemistry, 5st ed. Balzani, Wiley-VCH, Weinheim.
- Rajeshwar, K., de Tacconi, N. R. and Chenthamarakshan, C. R. 2001. Semiconductor-based composite materials: preparation, properties, and performance. Chemistry of Materials 13: 2765-2782.
- Ruan, C., Paulose, M., Varghese, O. K. and Grimes, C. A. 2006. Enhanced photoelectrochemical-response in highly ordered TiO₂ nanotube-arrays anodized in boric acid containing electrolyte. Solar Energy Mater. Solar Cells 90: 1283.
- Santato, C., Odziemkowski, M., Ulmann, M. and Augustynski, J. 2001. Crystallographically oriented mesoporous WO₃ films: synthesis, characterization, and applications. Journal of the American Chemical Society 123: 10639-10649.
- Schrank, S. G., José, H. J., and Moreira, R. F. P. M. 2002. Simultaneous photocatalytic Cr(VI) reduction and dye oxidation in a TiO₂ slurry reactor. Journal of Photochemistry and Photobiology A: Chemistry 147: 71-76.
- Shen, Q., Sato, T., Hashimoto, M., Chen, C. and Toyoda, T. 2006. Photoacoustic and photoelectrochemical characterization of CdSe-sensitized TiO₂ electrodes composed of nanotubes and nanowires. Thin Solid Films 499: 299-305.
- Shiyonovskaya, I. and Hepel, M. 1999. Bicomponent WO₃/TiO₂ Films as Photoelectrodes. Journal of The Electrochemical Society 146: 243-249.

- Somasundaram, S., Chenthamarakshan, C. R., de Tacconi, N. R., Basit, N. A. and Rajeshwar, K. (2006) Composite $\text{WO}_3\text{-TiO}_2$ films: Pulsed electrodeposition from a mixed bath versus sequential deposition from twin baths. Electrochemistry Communications 8: 539-543.
- Somasundaram, S., Tacconi, N., Chenthamarakshan, C. R., Rajeshwar, K. and de Tacconi, N. R. 2005. Photoelectrochemical behavior of composite metal oxide semiconductor films with a WO_3 matrix and occluded Degussa P 25 TiO_2 particles. Journal of Electroanalytical Chemistry 557: 167-177.
- Sonawane, R. S., Hegde, S. G. and Dongare, M. K. 2003. Preparation of titanium(IV) oxide thin film photocatalyst by sol-gel dip coating. Materials Chemistry and Physics 77: 744-750.
- Song, K. Y., Park, M. K., Kwon, Y. T., Lee, H. W., Chung, W. J. and Lee, W. I. 2001. Preparation of Transparent Particulate $\text{MoO}_3/\text{TiO}_2$ and WO_3/TiO_2 Films and their Photocatalytic Properties. Chemistry of Materials 13: 2349-2355.
- Therese, G. H. A., Kamath, P. V. 2000. Electrochemical Synthesis of Metal Oxide and Hydroxides. Chemistry of Materials 12: 1195-1204.
- Thomson, G. E. 1997. Porous anodic alumina: fabrication, characterization and applications. Thin Solid Films 297: 192-201.
- Tsuchiya, H., Macak, J. M., Taveira, L., Balaur, E., Ghicov, A., Sirotna, K. and Schmuki, P. 2005. Self-organized TiO_2 nanotubes prepared in ammonium fluoride containing acetic acid electrolytes. Electrochemistry Communications 7: 576-580.
- Tsuchiya, H., Macak, J. M., Ghicov, A., Taveira, L. and Schmuki, P. 2005. Self-organized porous TiO_2 and ZrO_2 produced by anodization. Corrosion Science 47: 3324.
- U.S. Environmental Protection Agency. (1998) Toxicological Review of Hexavalent Chromium. National Center for Environmental Assessment, Office of Research and Development, Washington, DC.
- Wahl, A. and Augustynski, J. 1998. Charge carrier transport in nanostructured anatase TiO_2 films assisted by the self-doping of nanoparticles. Journal of Physical Chemistry B 102: 7820-7828.

- Watcharenwong, A., Chanmanee, W., de Tacconi, N. R., Chenthamarakshan, C. R., Kajitvichyanukul, P. and Rajeshwar, K. 2007. Self-organized TiO₂ nanotube arrays by anodization of Ti substrate: Effect of anodization time, voltage and medium composition on oxide morphology and photoelectrochemical response. Physical Chemistry Chemical Physics (accepted).
- Wernick, S., Pinner, R. and Sheasby, P.G. (1987) The Surface Treatment and Finishing of Aluminum and its Alloys. Finishing Publications, Middlesex, England.
- Wolcott, A., Kuykendall, T. R., Chen, W., Chen, S. and Zhang, J. Z. 2006. Synthesis and characterization of ultrathin WO₃ nanodiscs utilizing long-chain poly(ethylene glycol). Journal of Physical Chemistry B 110: 25288-25296.
- Woodward, P. M. Description of Research in the Woodward Group. Available from: <http://www.chemistry.ohio-state.edu/~woodward/research.htm>[2007, November 1]
- Zhang, T., Oyama, T., Aoshima, A., Hidaka, H., Zhao, J. and Serpone, N. 2001. Photooxidative N-demethylation of methylene blue in aqueous TiO₂ dispersions under UV irradiation. Journal of Photochemistry and Photobiology A: Chemistry 140: 163–172.
- Zhitomirsky, I. 2000. Ceramic Films Using Cathodic Electrodeposition. Available from:<http://www.tms.org/pubs/journals/JOM/0001/Zhitomirsky/Zhitomirsky-0001.html#table1>[2007, November 1]
- Zhou, M., Lin, W-Y., de Tacconi, N. R. and Rajeshwar, K. 1996. Metal/semiconductor electrocomposite photoelectrodes: behavior of Ni/TiO₂ photoanodes and comparison of photoactivity of anatase and rutile modifications. . Journal of Electroanalytical Chemistry 402: 221.
- Zollinger, H. (1991) Color Chemistry: Synthesis, Properties and Applications of Organic Dyes and Pigments. 2nd revised ed., VCH.
- Zou, G., Xiong, K., Jiang, C., Li, H., Wang, Y., Zhang, S. and Qian, Y. 2005. Magnetic Fe₃O₄ nanodisc synthesis on a large scale via surfactant-assisted process. Nanotechnology 16: 1584-1588.



APPENDICES

สถาบันวิทยบริการ
จุฬาลงกรณ์มหาวิทยาลัย

APPENDIX A

Photocurrent and photocatalytic performances of films prepared by electrodeposition and anodization techniques

Table A-1 Photocurrent density of SS/WO₃ electrodeposition films with varying the electrodeposition time

Film	Electrodeposition Potential (mV)	Electrodeposition Time (min)	Photocurrent density ($\mu\text{A}/\text{cm}^2$)	
			1 st series	2 nd series
WO ₃	-450	5	253.3	186.7
		10	746.7	440.0
		15	53.3	26.7
		20	40.0	13.3
		25	26.7	13.3
		30	13.3	13.3

Table A-2 Photocurrent density of SS/TiO₂ electrodeposition films with varying the electrodeposition time

Film	Electrodeposition Potential (mV)	Electrodeposition Time (min)	Photocurrent density ($\mu\text{A}/\text{cm}^2$)	
			1 st series	2 nd series
TiO ₂	-950	15	21.3	9.3
		30	28.0	13.3
		45	16.0	8.0
		60	18.7	5.3
		95	14.7	5.3

Table A-3 Photocurrent density of SS/WO₃ electrodeposition films with varying the electrodeposition potential

Film	Electrodeposition Potential (mV)	Electrodeposition Time (min)	Photocurrent density ($\mu\text{A}/\text{cm}^2$)	
			1 st series	2 nd series
WO ₃	-250	10	200.0	160.0
	-300	10	213.3	360.0
	-350	10	426.7	653.3
	-400	10	480.0	453.3
	-450	10	386.7	186.7
	-550	10	133.3	40.0
			3 rd series	
WO ₃	-350	10	426.7	
	-350	10	480.0	
	-400	10	546.7	
	-400	10	493.3	

Table A-4 Photocurrent density of SS/TiO₂ electrodeposition films with varying the electrodeposition potential

Film	Electrodeposition Potential (mV)	Electrodeposition Time (min)	Photocurrent density ($\mu\text{A}/\text{cm}^2$)	
			1 st series	2 nd series
TiO ₂	-850	30	8.0	6.7
	-950	30	12.0	9.3
	-1050	30	6.7	6.7

Table A-5 Photocurrent density of SS/WO₃/WO₃/... multilayer films

Film	Electrodeposition Potential (mV)	Electrodeposition Time (min)	Photocurrent density ($\mu\text{A}/\text{cm}^2$)	
			1 st series	2 nd series
WO ₃	-450	10	533.3	546.7
		10 + 10	280.0	386.7
		10 + 10 + 10	333.3	160.0

Table A-6 Photocurrent density of SS/TiO₂/TiO₂/... multilayer films

Film	Electrodeposition Potential (mV)	Electrodeposition Time (min)	Photocurrent density ($\mu\text{A}/\text{cm}^2$)	
			1 st series	2 nd series
TiO ₂	-950	15	15.4	10.0
		15 + 15	7.7	3.3
		15 + 15 + 15	7.7	6.7
		15 + 15 + 15 + 15	7.7	6.7

สถาบันวิทยบริการ
จุฬาลงกรณ์มหาวิทยาลัย

Table A-7 Photocurrent density of SS/WO₃/TiO₂ films obtained by different electrodeposition steps

Film	Electrodeposition Potential (mV)	Electrodeposition Time (min)	Photocurrent density ($\mu\text{A}/\text{cm}^2$)	
			1 st series	2 nd series
SS/WO ₃ /TiO ₂	SS/WO ₃ /TiO ₂	SS/WO ₃ /TiO ₂	1 st series	2 nd series
	SS/-400/-950	SS/10/30 min (1 layer)	44.0	177.3
		SS/5/15 min (2 layers)	229.3	201.3
		SS/2/6 min (5 layers)	44.0	104.0

Table A-8 Photocurrent density of SS/WO₃/TiO₂ films prepared in different number of films layer

Film	Electrodeposition Potential (mV)	Electrodeposition Time (min)	Photocurrent density ($\mu\text{A}/\text{cm}^2$)
			1 st series
SS/WO ₃ /TiO ₂	SS/WO ₃ /TiO ₂	SS/WO ₃ /TiO ₂	1 st series
	SS/-400/-950	SS/2/6 min (1 layer)	176.0
		SS/2/6 min (2 layers)	56.0
		SS/2/6 min (3 layers)	52.0
		SS/2/6 min (4 layers)	77.3
		SS/2/6 min (5 layers)	44.0

Table A-9 Photocurrent density of SS/TiO₂/WO₃ films obtained by different electrodeposition steps

Film	Electrodeposition Potential (mV)	Electrodeposition Time (min)	Photocurrent density (μA/cm ²)	
			1 st series	2 nd series
SS/TiO ₂ /WO ₃	SS/TiO ₂ /WO ₃	SS/TiO ₂ /WO ₃	1 st series	2 nd series
	SS/-950/-400	SS/30/10 min (1 layer)	40.0	66.7
		SS/15/5 min (2 layers)	40.0	53.3
		SS/6/2 min (5 layers)	26.7	40.0

Table A-10 Photocurrent density of SS/TiO₂/WO₃ films prepared in different number of films layer

Film	Electrodeposition Potential (mV)	Electrodeposition Time (min)	Photocurrent density (μA/cm ²)
			1 st series
SS/TiO ₂ /WO ₃	SS /TiO ₂ /WO ₃	SS/TiO ₂ /WO ₃	1 st series
	SS/-950/-400	SS/6/2 min (1 layer)	66.7
		SS/6/2 min (2 layers)	53.3
		SS/6/2 min (3 layers)	40.0
		SS/6/2 min (4 layers)	26.7
		SS/6/2 min (5 layers)	26.7

สถาบันวิทยบริการ
จุฬาลงกรณ์มหาวิทยาลัย

Table A-11 Anodization conditions and photoelectrochemical performance of Ti/TiO₂ in this study

entry no.	electrolyte, medium modifier	voltage, time	j_{ph} , mA cm ^{-2 a)}
1	0.15 M NH ₄ F	20 V, 1 h	2.10
2	”	20 V, 3 h	1.83
3	”	20 V, 5 h	1.47
4	”	20 V, 10 h	1.43
5	0.15 M NH ₄ F/glycerol (~ 2-3% H ₂ O)	20 V, 3 h	2.38
6	”	20 V, 5 h	2.58
7	”	20 V, 10 h	2.82
8	0.36 M NH ₄ F/glycerol (~ 2-3% H ₂ O)	20 V, 5 h	n.d. ^{b)}
9	0.15 M NH ₄ F/PEG 200:H ₂ O (90:10)	20 V, 5 h	1.13 ^{c)}
10	0.15 M NH ₄ F/PEG 400:H ₂ O (90:10)	20 V, 5 h	2.65 ^{c)}
11	0.15 M NH ₄ F/PEG 600:H ₂ O (90:10)	20 V, 5 h	1.55 ^{c)}
12	0.15 M NH ₄ F/PEG 1000:H ₂ O (90:10)	20 V, 5 h	1.39 ^{c)}
13	0.15 M NH ₄ F/ethylene glycol:H ₂ O (90:10)	20 V, 5 h	1.31
14	0.36 M NH ₄ F/ethylene glycol:H ₂ O (90:10)	20 V, 5 h	n.d.
15	”	40 V, 5 h	n.d.
16	”	60 V, 5 h	n.d.

a) j_{ph} = photocurrent density in 0.5 M Na₂SO₄ at 2.0 V

b) n.d. = no data

c) Average value see table below

electrolyte, medium modifier	voltage, time	j_{ph} , mA cm ^{-2 a)}					
		Sample 1	Sample 2	Sample 3	Sample 4	Avg	SD
0.15 M NH ₄ F/ PEG 200:H ₂ O (90:10)	20 V, 5 h	1.15	1.19	1.11	1.07	1.13	0.04
PEG 400:H ₂ O (90:10)	20 V, 5 h	2.74	2.70	2.70	2.46	2.65	0.11
PEG 600:H ₂ O (90:10)	20 V, 5 h	1.43	1.79	1.59	1.39	1.55	0.16
PEG 1000:H ₂ O (90:10)	20 V, 5 h	1.19	1.63	1.35	1.39	1.39	0.16

Table A-12 Anodization conditions and photoelectrochemical performance of W/WO₃ in this study

entry no.	electrolyte, medium modifier	voltage, time	j_{ph} , mA cm ^{-2 a)}
1	0.15 M NaF	20 V, 3 h	0.99
2	„	40 V, 3 h	2.14
3	„	60 V, 3 h	2.82
4	„	80 V, 3 h	2.54
5	„	60 V, 1 h	3.21
6	„	60 V, 2 h	3.93
7	„	60 V, 3 h	2.82
8	„	60 V, 4 h	2.70
9	„	60 V, 6 h	2.78
10	0.3 M oxalic acid	20 V, 2 h	1.98
11	„	40 V, 2 h	2.14
12	„	60 V, 2 h	2.62
13	„	80 V, 2 h	2.62
14	„	60 V, 1 h	2.54
15	„	60 V, 2 h	2.62
16	„	60 V, 3 h	2.94
17	„	60 V, 4 h	3.33
18	„	60 V, 6 h	3.89
19	„	60 V, 10 h	4.13
20	0.15 M NaF/ PEG200:H ₂ O (40:60) ^{b)}	20 V, 3 h	1.57 ^{c)}
21	PEG400:H ₂ O (40:60)	20 V, 3 h	1.39 ^{c)}
22	PEG600:H ₂ O (40:60)	20 V, 3 h	1.38 ^{c)}
23	PEG1000:H ₂ O (40:60)	20 V, 3 h	1.30 ^{c)}
24	0.15 M NaF/ EG:H ₂ O (40:60) ^{b)}	20 V, 3 h	1.23

^{a)} j_{ph} = photocurrent density in 0.5 M Na₂SO₄ at 2.0 V

^{b)} PEG = poly (ethylene glycol); the number pertains to the molecular weight;
EG = ethylene glycol

^{c)} Average value see table below

electrolyte, medium modifier	voltage, time	j_{ph} , mA cm ^{-2 a)}					
		Sample 1	Sample 2	Sample 3	Sample 4	Avg	SD
0.15 M NaF/ PEG 200:H ₂ O (40:60)	20 V, 3 h	1.79	1.39	1.43	1.67	1.57	0.16
PEG 400:H ₂ O (40:60)	20 V, 3 h	1.59	1.15	1.53	1.31	1.39	0.17
PEG 600:H ₂ O (40:60)	20 V, 3 h	1.23	1.23	1.63	1.43	1.38	0.16
PEG 1000:H ₂ O (40:60)	20 V, 3 h	1.31	1.15	1.53	1.23	1.30	0.14

Table A-13 Anodization conditions and photoelectrochemical performance for W/WO₃/TiO₂ nanocomposite film preparation on W substrate

No.	Constant Anodization	Pulse Anodization	Ratio	j_{ph} , mA cm ^{-2 a)}
A1	0.15 M NaF, 60 V, 1 h	Add TiO(NO ₃) ₂ , 60 V/ -4 V, 20 min	90:10	6.75
Blank A1	0.15 M NaF, 60 V, 1 h	60 V/ -4 V, 20 min	-	2.86
A2	0.15 M NaF, 60 V, 1 h	Add TiO(NO ₃) ₂ , 60 V/ -4 V, 40 min	90:10	4.92
A3	0.15 M NaF, 60 V, 1 h	Add TiO(NO ₃) ₂ , 60 V/ -4 V, 1 h	90:10	4.05
A4	0.15 M NaF, 60 V, 1 h	Add TiO(NO ₃) ₂ , 60 V/ -4 V, 2 h	90:10	2.78
A5	0.15 M NaF, 60 V, 1 h	Add TiO(NO ₃) ₂ , 60 V/ -4 V, 3 h	90:10	2.78
B1	0.15 M NaF, 60 V, 1 h	Add TiO(NO ₃) ₂ , 60 V/ 0 V, 20 min	90:10	6.35
B2	0.15 M NaF, 60 V, 1 h	Add TiO(NO ₃) ₂ , 60 V/ 0 V, 40 min	90:10	7.86
Blank B2	0.15 M NaF, 60 V, 1 h	60 V/ 0 V, 40 min	-	3.49
B3	0.15 M NaF, 60 V, 1 h	Add TiO(NO ₃) ₂ , 60 V/ 0 V, 1 h	90:10	7.78
B4	0.15 M NaF, 60 V, 1 h	Add TiO(NO ₃) ₂ , 60 V/ 0 V, 2 h	90:10	7.06
B5	0.15 M NaF, 60 V, 1 h	Add TiO(NO ₃) ₂ , 60 V/ 0 V, 3 h	90:10	6.90

^{a)} j_{ph} = photocurrent density in 0.5 M Na₂SO₄ at 2.0 V

Table A-14 Anodization conditions and photoelectrochemical performance for Ti/TiO₂/WO₃ nanocomposite film preparation on Ti substrate

No.	Constant Anodization	Pulse Anodization	Ratio	j_{ph} , mA cm ^{-2 a)}
C1	0.15 M NH ₄ F, 20 V, 30 min	Add W ₂ O ₁₁ ²⁻ , 20 V/-4 V, 30 min	90:10	5.16
Blank C1	0.15 M NH ₄ F, 20 V, 30 min	20 V/-4 V, 30 min	-	4.68
C2	0.15 M NH ₄ F, 20 V, 30 min	Add W ₂ O ₁₁ ²⁻ , 20 V/-4 V, 1 h	90:10	3.65
C3	0.15 M NH ₄ F, 20 V, 30 min	Add W ₂ O ₁₁ ²⁻ , 20 V/-4 V, 2 h	90:10	2.82
C4	0.15 M NH ₄ F, 20 V, 30 min	Add W ₂ O ₁₁ ²⁻ , 20 V/-4 V, 3 h	90:10	1.55
D1	0.15 M NH ₄ F, 20 V, 30 min	Add W ₂ O ₁₁ ²⁻ , 20 V/0 V, 30 min	90:10	6.65
Blank D1	0.15 M NH ₄ F, 20 V, 30 min	20 V/0 V, 30 min	-	5.24
D2	0.15 M NH ₄ F, 20 V, 30 min	Add W ₂ O ₁₁ ²⁻ , 20 V/0 V, 1 h	90:10	5.75
D3	0.15 M NH ₄ F, 20 V, 30 min	Add W ₂ O ₁₁ ²⁻ , 20 V/0 V, 2 h	90:10	5.60
D4	0.15 M NH ₄ F, 20 V, 30 min	Add W ₂ O ₁₁ ²⁻ , 20 V/0 V, 3 h	90:10	5.48

a) j_{ph} = photocurrent density in 0.5 M Na₂SO₄ at 2.0 V

Table A-15 Anodization conditions and photoelectrochemical performance for the study of effect of electrolyte composition on the resulting W/WO₃/TiO₂ films prepared on W substrate

No.	Constant Anodization	Pulse Anodization	Ratio	j_{ph} , mA cm ^{-2 a)}
1	0.15 M NaF, 60 V, 1 h	60 V/ -4 V, 20 min	100:0	2.86
2	0.15 M NaF, 60 V, 1 h	Add TiO(NO ₃) ₂ , 60 V/ -4 V, 20 min	90:10	6.75
3	0.15 M NaF, 60 V, 1 h	Add TiO(NO ₃) ₂ , 60 V/ -4 V, 20 min	70:30	5.87
4	0.15 M NaF, 60 V, 1 h	Add TiO(NO ₃) ₂ , 60 V/ -4 V, 20 min	50:50	5.71
5	0.15 M NaF, 60 V, 1 h	60 V/ 0 V, 40 min	100:0	3.49
6	0.15 M NaF, 60 V, 1 h	Add TiO(NO ₃) ₂ , 60 V/ 0 V, 40 min	90:10	7.86
7	0.15 M NaF, 60 V, 1 h	Add TiO(NO ₃) ₂ , 60 V/ 0 V, 40 min	70:30	5.79
8	0.15 M NaF, 60 V, 1 h	Add TiO(NO ₃) ₂ , 60 V/ 0 V, 40 min	50:50	5.16

a) j_{ph} = photocurrent density in 0.5 M Na₂SO₄ at 2.0 V

Table A-16 Anodization conditions and photoelectrochemical performance for the study of effect of electrolyte composition on the resulting Ti/TiO₂/WO₃ films prepared on Ti substrate

No.	Constant Anodization	Pulse Anodization	Ratio	j_{ph} , mA cm ^{-2 a)}
1	0.15 M NH ₄ F, 20 V, 30 min	20 V/-4 V, 30 min	100:0	4.68
2	0.15 M NH ₄ F, 20 V, 30 min	Add W ₂ O ₁₁ ²⁻ , 20 V/-4 V, 30 min	90:10	5.16
3	0.15 M NH ₄ F, 20 V, 30 min	Add W ₂ O ₁₁ ²⁻ , 20 V/-4 V, 30 min	70:30	4.60
4	0.15 M NH ₄ F, 20 V, 30 min	Add W ₂ O ₁₁ ²⁻ , 20 V/-4 V, 30 min	50:50	4.01
5	0.15 M NH ₄ F, 20 V, 30 min	20 V/0 V, 30 min	100:0	5.24
6	0.15 M NH ₄ F, 20 V, 30 min	Add W ₂ O ₁₁ ²⁻ , 20 V/0 V, 30 min	90:10	6.65
7	0.15 M NH ₄ F, 20 V, 30 min	Add W ₂ O ₁₁ ²⁻ , 20 V/0 V, 30 min	70:30	6.55
8	0.15 M NH ₄ F, 20 V, 30 min	Add W ₂ O ₁₁ ²⁻ , 20 V/0 V, 30 min	50:50	5.56

a) j_{ph} = photocurrent density in 0.5 M Na₂SO₄ at 2.0 V

Table A-17 Anodization conditions and photoelectrochemical performance for Ti/TiO₂/WO₃ nanotubes film preparation

No.	Constant Anodization 0.15 M NH ₄ F/PEG400:H ₂ O (90:10)	Pulse Anodization Add W ₂ O ₁₁ ²⁻	Ratio	j_{ph} , mA cm ^{-2 a)}
CT 1	20 V, 10 min	20 V/0 V, 10 min	90:10	6.67
CT 2	20 V, 10 min	20 V/0 V, 30 min	90:10	6.83
CT 3	20 V, 10 min	20 V/0 V, 1 h	90:10	6.83
CT 4	20 V, 30 min	20 V/0 V, 10 min	90:10	6.59
CT 5	20 V, 30 min	20 V/0 V, 30 min	90:10	6.67
CT 6	20 V, 30 min	20 V/0 V, 1 h	90:10	7.14
CT 7	20 V, 1 h	20 V/0 V, 10 min	90:10	6.35
CT 8	20 V, 1 h	20 V/0 V, 30 min	90:10	6.35
CT 9	20 V, 1 h	20 V/0 V, 1 h	90:10	6.59
CT 10	20 V, 2 h	20 V/0 V, 30 min	90:10	6.59
CT 11	20 V, 2 h	20 V/0 V, 1 h	90:10	7.30
CT 12	20 V, 2 h	20 V/0 V, 2 h	90:10	7.14
CT 13	20 V, 2 h	20 V/0 V, 3 h	90:10	6.83
CT 14	20 V, 3 h	20 V/0 V, 30 min	90:10	6.43
CT 15	20 V, 3 h	20 V/0 V, 1 h	90:10	7.22
CT 16	20 V, 3 h	20 V/0 V, 2 h	90:10	7.70
CT 17	20 V, 3 h	20 V/0 V, 3 h	90:10	6.90

a) j_{ph} = photocurrent density in 0.5 M Na₂SO₄ at 2.0 V

Table A-18 Photocatalytic reduction of Hexavalent Chromium, Cr(VI) by Ti/TiO₂ film

Electrolyte: 0.15 M NH₄F

Anodization condition: 20 V 1 h

Time	Concentration of Cr(VI)	C/C ₀
00	100.00	
0	99.11	1.00
5	81.76	0.82
10	67.10	0.68
15	48.73	0.49
20	35.37	0.36
25	21.02	0.21
30	4.57	0.05
35	0.00	0.00
40	0.00	0.00
45	0.00	0.00

สถาบันวิทยบริการ
จุฬาลงกรณ์มหาวิทยาลัย

Table A-19 Photocatalytic reduction of Hexavalent Chromium, Cr(VI) by Ti/TiO₂ film

Electrolyte: 0.15 M NH₄F + Glycerol

Anodization condition: 20 V 5 h

Time	Concentration of Cr(VI)	C/C ₀
00	100.00	
0	98.77	1.00
5	80.78	0.82
10	65.23	0.66
15	50.37	0.51
20	37.18	0.38
25	19.08	0.19
30	7.45	0.08
35	0.00	0.00
40	0.00	0.00
45	0.00	0.00

Electrolyte: 0.15 M NH₄F + PEG400

Anodization condition: 20 V 5 h

Time	Concentration of Cr(VI)	C/C ₀
00	100.00	
0	99.44	1.00
5	82.95	0.83
10	72.40	0.73
15	56.19	0.57
20	42.43	0.43
25	29.33	0.29
30	17.73	0.18
35	5.68	0.06
40	0.00	0.00
45	0.00	0.00

Table A-20 Photocatalytic reduction of Hexavalent Chromium, Cr(VI) by W/WO₃/TiO₂ film

Constant anodization: 0.15 M NaF, 60 V 1 h

Pulse anodization: added TiO₂ precursor, 60/-4 V 20 min

Time	Concentration of Cr(VI)	C/C ₀
00	100.00	
0	98.33	1.00
5	89.02	0.91
10	75.87	0.77
15	61.54	0.63
20	42.62	0.43
25	29.51	0.30
30	20.51	0.21
35	10.94	0.11
40	4.58	0.05
45	2.39	0.02
50	1.24	0.01

Constant anodization: 0.15 M NaF, 60 V 1 h

Pulse anodization: added TiO₂ precursor, 60/0 V 40 min

Time	Concentration of Cr(VI)	C/C ₀
00	100.00	
0	93.92	1.00
5	85.47	0.91
10	72.03	0.77
15	57.30	0.61
20	45.67	0.49
25	29.15	0.31
30	16.77	0.18
35	6.15	0.07
40	0.00	0.00
45	-	-
50	-	-

Table A-21 Photocatalytic reduction of Hexavalent Chromium, Cr(VI) by Ti/TiO₂/WO₃ film

Constant anodization: 0.15 M NH₄F, 20 V 30 min

Pulse anodization: added WO₃ precursor, 20/-4 V 30 min

Time	Concentration of Cr(VI)	C/C ₀
00	100.00	
0	99.81	1.00
5	85.25	0.85
10	72.27	0.72
15	59.25	0.59
20	46.01	0.46
25	32.65	0.33
30	19.24	0.19
35	9.58	0.10
40	2.48	0.02
45	-	-
50	-	-

Constant anodization: 0.15 M NH₄F, 20 V 30 min

Pulse anodization: added WO₃ precursor, 20/0 V 30 min

Time	Concentration of Cr(VI)	C/C ₀
00	100.00	
0	98.03	1.00
5	83.28	0.85
10	67.16	0.69
15	57.37	0.59
20	42.08	0.43
25	32.07	0.33
30	18.26	0.19
35	9.83	0.10
40	1.93	0.02
45	-	-
50	-	-

Table A-22 Photocatalytic reduction of Hexavalent Chromium, Cr(VI) by Ti/TiO₂/WO₃ nanotubes film

Constant anodization: 0.15 M NH₄F+PEG400, 20 V 3 h

Pulse anodization: added WO₃ precursor, 20/0 V 2 h

Time	Concentration of Cr(VI)	C/C ₀
00	100.00	
0	99.91	1.00
5	79.96	0.80
10	46.85	0.47
15	4.90	0.05
20	1.37	0.01
25	1.00	0.01
30	0.15	0.00
35	0.00	0.00
40	-	-
45	-	-
50	-	-

Table A-23 Photocatalytic reduction of Methylene blue, MB by Ti/TiO₂ filmElectrolyte: 0.15 M NH₄F

Anodization condition: 20 V 1 h

Time	Concentration of MB	C/C ₀
00	30.00	
0	27.03	1.00
5	25.36	0.94
10	23.40	0.87
15	21.44	0.79
20	19.39	0.72
30	16.22	0.60
45	12.20	0.45
60	8.79	0.33
90	4.32	0.16
120	1.92	0.07

สถาบันวิทยบริการ
จุฬาลงกรณ์มหาวิทยาลัย

Table A-24 Photocatalytic reduction of Methylene blue, MB by Ti/TiO₂ filmElectrolyte: 0.15 M NH₄F + Glycerol

Anodization condition: 20 V 5 h

Time	Concentration of MB	C/C ₀
00	30.00	
0	26.87	1.00
5	25.07	0.93
10	23.02	0.86
15	21.34	0.79
20	19.78	0.74
30	15.87	0.59
45	11.68	0.43
60	8.33	0.31
90	3.79	0.14
120	1.77	0.07

Electrolyte: 0.15 M NH₄F + PEG400

Anodization condition: 20 V 5 h

Time	Concentration of MB	C/C ₀
00	30.00	
0	26.90	1.00
5	24.90	0.93
10	22.79	0.85
15	20.40	0.76
20	18.27	0.68
30	14.69	0.55
45	9.87	0.37
60	6.34	0.24
90	2.46	0.09
120	1.12	0.04

Table A-25 Photocatalytic reduction of Methylene blue, MB by W/WO₃/TiO₂ film

Constant anodization: 0.15 M NaF, 60 V 1 h

Pulse anodization: added TiO₂ precursor, 60/-4 V 20 min

Time	Concentration of MB	C/C ₀
00	30.00	
0	27.14	1.00
5	25.60	0.94
10	23.58	0.87
15	21.62	0.80
20	19.82	0.73
30	16.68	0.61
45	12.45	0.46
60	9.02	0.33
90	4.33	0.16
120	2.04	0.07

Constant anodization: 0.15 M NaF, 60 V 1 h

Pulse anodization: added TiO₂ precursor, 60/0 V 40 min

Time	Concentration of MB	C/C ₀
00	30.00	
0	26.85	1.00
5	25.25	0.94
10	23.67	0.88
15	22.29	0.83
20	20.51	0.76
30	17.73	0.66
45	13.18	0.49
60	9.84	0.37
90	4.72	0.18
120	2.57	0.10

Table A-26 Photocatalytic reduction of Methylene blue, MB by Ti/TiO₂/WO₃ filmConstant anodization: 0.15 M NH₄F, 20 V 30 minPulse anodization: added WO₃ precursor, 20/-4 V 30 min

Time	Concentration of MB	C/C ₀
00	30.00	
0	27.09	1.00
5	25.24	0.93
10	23.08	0.85
15	20.95	0.77
20	18.68	0.69
30	15.18	0.56
45	11.42	0.42
60	7.99	0.29
90	3.92	0.14
120	1.95	0.07

Constant anodization: 0.15 M NH₄F, 20 V 30 minPulse anodization: added WO₃ precursor, 20/0 V 30 min

Time	Concentration of MB	C/C ₀
00	30.00	
0	27.37	1.00
5	25.50	0.93
10	23.62	0.86
15	21.36	0.78
20	19.35	0.71
30	15.74	0.58
45	11.88	0.43
60	7.89	0.29
90	3.74	0.14
120	1.74	0.06

Table A-27 Photocatalytic reduction of Methylene blue, MB by Ti/TiO₂/WO₃ nanotubes film

Constant anodization: 0.15 M NH₄F+PEG400, 20 V 3 h

Pulse anodization: added WO₃ precursor, 20/0 V 2 h

Time	Concentration of MB	C/C ₀
00	30.00	
0	27.48	1.00
5	25.56	0.93
10	23.30	0.85
15	20.76	0.76
20	18.21	0.66
30	14.33	0.52
45	9.26	0.34
60	5.65	0.21
90	1.96	0.07
120	0.87	0.03

สถาบันวิทยบริการ
จุฬาลงกรณ์มหาวิทยาลัย

APPENDIX B

Photon flux and quantum yield calculations

Photon flux, P, of the UV light source was calculated from equation 3.2 in Chapter III.

$$P = \left[\frac{(A_s - A_b) \times V_d \times V_p \times N_A}{\epsilon_{Fe^{2+}} \times l \times \Phi_{Fe^{2+} \text{ at } 0.006M} \times V_a \times t} \right] \quad (3.2)$$

A_s , developed absorbance of sample at 510.0 nm	=	2.73696
A_b , developed absorbance of blank at 510.0 nm	=	0.12508
V_d , final developed volume	=	0.01 L
V_p , photolyzed volume	=	0.01 L
N_A , Avogadro number	=	$6.023 \times 10^{23} \text{ mol}^{-1}$
$\epsilon_{Fe^{2+}}$, specific molar absorbance for $[Fe(phen)_3]^{2+}$ at 510.0 nm	=	$11,110 \text{ L cm}^{-1} \text{ mol}^{-1}$
l , the spectrophotometer cell path length	=	1.80 cm
$\Phi_{Fe^{2+}}$, quantum yield for the photoreduction of the ferrioxalate ions	=	1.2
V_a , aliquot volume	=	0.001 L
t , irradiation time	=	120 s

$$\therefore P = 5.45 \times 10^{16} \text{ photon/s}$$

The apparent quantum yield (Φ_{app}) of the reaction can be defined as the initial degradation rate of hexavalent chromium ($r_{initial}$) (photon/s) divided by the photon flux (P) (photon/s).

$$\Phi_{app} = \frac{r_{initial}}{P}$$

Example:

Initial rate of hexavalent chromium reduction by Ti/TiO₂ film obtained from 0.15 M NH₄F at 20 V for 1 h is 3.25 μM/min (Table 4.15).

$$r_{\text{initial}} = 3.25 \mu\text{M}/\text{min} \times V_i \times N_A$$

where V_i = irradiated volume (10 ml from this experiment)

$$r_{\text{initial}} = \frac{3.25 \times 10^{-6} M}{60s} \times 0.01L \times 6.023 \times 10^{23} \text{ mol}^{-1}$$

$$r_{\text{initial}} = 3.26 \times 10^{14} \text{ photon/s}$$

From $\Phi_{\text{app}} = \frac{r_{\text{initial}}}{P}$

$$\Phi_{\text{app}} = \frac{3.26 \times 10^{14}}{5.45 \times 10^{16}} \quad \frac{\text{photon} / s}{\text{photon} / s}$$

$$\therefore \Phi_{\text{app}} = 0.60 \times 10^{-2}$$

สถาบันวิทยบริการ
จุฬาลงกรณ์มหาวิทยาลัย

APPENDIX C

Journal publication list

1. **Watcharenwong, A.**, Chanmanee, W., de Tacconi, N. R., Chenthamarakshan, C. R., Kajitvichyanukul, P. and Rajeshwar, K. (2007) Anodic growth of nanoporous WO₃ films: morphology, photoelectrochemical response and photocatalytic activity for methylene blue and hexavalent chrome conversion. *Journal of Electroanalytical Chemistry*, (Accepted)
2. **Watcharenwong, A.**, Chanmanee, W., de Tacconi, N. R., Chenthamarakshan, C. R., Kajitvichyanukul, P. and Rajeshwar, K. (2007) Self-organized TiO₂ nanotube arrays by anodization of Ti substrate: Effect of anodization time, voltage and medium composition on oxide morphology and photoelectrochemical response. *Journal of Materials Research*, Vol. 22, pp. 3186-3195.
3. Chanmanee, W., **Watcharenwong, A.**, Chenthamarakshan, C. R., Kajitvichyanukul, P., de Tacconi, N. R. and Rajeshwar, K. (2007) Titania nanotubes from pulse anodization of titanium foils. *Electrochemistry Communications*, Vol. 9 , pp. 2145–2149.
4. Chanmanee, W., **Watcharenwong, A.**, Chenthamarakshan, C. R., Kajitvichyanukul, P., de Tacconi, N. R. and Rajeshwar, K. (2007) Formation and Characterization of Self-Organized TiO₂ Nanotube Arrays by Pulse Anodization. *Journal of the American Chemical Society*, (Accepted)
5. de Tacconi, N. R., Chenthamarakshan, C. R., Yogeeswaran, G., **Watcharenwong, A.**, de Zoysa, R. S., Basit, N. A. and Rajeshwar, K. (2006) Nanoporous TiO₂ and WO₃ Films by Anodization of Titanium and Tungsten Substrates: Influence of Process Variables on Morphology and Photoelectrochemical Response. *Journal of Physical Chemistry B*, Vol. 110, pp. 25347-25355.

REFEREED CONFERENCE PROCEEDINGS

1. **Watcharenwong, A.**, Chanmanee, W., Kajitvitchyanukul, P., Chenthamarakshan, C. R., de Tacconi, N. R., Rajeshwar, K. (2007) Anodic Growth of Nanoporous TiO₂ and WO₃ films: Influence of Process Variables on Morphology, Photoelectrochemical response and Photocatalysis applications. Proceedings of the 2nd international conference on Advances in Petrochemicals and Polymers (ICAPP 2007) June 25 – 28, 2007, Bangkok, Thailand,



สถาบันวิทยบริการ
จุฬาลงกรณ์มหาวิทยาลัย

BIOGRAPHY

Mr. Apichon Watcharenwong was born on August 26, 1978 in Buriram, Thailand. He received his Bachelor's degree in Civil Engineering from Department of Civil Engineering, Faculty of Engineering, Khon Kaen University, Khon Kaen, Thailand in 2001. He received his Master's degree in Environmental Engineering from Department of Environmental Engineering, King Mongkut's University of Technology Thonburi in 2004. He pursued his Philosophy of Doctoral Degree studies in the International Postgraduate Program in Environmental Management (Hazardous Waste Management), Inter-Department of Environmental Management Chulalongkorn University, Bangkok, Thailand on October, 2004. He finished his Philosophy of Doctoral Degree in December 2007.



สถาบันวิทยบริการ
จุฬาลงกรณ์มหาวิทยาลัย